Petrophysical and textural properties of carbonate and non-carbonate depositional systems (Carboniferous-Permian, Spitsbergen)

Jafarian, E.

2018

document version
Publisher's PDF, also known as Version of record

Petrophysical and textural properties of carbonate and non-carbonate depositional systems (Carboniferous-Permian, Spitsbergen)

Elham Jafarian

The research presented in this thesis was conducted at the:

Vrije Universiteit Amsteram
Faculty of Science
Department of Earth Sciences
De Boelelaan 1085
1081HV Amsterdam
The Netherlands

Cover design by Elham Jafarian
Front cover illustration: Photo by Dierk Blomeier/ Norwegian Polar Institute

ISBN: 978-90-8659-775-8
Printed by HAVEKA

VRIJE UNIVERSITEIT

Petrophysical and textural properties of carbonate and non-carbonate depositional systems (Carboniferous-Permian, Spitsbergen)

ACADEMISCH PROEFSCHRIFT

ter verkrijging van de graad Doctor aan
de Vrije Universiteit Amsterdam,
op gezag van de rector magnificus
prof.dr. V. Subramaniam,
in het openbaar te verdedigen
ten overstaan van de promotiecommissie
van de Faculteit der Bètawetenschappen
op dinsdag 6 februari 2018 om 9.45 uur
in de aula van de universiteit,
De Boelelaan 1105

door

Elham Jafarian

geboren te Tehran, Iran

promotor: prof.dr. J.J.G. Reijmer

copromotoren: dr. L.M. Kleipool
dr. D.P.G. Blomeier
dr. C. Scheibner

Reading Committee

prof. dr. Christian Betzler
prof. dr. Jean Borgomano
prof. dr. Maria Mutti
prof. dr. W. van Westrenen
dr. Jan Stafleu

Table of Contents

Chapter 1

Introduction

1.1 Marine carbonates

Marine carbonate sediments, the result of biogenic and inorganic precipitation from seawater, occur in all marine environments, from the tropics to the polar circle. They have high economic importance since their buried counterparts hold major hydrocarbon reserves e.g. Ghawar field in Saudi Arabia, Asmari field and South Pars Gasfield in Iran, Ypresian carbonate reservoirs in Jebel Ousselat, northern Tunisia, Prudhoe Bay field in Alaska, and Agbami oil field in Nigeria.

Exploring and producing hydrocarbons from carbonate reservoirs are proven to be difficult due to the heterogeneous appearance and behaviour of the rocks. Therefore, understanding the textural and spatial petrophysical distribution of carbonate rocks is very challenging and will aid in finding and producing hydrocarbon-bearing reservoirs.

Marine carbonate depositional settings comprise a variety of morphologies such as shallow water epeiric platforms, flat-topped platforms with steep slopes, ramps, and mounds. The depositional morphology is controlled by (i) the environment in which they develop, the so-called extrinsic controls (e.g. tectonics, eustasy, climate, environmental variables, and antecedent topography) and (ii) the production and depositional factors, the intrinsic controls (Schlager, 2005). The geometric style of the system is to a large extent decisive in the depositional character within the basin. For example, during sea-level falls, the entire shelf environment in steep slope shelf systems will be exposed and consequently reduce potential sites for carbonate production significantly, while the only shift in facies belts occur a long ramp settings (Tucker and Wright, 2009).

Following Schlager (2005) carbonate precipitation can be subdivided into biotically controlled, biotically induced and abiotic processes. The types and abundances of organisms in marine carbonate-forming settings are largely controlled by the biochemistry of the respective organisms and environmental factors e.g. light, temperature and water chemistry. The biotically controlled production can be subdivided into heterotrophic, and autotrophic production (Schlager, 2005). The biotically induced carbonate precipitation, autotrophic and heterotrophic production cluster into three different carbonate factories: mud-mound, tropical and cool/cold-water factories respectively. Changes in the environment (extrinsic) as a result of large-scale tectonic instability or climate variability, have a strong influence on the type of carbonate factories and resulting depositional geometry (Schlager, 2005). In addition to these complex primary depositional processes, carbonate systems are subject to extensive alterations due to post-depositional processes such as fracturing and

diagenesis. The latter (e.g. dissolution, cementation, and recrystallization) can easily modify porosity, crystal morphology, and the rigidity of the solid framework. The spatial heterogeneity in carbonate sediments is a result of early environmental mechanical-chemical conditions and associated biological and non-biological precipitation and subsequent post-depositional modifications.

1.2 Study area

During the Late Palaeozoic, the northern rim of the supercontinent Pangea (at the present day in different circum-Arctic areas) documented gradual cooling and deepening of depositional settings with a change from warm and arid to cool and cold-water climatic conditions (Steel and Worsley, 1984; Beauchamp, 1994; Beauchamp and Desrochers, 1997; Ehrenberg et al., 1998). The drop in water temperature is caused by the upwelling of dense, cold and nutrient-rich deep waters within Panthalassa along the western and northern sides of Pangea. This process was set in motion after the seasonal melting of northern sea ice sheets. Furthermore, the closure of the Uralian Gateway during the northwards movement of Pangea led to the cut-off of the influx of warm-water masses from the Paleo-Tethys Ocean. These changes, in turn, resulted in sedimentological shifts and introduced different types of depositional systems (Beauchamp, 1994; Beauchamp and Desrochers, 1997; Blomeier et al., 2011, 2013). Understanding these shifts in the Late Palaeozoic carbonate systems and their spatial distribution of textural and physical properties is the reason why the Late Palaeozoic deposits on Spitsbergen (Svalbard Archipelago, NW Barents Shelf) were investigated. Spitsbergen is the main island of the Svalbard Archipelago, and is located between 74° and 81°N latitude and 10° and 35°E longitude, high above the Arctic Circle on the northwestern part of the Barents Shelf. The sediments recorded in well-exposed outcrops can be subdivided into two main lithostratigraphic units, the Gipsdalen Group (Early Carboniferous to Early Permian) and the Tempelfjorden Group (Early to Late Permian) (Dallmann et al., 1999; Ehrenberg et al., 2001; Blomeier et al., 2009, 2011, 2013).

In the Gipsdalen Group, the Treskeloden Formation (Kasimovian-Artinskian) comprises two intervals: a siliciclastic-dominated lower interval, and a cyclic succession of siliciclastic and carbonate rocks dominated by coral horizons (Birkenmajer, 1964). These deposits accumulated in shallow-marine to lagoonal and alluvial environments.

A lateral equivalent of the Treskeloden Formation, the Wordiekammen Formation (Moscovian-Sakmarian) is marked by siliciclastics and shallow

marine limestone (e.g. algae and benthic foraminifers) depositing in shallow subtidal and intertidal to supratidal areas of a tropical carbonate platform (Blomeier et al., 2009). The variations in lithology relate to a sea-level rise and subsequent varying timing of flooding of different siliciclastic source areas (Larssen et al., 2002). These sedimentary successions are overlain by stacked photozoan limestone/evaporite cycles of the Gipshuken Formation displaying sedimentation in a restricted peritidal platform and supratidal sabkha setting. The Templet Member is the uppermost part of the Gipshuken Formation and shows a decrease in evaporates upwards; however, carbonate breccias and *Microcodium* facies become more abundant, suggesting periods of subaerial exposure.
A disconformity with karst features and reworked sediments formed during a widespread transgression in the late Artinskian separates the Gipsdalen Group from the overlying Tempelfjorden Group.
The sediments of the Tempelfjorden Group (Artinskian-Tatarian) consist of sparitic heterozoan limestones at the base (Vøringen Member) that are overlain by shale and spiculitic chert horizons (Kapp Starostin strata). These successions pass upwards into glauconitic sandstones and silicified, bioclastic limestones (Stensiöfjellet Member). The sediments of the Tempelfjorden Group are deposited in a cool- to cold-water setting including open-marine, shallow nearshore, to deeper offshore realms of a storm-dominated ramp.

1.3 Aim of the study

In subsurface reservoirs, observations are restricted to cores, well logs and seismic lines or cubes. Borehole data present only 1D information of the reservoir and capture heterogeneity on a limited scale. Seismic datasets provide 2D or 3D information of the reservoir. However, seismic datasets are marked by finite horizontal and vertical resolution, which cannot resolve the detailed distribution of meter-scale heterogeneities. Thus seismic profiles already contain major uncertainties limiting the prediction of subsurface geology, and the assessment of reservoir productivity and its economics. The subsurface seismic images require quantitative validation, for example with analogous high-resolution outcrop studies (Helland-Hansen et al., 1994). Outcrops are the favoured choice to understand the geometry of depositional systems and the lateral and vertical heterogeneity of the sediments due to the fine scale in which observations can be made, the data continuity and the 3D accessibility of the sedimentary systems. In addition, quantification of the petrophysical properties (e.g. porosity and permeability) of hydrocarbon reservoir rocks as found in outcrop will help to determine the reservoir

capacity and production capability, and thereby its petroleum geological significance.
In order to compare outcrops with subsurface data, high-resolution outcrop observations are translated into lower resolution seismic images by synthetic seismograms. The latter illustrates the loss or conservation of geological information in seismic datasets.
In this study, we pursue a relationship between outcrop-derived sedimentological and petrophysical attributes (e.g. lithology, facies, diagenesis, porosity, density) and seismic response of a carbonate and non-carbonate succession. This mixed depositional system is marked by a wide variability of textural and petrophysical properties, which in turn complicate subsurface seismic interpretation. The result of this study can contribute to predicting the characteristics of comparable depositional systems in the subsurface.

1.4 Scope

In order to have a better insight in the lateral and vertical variations in the Late Palaeozoic sediment distribution on Spitsbergen, stratigraphic sections have been studied. Several studies have examined the sedimentological character of the Late Palaeozoic outcrop successions of the Svalbard Archipelago (Ehrenberg et al., 2001; Beauchamp and Baud, 2002; Blomeier et al., 2009, 2011, 2013).
The spatial facies distributions and depositional models presented in this thesis were primarily based on previous studies and subsequently complemented by own information derived from field observations and thin sections. This information was used to create a sequence stratigraphic framework that provided the correlation between the individual sections and consequently produced the geological model needed for modelling purposes.
The developments in impedance and synthetic seismic models are so far based on accuracies of the researched geological models. To create efficient 3D geological models which show large-scale lithofacies correlation, we need to further improve the existing information about the geometries of sedimentary settings and their internal facies architectures. Digital outcrop models for example, in which the high-resolution aerial photograph is draped over the regional digital elevation model, may help to better understand the stratal geometries of the individual sedimentary systems (Bellian et al., 2005; Warrlich et al., 2005; Tomás et al., 2009; Verwer et al., 2009; Benson et al., 2014).
The reasons why we used geological models which have been built according to sequence stratigraphic principles are listed below:

- The studied depositional setting is constant and laterally extensive, as is evident from limited lateral microfacies variations and the similarities of sedimentation patterns amongst the studied sections. The minor lateral changes over large distances can only be identified in the stratigraphic framework (not covered by aerial photograph).

- The selected samples collected from the sections are representative for various microfacies types covering the proximal and distal part of the depositional system.

- The size and dimensions of real seismic lines are much closer to our models. "Regular" outcrop models are often much smaller and therefore hard to link to the actual seismic.

- The outcrops are commonly characterized by steep cliffs that are difficult to access. In the future, photographs from RC-drones or high-resolution satellite images may help to acquire datasets

The petrophysical properties, which consist of porosity, density, mineral composition, grain-size and acoustic velocities, were measured on dry plug samples derived from the outcrops. The next step was the analysis of the petrophysical and textural effects such as mineralogy, porosity, density and grain size on the acoustic velocities, which are critical in identifying the origin of seismic reflections (Anselmetti and Eberli, 1993).
The petrophysical and sedimentological information are consequently used to produce synthetic seismic models, which could serve as guidelines for subsurface petroleum system characterization in similar palaeogeographic settings.
Fig. 1.1 illustrates the main organization of the workflow for generating synthetic seismic models and logs of the outcrops.

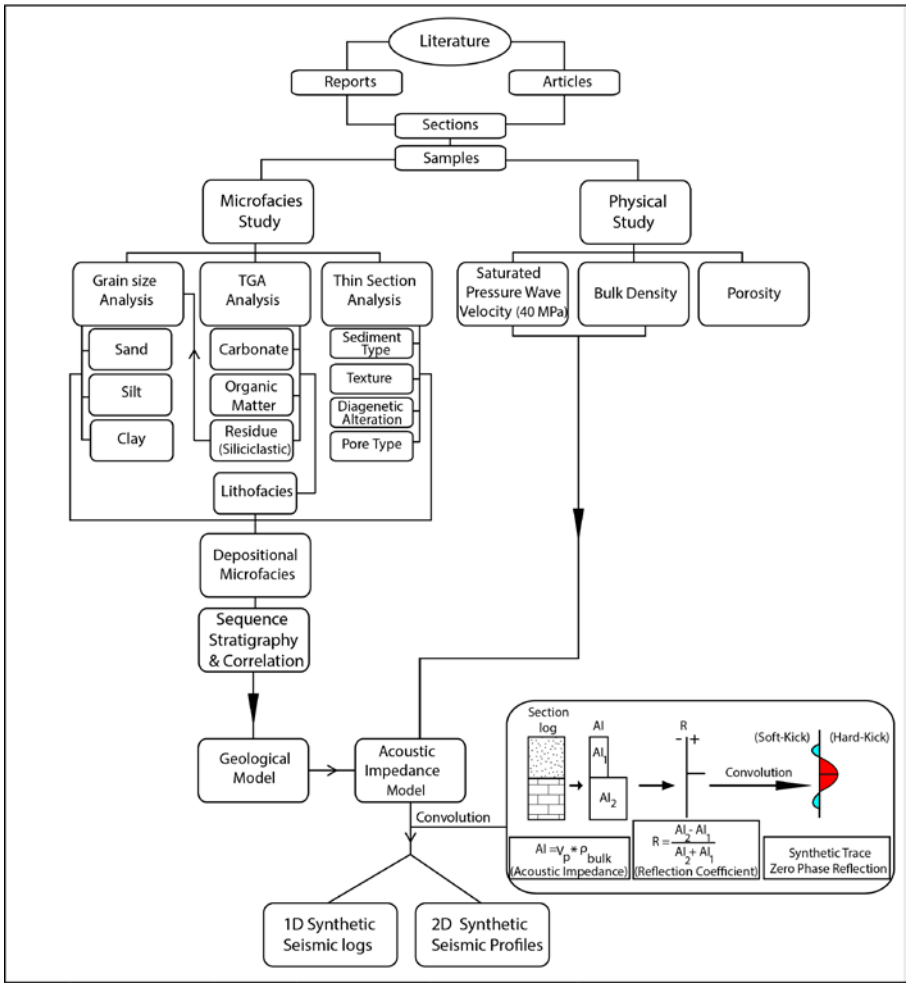

Fig. 1.1 Workflow used for generating synthetic seismic models of the outcrop based on field- and laboratory work.

1.5 Outline

This dissertation starts off with an introduction (Chapter 1), which is followed by the core of the thesis (Chapter 2, 3 and 4; based on submitted and articles). The overall results and conclusions are presented in the synthesis (Chapter 5).

Chapter 2: Facies arrangement and cyclostratigraphic architecture of a Permian biosiliceous carbonate–carbonate depositional system
Goal: Identify depositional system, lateral and vertical facies distribution and to establish of sequence stratigraphic framework of tropical to cool and cold-water carbonate sediments.

Chapter 3: Rock properties of a Carboniferous-Permian mixed carbonate and non-carbonate depositional system
Goal: Relate the acoustic properties to petrophysical and textural parameters (e.g. rock composition, density, porosity, and texture) and link these properties to the facies distribution along the mixed carbonate and non-carbonate depositional system.

Chapter 4: Synthetic seismic model of a Permian biosiliceous carbonate–carbonate depositional system
Goal: Construct synthetic seismic models (using the sedimentological and petrophysical studies presented in Chapters 2 and 3) to evaluate the expression of the outcrop observations into synthetic seismic data, which can be used for comparison with subsurface analogues.

Chapter 5: Synthesis
Goal: Combine the findings to produce a comparison of the geological and petrophysical properties of the sediments of the studied area with those known from other settings. In addition, final conclusions, implications of the results achieved in this study as well as suggestions for further studies are presented.

Chapter 2

Facies arrangement and cyclostratigraphic architecture of the Templet Member and the Kapp Starostin Formation (Permian) on Spitsbergen, Svalbard

E. Jafarian
R.D. Groen
C. Nooitgedacht
C. Scheibner
D.P.G. Blomeier
J.J.G. Reijmer

Chapter based on: Facies arrangement and cyclostratigraphic architecture of the Templet Member and the Kapp Starostin Formation (Permian) on Spitsbergen, Svalbard. Norwegian Journal of Geology 97, 213-231.

2.1 Abstract

Because of outstanding outcrops, Spitsbergen (Svalbard archipelago) provides unique opportunities to investigate the whole Upper Palaeozoic succession in great detail. This study can help to interpret the stratigraphic history and depositional evolution at other locations exposing coeval shelf strata along the northern margin of Pangea, e.g., the southern Barents Sea and Arctic Canada. Bed-scale outcrop observations are combined with microfacies studies to interpret the sedimentary settings and depositional environment of the Upper Palaeozoic strata. A sequencestratigraphic analysis has been carried out to evaluate the relative timing of sediment facies deposition in response to sea-level changes. The Early Artinskian to Kazanian successions of the Templet Member and the Kapp Starostin Formation were divided into five parasequences that are superimposed on a long-term, second-order, sea-level fall. These parasequences record a fundamental change of the sedimentary setting, from a restricted-marine, warm-water carbonate platform to an open-marine, cold-water, biosiliceous-carbonate ramp system.

A cross-section across Svalbard comprising nine onshore sections shows that during deposition of the Kapp Starostin Formation a major depocentre marked by thick parasequences and a higher proportion of deep-water facies (bedded cherts) is located in the southwest of Spitsbergen (at Akseløya), whereas northeastern Svalbard records shallow-water microfacies. Svalbard was tectonically passive during the Permian; the local differences in accommodation space and facies were most likely linked to the rejuvenation of pre-existing structural elements, inherited from the Carboniferous.

A deepening of the depositional environment combined with cold-water climatic conditions as recorded in our study area has also been documented in other Upper Palaeozoic successions around the Arctic, such as the Finnmark Platform (Norwegian Barents Sea) and the Sverdrup Basin (Arctic Canada). This transition in the depositional environment along the northern margin of Pangea is the result of large-scale changes in oceanic circulation patterns and local palaeogeographic changes during the northward movement of Pangea.

2.2 Introduction

The Permian was a dynamic period in Earth history because it was then that the supercontinent Pangea formed; an event that affected many global processes including tectonics, climate and ocean circulation (Ziegler et al., 1997; Laya and Tucker, 2012). The Franklinian shelf, located on the northern

rim of the supercontinent Pangea, preceded the formation of basins in Arctic Canada (the Sverdrup Basin), the Barents Sea (the Finnmark Platform, the Hammerfest Basin and onshore Svalbard), Greenland (the Wandel Sea Basin), and Russia (the Timan Pechora Basin) (Scotese and Langford, 1995; Golonka, 2002). During the Late Palaeozoic, the sediments within these basins recorded a gradual cooling from warm and arid to cold-water conditions and an associated deepening of the depositional environments (Steel and Worsley, 1984; Beauchamp, 1994; Beauchamp and Desrochers, 1997; Ehrenberg et al., 1998).

This study focuses on the Barents shelf, which consists of a complex series of basins, platforms and highs (e.g., Anell et al., 2014). The Svalbard archipelago is situated between 74° and 81° latitude and 10° and 35° longitude, high above the Arctic Circle in the northwestern part of the Barents Shelf (Fig. 2.1A) (Johannessen and Steel, 1992; Dallmann et al., 1999; Jafarian et al., 2017a). Spitsbergen is the main island of Svalbard and is host to many outstanding outcrops of the entire Upper Palaeozoic succession including carbonates and biosiliceous sedimentary rocks (Fig. 2.1A). We summarise the stratigraphy of three onshore sections that range in age from the Early Artinskian to Kazanian (Early to Late Permian). The logs cover the uppermost part of the Gipsdalen Group (Templet Member) and the succeeding Tempelfjorden Group on central Spitsbergen. The measured sections are compared with four sections in NE Svalbard (Blomeier et al., 2011, 2013) and two sections in central and SW Spitsbergen (Ehrenberg et al., 2001). Combining the results of this study and previous studies we aim to produce a comprehensive sequencestratigraphic model, covering the larger part of the archipelago. This will provide a better understanding of the spatial and temporal microfacies distribution and the depositional morphology and development. These findings can help to improve the interpretation of similar systems in the geological record.

Studies have shown that biosiliceous sediments are a potentially good source and reservoir rocks for hydrocarbons (e.g., Surdam and Stanley, 1981; Rogers and Longman, 2001). The Permian was a time of extensive spiculitic chert accumulation along the northern margin of Pangea, and several seismic-based sequencestratigraphic studies have resulted in findings of reservoir rocks for hydrocarbon exploitation, e.g., the Finnmark Platform (Norwegian Barents Sea) (Ehrenberg et al., 1998, 2001; Beauchamp and Baud, 2002; Larssen et al., 2002; Gates et al., 2004; Colpaert et al., 2007). Therefore, the study presented here will be of benefit to our understanding of the depositional environment and bedscale, lateral and vertical, microfacies variations in the source and reservoir rocks of the Barents Sea oil and gas plays. Furthermore, synthetic seismograms, which could be constructed based on the facies variations within a well-defined sequence-stratigraphic framework, and associated

petrophysical properties (Jafarian et al., 2017a) will provide useful analogues for subsurface equivalents (Jafarian et al., in press).

2.3 Study interval

The Upper Palaeozoic succession of Spitsbergen contains two main lithostratigraphic units, the Lower Carboniferous to Lower Permian Gipsdalen Group and the Early to Late Permian Tempelfjorden Group (Fig. 2.1B).
The Gipshuken Formation (Sakmarian–Artinskian) is the upper formation of the Gipsdalen Group and is exposed over the whole archipelago except for the southernmost part of Spitsbergen (Sørkapp–Hornsund High) (Blomeier et al., 2009). In central Spitsbergen, the uppermost part of the Gipshuken Formation is marked by the deposition of evaporite/carbonate cycles of the Templet Member representing restricted, peritidal platform and sabkha environments (Dallmann et al., 1999). In the Early Permian (Artinskian), evidence of subaerial exposure, intense karstification and the collapse of the Gipshuken Platform implies a significant regression. The latter ultimately produced a hiatus in sedimentation separating the Gipsdalen and Tempelfjorden groups (Fig. 2.1B) (Ehrenberg et al., 2001; Groen, 2010). According to Blomeier et al. (2011), this hiatus represents a period between 1 and 9 Myr, but this may vary locally.
The overlying Tempelfjorden Group contains the Kapp Starostin Formation (Late Artinskian–Kazanian/ Earliest Tatarian) in central and northern Spitsbergen (Fig. 2.1B). In east Svalbard, the Tempelfjorden Group consists of the Tokrossøya Formation at Hornsund and the Miseryfjellet Formation on Bjørnøya (Cutbill and Challinor, 1965; Dallmann et al., 1999). The Vøringen Member, Late Artinskian to Kungurian, is the oldest member of the Kapp Starostin Formation and occurs in most areas of Spitsbergen except on Brøggerhalvøya in the northwest of the island (Dallmann et al., 1999). The member contains coarse-grained, bioclastic limestones deposited on the shoreface in storm-dominated ramp settings (Dallmann et al., 1999; Blomeier et al., 2011). Deposits covering the Vøringen Member include dark to light-coloured, spiculitic chert horizons with shale partings (Groen, 2010; Blomeier et al., 2011). In central Spitsbergen, the Stensiöfjellet Member forms the uppermost strata of the Kapp Starostin Formation and consists of green, glauconitic sandstones (with up to 30% glauconite) and spiculitic cherts deposited in a nearshore environment (Fig. 2.1B) (Dallmann et al., 1999). The transition from the Tempelfjorden Group to the overlying Sassendalen Group is marked by a sharp change to marine siliciclastics. It also marks the termination of the deposition of biota-dominated sediments, e.g., spiculitic

cherts and bioclastic limestones (Ehrenberg et al., 2001; Blomeier et al., 2011). No evidence of subaerial exposure or a hiatus has been recorded in central Spitsbergen (Mangerud and Konieczny, 1993). However, whether or not the Permo Triassic boundary represents a period of erosion, non-deposition or conformable sedimentation remains controversial (Mørk et al., 1989; Stemmerik and Worsley, 1989; Mangerud and Konieczny, 1993; Ehrenberg et al., 2001; Nakrem et al., 2008; Dustira et al., 2013).

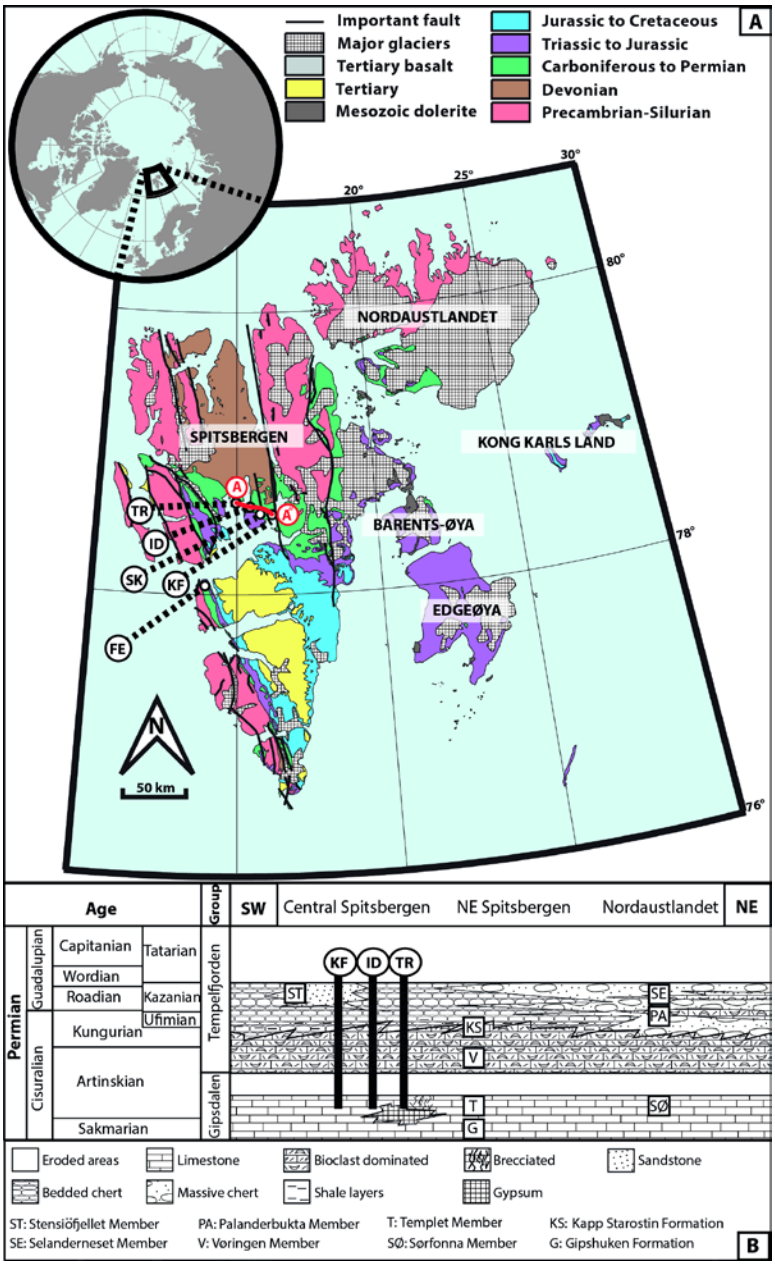

Fig. 2.1 (A) Geological map of the Svalbard archipelago. Strata investigated for this study are of Permian age and are represented by the greenshaded areas on the map and in the legend. Sections location indicated: Tålmodryggen (TR); Idodalen (ID); Skansen (SK); Kapp Fleur de Lys (KF) and Festningen (FE). A–A" indicates cross-sections used for the correlation profile in figure 2.5 (modified from http: //npolar.no/geonet/ items general/frame.html). (B) Chronostratigraphic framework and main lithologies of the Permian of Svalbard (adapted from Dallmann et al., 1999). The stratigraphic positions of the investigated sections are indicated: Tålmodryggen (TR), Idodalen (ID) and Kapp Fleur de Lys (KF).

2.4 Methods

Three sections were logged in central Spitsbergen at selected locations: (i) section KF located at Kapp Fleur de Lys, on the western coast of Billefjorden; (ii) section ID positioned at Idodalen, on the eastern coast of Dicksonfjorden, and (iii) section TR located at Tålmodryggen, on the western coast of Dicksonfjorden. The sedimentological sections were logged measuring layer thicknesses and defining colour, lithology, texture (Dunham, 1962), components, sedimentary structures and key stratigraphic surfaces. These data are supplemented with some samples from the type-section of the Kapp Starostin Formation at Festningen (FE) (Outer Isfjorden) and data from a section at Skansen (SK) (western coast of Billefjorden) (Blomeier et al., 2011, 2013). Thermogravimetric analysis (TGA) was performed on selected samples to determine the amount of organic matter, carbonate and non-carbonate residue (Dean, 1974; Earnest, 1984). A total of 111 thin-sections (Idodalen: n = 35, Kapp Fleur de Lys: n = 21, Tålmodryggen: n = 37, Festningen: n = 10, and Skansen: n = 8), 2 x 5 cm size, were prepared for petrographic analysis. The siliciclastics were categorised following the grain-size based classification of Wentworth (1922), and carbonates were classified according to Dunham (1962). Biosiliceous sedimentary rocks were defined based on the main components and characteristic fabrics. In total, fourteen microfacies types have been identified of which the detailed information is listed in Table 2.1. The interpretation of the microfacies environment was used to determine variations in relative sea level, and it also provided the basis for a correlation between the individual sections and the construction of a sequence-stratigraphic framework.

2.5 Results

2.5.1 Microfacies analysis

Previous work on the Svalbard exposures (Ehrenberg et al., 1998, 2001; Hüneke et al., 2001; Blomeier et al., 2011, 2013; Buggisch et al., 2012) consisted of highly detailed logging, facies descriptions and geochemical analyses. The microfacies studies discussed in these earlier studies are used as a basis for the definition and identification of the microfacies types presented in this study. During the fieldwork, three new sections at Kapp Fleur de Lys (KF), Idodalen (ID) and Tålmodryggen (TR) were investigated enclosing all previously encountered microfacies types. A total of fourteen microfacies types has been defined based on lithology, texture, components and sedimentary

structures (Fig. 2.2; Table 2.1). Each microfacies is linked to specific depositional processes and settings. Evaporites (MFT–1; n = 2), microbial limestones (MFT–2; n = 7), mudstones (MFT–3; n = 5), peloidal, bioclastic wacke- to packstones (MFT–4; n = 1), *Microcodium* bearing sediments (MFT–5; n = 2) and lithoclastic rudstones (carbonate breccias) (MFT–6; n = 3) occur predominantly in the Templet Member. Coarse-grained, brachiopod limestones (MFT–7; n = 5), coarse-grained, mixed-bioclastic limestones (MFT–8; n = 7) and finegrained, mixed-bioclastic limestones (MFT–9; n = 9) are restricted to the strata of the Vøringen Member. Coarse-grained, bryozoan limestones (MFT–10; n = 15) and coarse-grained, echinoderm limestones (MFT–11; n = 2) are present within the Kapp Starostin Formation. Spiculites (MFT–12; n = 50), locally interbedded with thin horizons of shale (MFT–13; n = 1), are a dominant microfacies within the Kapp Starostin Formation. In addition, glauconitic calcareous sandstones (MFT–14; n = 2) are a typical microfacies within the Stensiöfjellet Member.

Thermogravimetric analysis (TGA) shows that carbonate content decreases when moving from the microfacies of the Templet Member to the Kapp Starostin Formation. At the same time, the biogenic silica (spicule) content increases (Jafarian et al., 2017a).

Table 2.1 Characteristics, occurrence, and environmental reconstruction of the microfacies types (MFTs) of central Spitsbergen.

MFT-No.	MFT-name	Lithology, colour and texture	Components		Occurrence & facies association	Depositional environments
			Skeletal	Nonskeletal		
1	**Evaporite**	Evaporites usually form massive to nodular horizons. Silicified patches and chert nodules are commonly present			Templet Mb., associated with MFT–2	Points to a supratidal, sabkha environment
2	**Microbial limestone**	Thick to medium-bedded, greyish to partly brownish, fine-grained limestones show horizontal to wavy laminated algal mats. Sparry-filled fenestral cavities, desiccation cracks and strong fragmentation occur frequently	Algal mats and few siliceous sponge spicules	Dense micritic peloids, sand-sized quartz grains and locally *Microcodium*	Templet Mb., associated with MFTs–1, 3, 4, 5 & 6	Reflect marginal marine, tidal flats of a carbonate platform. Presence of evaporites and *Microcodium* crystals suggest the vicinity to the supratidal sabkha environment
3	**Mudstone**	Massive, thick to medium-bedded, fine-grained limestones (mudstones and minor wackestones) are characterized by grey or reddish micrite/microsparite	Algal mats, few sponge spicules, foraminifers and ostracods	Quartz grains, rare *Microcodium*, dolomite crystals, peloids and pyrite crystals	Templet Mb., associated with MFTs–2, 4, 5 & 6	Reflect deposition under low-energy, calm-water conditions within the tidal flats of the marginal marine platform
4	**Peloidal, bioclastic wacke- to packstone**	Grey, partly reddish or brownish limestones comprise micrite/microsparite matrix, with blocky sparite in some well-washed areas	Restricted photozoan bioclasts (mainly Ealandia sp. foraminifera)	Abundant peloids, rare quartz grains, *Microcodium* and dolomite crystals	Templet Mb., associated with MFTs–2, 3 & 5	Typical for the platform interior, under moderate-energy conditions (tides, waves), the components were washed into lateral restricted accumulations behind the platform edge
5	***Microcodium* bearing sediment**	Subhedral, light brownish equant to bladed sparry calcite crystals embedded in micritic/microsparitic matrix forming wacke- to packstones	Algal mats, few siliceous sponge spicules, foraminifers and ostracods	*Microcodium*, quartz grains, peloids and dolomite crystals	Templet Mb., associated with MFTs–2, 3 & 6	Reveal a meteoric influenced environment, pause of marine sedimentation and subaerial exposure
6	**Lithoclastic rudstone (carbonate breccia)**	Massive, medium to thick-bedded, multicoloured rudstones are marked by angular to well-rounded intraformational clasts. Sediments are intensively altered (stained, recrystallized, dolomitized and/or marginally dissolved) and embedded in micritic/microsparitic matrix	Few siliceous sponge spicules, foraminifers and ostracods	Peloids, quartz grains and locally *Microcodium*	Templet Mb., associated with MFTs–2, 3 & 5. Locally occurs in the lowermost strata of the Vøringen Mb.	During the marine regression, subaerially exposed carbonate platform deposits are affected by desiccation, meteoric alteration and reworking within sabkha like environment
7	**Coarse-grained, brachiopod limestone**	Massive, medium to thick-bedded rudstones (in addition to loosely packed floatstones) are locally intensely silicified. Sparite cement is common	Thick-shelled brachiopods in brachiopod coquinas or whole specimens in brachiopod pavements, rare debris of bivalves, gastropods, bryozoans and echinoderms	Rare glauconite minerals	In the Vøringen Mb., forms the lower bed of distinct sediment couplets, associated with MFTs–8, 9	Coarse grain size with high degree of abrasion, sparite cement, graded bedding and the association with fine-grained limestones (MFT–9) reflect high-energy periodic storm events. During this time the skeletal material was reworked from their origin (between FWWB and SWWB) and accumulated across the inner ramp (above FWWB) to form brachiopod coquinas
8	**Coarse-grained, mixed-bioclastic limestone**	Grey to slightly brownish and yellowish, thick to thin-bedded rud- to floatstones that contain recrystallized, marginally dissolved and broken bioclastic debris. The deposits are affected by silicification. Sparry-filled inter- and intraparticle voids present	Fragments of brachiopods, bryozoans, echinoderms, sponge spicules, rare debris of foraminifers and ostracods	Peloids, carbonate extraclasts and rare allochthonous glauconite minerals	Kapp Starostin Fm., associated with MFTs–10, 11. In the Vøringen Mb., associated with MFTs–7, 9	Presence of broken debris of heterozoan biota and blocky sparite indicate storm-dominated, cool-water conditions within the inner and mid ramp setting

MFT-No.	MFT-name	Lithology, colour and texture	Components		Occurrence & facies association	Depositional environments
			Skeletal	Nonskeletal		
9	**Fine-grained, mixed-bioclastic limestone**	Medium-bedded to massive grainstones are affected by an intense silicification and bioturbation (mostly *Skolithos* burrows)	Well-sorted, fine- to medium brachiopod debris and sometimes sponge spicules	Peloids, quartz grains and glauconite minerals	In the Vøringen Mb,. forms the upper horizon of storm beds (tempestites), associated with MFTs–7, 8	Grainstone fabric reflects agitated-water condition around the FWWB. The deposits show the normal background sedimentation in periods without storm activity
10	**Coarse-grained, bryozoan limestone**	Thin to medium-bedded float- to rudstones that are silicified and recrystallized. The components are commonly altered (recrystallized, marginally dissolved, fragmented and Fe-stained) indicating reworking. Matrix mainly is composed of micrite/microsparite. Locally blocky or sytaxial sparite cements are present	Poorly-sorted debris of bryozoans, echinoderms, brachiopods, siliceous sponges and rare solitary rugose corals and gastropods	Glauconite minerals, peloids and dolomite crystals	Kapp Starostin Fm., associated with MFTs–8, 11	The dominant micritic matrix represents a more distal area with respect to brachiopod limestones. The main environment of robust, bush-like trepostome bryozoan comprises the distal mid ramp around the SWWB. During storms, bryozoan debris was transported (from the primarily habitat) across the mid and proximal outer ramp setting
11	**Coarse-grained, echinoderm limestone**	Greyish to brownish, thin to medium-bedded float- to rudstones with a micritic/microsparitic matrix, and locally sparite cement. The biotic constituents are commonly altered representing reworking. Sediments are partly strongly silicified	Poorly-sorted fragments of echinoderms, bryozoans, brachiopods, siliceous sponges, foraminifers and ostracods	Glauconite minerals and dolomite crystals	Kapp Starostin Fm., associated with MFTs–7, 8 & 10	The dominance of matrix-supported fabric points to deposition under distal, low to moderate-energy conditions below the FWWB of the mid ramp setting. Rarely occurring grainstone fabrics suggest proximal, higher-energy conditions
12	**Spiculite**	Two types of spiculitic cherts could be identified: (1)Dark-coloured, thin to medium-bedded spiculitic cherts marked by the abundance of microspicules, the micritic matrix, the low-diversity biotic association and the local occurrence of shale horizons. (2) Light-coloured massive to nodular-bedded cherts characterized by the abundance of megaspicules, burrows and a lower concentration of micritic matrix. Sediments are intensively silicified and bioturbated	Well to poorly-sorted monaxon spicules, brachiopods, echinoderms, bryozoans and ostracods	Glauconite grains, peloids and rare quartz grains	Kapp Starostin Fm., associated with MFTs–8, 10 & 11	Dark-coloured bedded cherts reflect deposition in calm-water, low-energy conditions of the outer ramp setting far below the SWWB. Light-coloured cherts suggest a transition of this facies toward proximal area on the outer mid ramp margin around SWWB
13	**Clay-siltstone (shales)**	Dark-coloured clay-siltstones are present either as linings or very thin to medium bedded (internally laminated) layers	Components are not clear recognizable due to obliteration of primarily origin	Silt-sized quartz grains	Kapp Starostin Fm., associated with MFT–12. Separates the Vøringen Mb. from the Templet Mb.	Reflect calm-water, anaerobic conditions of the outer ramp setting, probably representing somewhat condensed sedimentation
14	**Glauconitic calcareous sandstone**	Massive, thin to medium-bedded, greenish to whitish sandstones show well-sorted and well-rounded quartz grains mainly cemented by blocky sparite. Silicification occurs in the sediments	Fragments of brachiopods, bryozoans and crinoids	Well sorted, edge-rounded to rounded, sand-sized quartz grains, less than 5% glauconite minerals	In the Stensiöfjellet Mb., associated with MFTs–7, 9	Reflect deposition in the foreshore to shoreface areas of the inner ramp

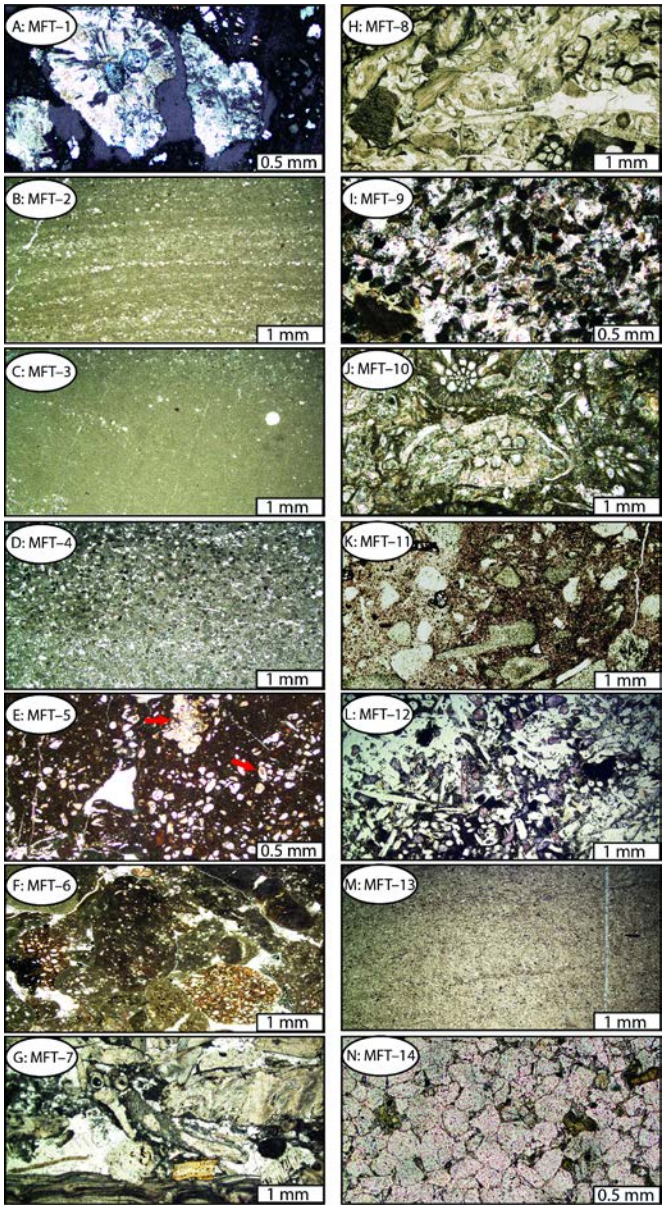

Fig. 2.2 Thin-section photographs of each microfacies type. Scales indicated. (A) MFT–1: evaporite; (B) MFT–2: microbial limestone; (C) MFT–3: mudstone; (D) MFT–4: peloidal bioclastic wacke- to packstone; (E) MFT–5: *Microcodium*-bearing sediments (*Microcodium* aggregate and single crystal are indicated by arrows); (F) MFT–6: lithoclastic rudstone (breccia); (G) MFT–7: coarse-grained, brachiopod limestone; (H) MFT–8: coarse-grained, mixed-bioclastic limestone; (I) MFT–9: fine-grained, mixed-bioclastic limestone; (J) MFT–10: coarse-grained, bryozoan limestone; (K) MFT–11: coarse-grained, echinoderm limestone; (L) MFT–12: spiculite; (M) MFT–13: clay-siltstone; (N) MFT–14: glauconitic calcareous sandstone.

2.5.2 Section descriptions

Kapp Fleur de Lys section (KF)

The section at Kapp Fleur de Lys (Fig. 2.1) is 139 m thick and encloses the upper 2 m of the Templet Member and 137 m of the overlying Kapp Starostin Formation. The latter formation includes a 7.5 m-thick Vøringen Member at its base and a 17 m-thick Stensiöfjellet Member at the top.

The Templet Member consists of grey-coloured, micritic limestones (MFTs–2, 3 and 4) followed by medium-bedded, lithoclastic rudstones (MFT–6) and *Microcodium* bearing sediments (MFT–5). In this section, the boundary between the Templet and Vøringen Members is not exposed. The Vøringen Member is characterised by a series of 2–3 m-thick beds of fossiliferous limestones (Groen, 2010; Blomeier et al., 2013). The coarse-grained, brachiopod limestones (MFT–7) grade into fining-upward horizons (graded bedding) with various other biota such as echinoderms and bryozoans (MFTs 8, 9). Local bioturbation by Skolithos burrows has ostensibly led to silicification. Above this member, a monotonous series of thin- to medium-bedded cherts (MFT–12) with claystone partings (MFT–13) occurs, marking the overall appearance of the Kapp Starostin Formation. At the top, the Stensiöfjellet Member consists of thick, greenish, glauconitic sandstone beds (MFT–14), whitish massive to nodular-bedded cherts (MFT–12) and minor allochemical limestones (MFT–7).

Idodalen section (ID)

Section Idodalen (Fig. 2.1) contains 6 m of the Templet Member and 91 m of the Kapp Starostin Formation, including a 7.5 m-thick Vøringen Member at the base.

The Templet and Vøringen members in this section are lithologically similar to those present in section Kapp Fleur de Lys. The strata above the Vøringen Member are also analogous to those encountered in section Kapp Fleur de Lys. However, after 60 m from the base of the section, the uniform chert series (MFT–12) is interrupted by a distinctive series of coarse-grained, bioclastic (bryozoans, brachiopods, crinoids) limestones (MFTs–10 and 11). Above this sequence, the section continues with 25 m of dark to ochre-coloured, massive to nodular-bedded cherts (MFT–12).

Tålmodryggen section (TR)

Section Tålmodryggen (Fig. 2.1) comprises 20 m of the Templet Member and 98 m of the Kapp Starostin strata, including a 7.5 m-thick Vøringen Member at the base. The Templet Member is characterised by intercalations of white evaporates (MFT–1) and algal limestones (MFT– 2) that are overlain by

lithoclastic rudstone (breccia) layers (MFT–6). The Vøringen Member is marked by transgressive horizons of grey to light brown, carbonate breccia (MFT–6) followed by thin- to medium-bedded, multicoloured claystone horizons (MFT–13). Higher up in the succession, sediment couplets occur consisting of an alternation of brachiopod limestones and finegrained, bioclastic limestones (MFTs–7 and 9) with abundant Skolithos burrows. Unlike in the sections at Idodalen and Kapp Fleur de Lys, section Tålmodryggen contains lenses and horizons of coarse lithoclasts (pebbles). Sandy horizons crop out in the topmost massive chert units of the Vøringen Member.
The sediments of the Kapp Starostin Formation continue with a monotonous series of dark to ochre-coloured cherts (MFT–12) with dark claystone linings and horizons (MFT–13). At 60 m from the base of the section, a 5 m-thick interval of silicified, bioclastic limestones containing fragments of bryozoans, brachiopods, corals and siliceous sponges (MFT–10) is present which is followed by shale horizons. At 86 m from the base of the section, a second series of bioclastic carbonates (MFTs–10 and 11; 14 m) is present. The uppermost part of this section is marked by units of white, massive chert (MFT–12; 20 m).

2.6 Discussion

2.6.1 Depositional model

Depositional model of the Templet Member

The various microfacies of the Templet Member (MFTs– 2, 3 and 4) show an abundance of peloids and a poorly diversified photozoan biotic association (predominantly algae), which reflects warm and hypersaline, restricted shallow-water conditions (Fig. 2.3) (Groen, 2010). The carbonate sediments of the Templet Member, which have mud-supported textures, most likely accumulated in a marginal marine, peritidal setting of a tropical carbonate platform, above the FWWB (Blomeier et al., 2011). The presence of sabkha setting evaporites (MFT–1) in the Templet Member is indicative of an arid to semiarid climate. The occurrence of quartz grains in this member confirms its proximity to the hinterland. During a marine regression in Sakmarian–Artinskian time, limestone strata of the Templet Member emerged and were subjected to erosion and karstification. The lithoclastic rudstone (MFT–6) is interpreted as the end product of this process.

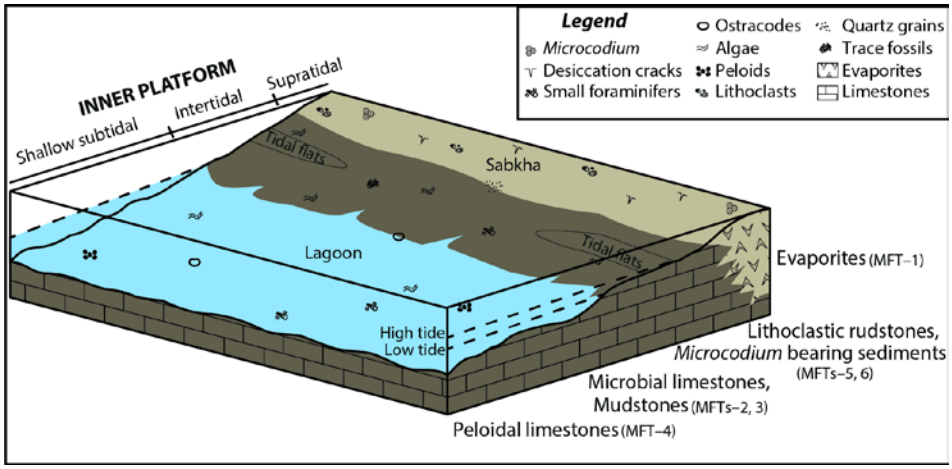

Fig. 2.3 Schematic 3D model of a flat-topped carbonate platform for the Templet Member in central Spitsbergen, showing distribution of the main microfacies and biota across the platform. Adapted from Blomeier et al. (2011). Symbols show the main components of the sediments.

Depositional model of the Tempelfjorden Group

The Kapp Starostin Formation was deposited in an intracratonic basin characterized by gentle uniform depositional slopes, which is the most common basin type for the development of a ramp-type system (Ehrenberg et al., 2001). It consists of chert horizons in combination with cold-water carbonate sediments marked by gravel sized heterozoan biota and the presence of glauconite grains. Ooids and aggregate grains are absent. These sediments were deposited on a ramp-type morphology. The depositional anatomy is constant and laterally extensive, as is evident from limited lateral microfacies variations and the similarities of sedimentation patterns amongst the studied sections. The ramp system displays various sub-environments from the inner (around foreshore to fair-weather wave base, FWWB) to mid (between FWWB and stormweather wave base, SWWB) to the outer ramp (below SWWB) that are characterised by particular microfacies types (Fig. 2.4).

Depositional model of the Vøringen Member

Sediments of the Vøringen Member show a different depositional environment than the warm and hypersaline conditions of the Templet Member. In the transgressive deposit of the Vøringen Member, the photozoan association switched to a heterozoan assemblage, represented by crinoids, brachiopods and bryozoans, as well as siliceous sponge spicules (Bryonoderm facies; Hüneke et al., 2001). Brachiopods are the main constituent and accumulated

on shell banks (coquinas) within an inner ramp system (Fig. 2.4), forming coarse grained, brachiopod limestones (MFT–7). The predominance of the sparite-filled primary pore space and the high degree of roundness of the individual grains implies that high-energy conditions predominated during deposition of the inner and mid ramp microfacies (Groen, 2010; Blomeier et al., 2011). This microfacies (MFT–7) occurs associated with coarse-grained, mixedbioclastic limestones (MFT–8) consisting of broken fragments of bryozoans, echinoderms and siliceous sponge spicules, which were transported from the midramp area by strong onshore storm surges (Blomeier et al., 2011, 2013). The fine-grained, mixed-bioclastic limestones (MFT–9) form the upper part of the Vøringen Member and reflect sedimentation under normal conditions in an agitated shoreface area (Groen, 2010; Blomeier et al., 2011).

The coarse grain size of the skeletal debris, the finingupward trend, and occasional erosive surfaces provide evidence for the deposition of proximal tempestites in the inner-ramp setting (Flügel, 2004). Hence, the ramp system has been subjected to the impact of storms repeatedly. In the fine-grained, mixed-bioclastic limestones (MFT–9), extensive bioturbation (mainly by Skolithos and Zoophycos trace fossils) and occasional glauconite minerals indicate low sedimentation rates and suggest breaks in the storm activity. Reid et al. (2007) and Blomeier et al. (2013) interpreted the occurrence of trace fossils in the upper part of storm deposits as the increased activity of opportunistic sediment feeders in the aftermath of a storm.

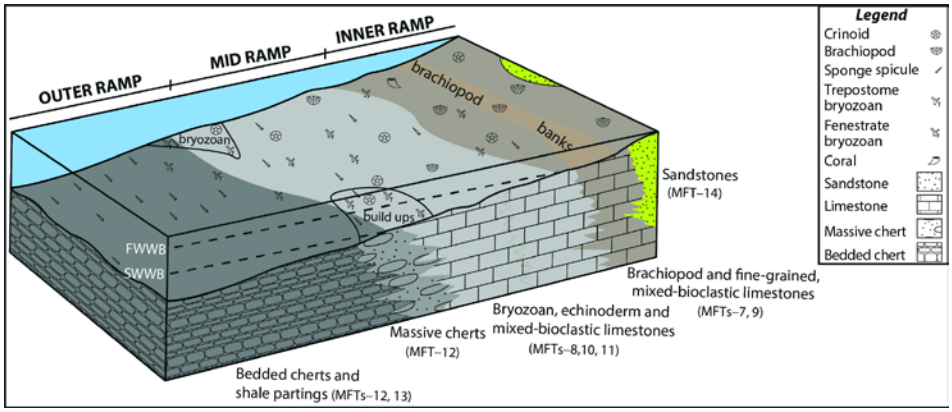

Fig. 2.4 Schematic 3D carbonate ramp model for the Kapp Starostin Formation in central Spitsbergen, showing distribution of the main microfacies and biota across the inner, mid and outer ramp settings. Adapted from Blomeier et al. (2013). Symbols show the main components of the sediments.

Depositional model of the Kapp Starostin strata

Bryozoans and echinoderms are the minor carbonate producing elements in the mid-ramp setting (Blomeier et al., 2011, 2013). Their carbonate production rates are significantly lower than the photozoan biota that dominate the tropical carbonate deposits of the Gipshuken Formation. This is compatible with reduced accumulation rates of cold-water carbonate ramps in comparison with high rates in tropical environments (James, 1997; Blomeier et al., 2013). The correlation of outcrop sections on Spitsbergen and results of seismic mapping on the Finnmark Platform show that limestone beds that are rich in large, little-abraded, bryozoan debris, crinoids and sponges (MFT–10) formed as isolated banks. They gradually change into spiculite and shale-dominated deposits (Malkowski and Hoffman, 1979; Fredriksen, 1988; Ehrenberg et al., 2001). Autochthonous bryozoans, echinoderms and siliceous sponges may even contribute to the formation of local build-ups in areas of favourable topography or nutrient supply around the SWWB (Ehrenberg et al., 1998).

In the study area, allochthonous bryozoan and echinoderm limestones (MFTs–10 and 11) within the Kapp Starostin strata are characterised by thinner, mud-rich beds that show minor grading. Toward deeper depositional environments these deposits are interbedded with shale and spiculitic cherts representing distal tempestites that probably formed during a sea-level fall (Fig. 2.4). The phenomenon of storm activities perturbing the mid-ramp ocean floor is in agreement with a mid-latitude location (Morton, 1981).

The thin- to medium-bedded, dark-coloured spiculitic cherts (MFT–12) with shale partings (MFT–13), which constitute the main lithology of the Kapp Starostin Formation, formed within the cold-water, low-energy conditions of the outer ramp (Fig. 2.4). The presence of glauconite suggests a low sedimentation rate, most likely below the SWWB, and the presence of burrows is indicative of aerobic conditions (Beauchamp and Baud, 2002). The occurrence of shale horizons and a lime-mud matrix might have led to the dark colour of the bedded cherts (Gates et al., 2004).

In the investigated area, the light-coloured, massive cherts (MFT–12) are succeeded by dark-coloured, bedded cherts suggesting that they have closely related depositional histories. The massive cherts contain larger spicules, a lower matrix content and more recognizable bioclasts of brachiopods, ostracods and bryozoans, which are evidence of a more energetic environment with respect to the bedded cherts (Ehrenberg et al., 2001) This unit was likely deposited on the outer mid-ramp margin around SWWB. The light-coloured nature, and the occurrence of extensive bioturbation and various biota in these deposits point to oxygenated depositional conditions.

The presence of glauconite and silica deposits specifically in the mid- to outer-ramp

microfacies is related to upwelling currents, which could have brought substantial amounts of nutrients onto the ramp (Beauchamp and Baud, 2002; Gates et al., 2004). Seasonal thawing of northern seaice sheets led to the production of dense, cold water in the deep northern Panthalassan Ocean, displacing nutrients and silica-rich water to the western and northern shelfal areas of Pangea via upwelling. This process created an environment favouring siliceous biogenic productivity (Beauchamp and Baud, 2002). Additionally, the closure of the Uralian seaway during the Kungurian caused the cutoff of the supply of warm waters of the Tethys (Blomeier et al., 2011). Changes in oceanic circulation patterns accompanied by local palaeogeographical changes during the northward movement of Pangea hence resulted in the decrease of the water temperature from warm to temperate and cold marine conditions along the western and northern margin of Pangea (Beauchamp, 1994; Stemmerik and Worsley, 1995; Reid et al., 2007; Beauchamp and Grasby, 2012).

Depositional model of the Stensiöfjellet Member

The microfacies types of the Stensiöfjellet Member grade from massive spiculitic cherts (MFT–12) at the base to distinct, green, glauconitic sandstones (MFT–14) with sporadic brachiopod limestone horizons (MFT–7) (Fig. 2.4). The well-sorted and well-rounded quartz grains indicate that the sediments have been deposited in a high-energy near-shore area. Glauconite also has been found within this member, which according to Blomeier et al. (2013) was formed by post-depositional, early diagenetic processes that occurred when deeper, quiet-water conditions of the overlying Sassendalen Group dominated the region. During latest Permian time, rapid global warming and complete melting of the northern sea ice entirely rearranged the palaeo-oceanographic setting which led to the extinction of several families of silicasecreting organisms (Wignall et al., 1998; Beauchamp and Baud, 2002).

2.6.2 Microfacies arrangement and cycle stacking pattern

Third-order cyclicity

Based on outcrop observations and the microfacies analysis, five parasequences (S0, S1, S2, S3 and S4) as components of individual systems tracts were recognized within all stratigraphic sections. A parasequence is defined as a package of beds that is deposited as a result of third-order sea-level fluctuations, probably caused by glacio-eustatic processes, with a magnitude of several tens of metres and a periodicity of 1–10 Myr (Nichols, 1999). Each parasequence reflects sedimentation from the deepest to the shallowest marine environments at the top. Marine flooding surfaces mark the boundary between parasequences (PSB) and are characterized by an abrupt

increase in relative sea level and a sudden shift from shallowest to deepest microfacies (Nichols, 1999). Therefore, the parasequence boundaries (PSB) are defined at the top of the shallowest marine unit.
Fourth- and fifth-order cycles (periodicity of 10–500 Kyr), together with high energy storms, locally affected the chert-dominated parasequences and subdivided them into a number of temporally restricted, shallowing-upward cycles (Fig. 2.5). Waves and currents set up by storms transported sediments such as single bioclastic limestones or sand grains from the inner or mid ramp towards the chert-rich outer ramp setting. These storm beds (tempestites) have limited extension and are common in the shallowing-upward sequences.

Parasequence S0: Templet Member

In S0, the microbial limestones and mudstones (MFTs–2 and 3) grade into lithoclastic rudstones and *Microcodium*-bearing sediments (MFTs–5 and 6) to form a shallowing and coarsening-upward pattern (Fig. 2.5). The occurrence of *Microcodium* and intraclasts is indicative of the prevalence of terrestrial conditions with subaerial exposure. The top of this regressive cycle represents a hiatus and is defined as the sequence boundary (SB) separating S0 from S1. The thickness of S0 varies between ~2 m in section Kapp Fleur de Lys to ~20 m in section Tålmodryggen.

Parasequence S1: Vøringen Member

Above the sequence boundary (SB), a claystone horizon (MFT–13) forms the base of S1 in section Idodalen. We assume it is also present in section Kapp Fleur de Lys, but it was not observed there due to limited exposure. The claystone represents a substantial relative rise in sea level and reflects a period with sediment-starved conditions in a deep-marine setting (Fig. 2.5).
In section Tålmodryggen, the presence of extraclasts (MFT–6) at the base of S1 indicates that erosion took place as a result of high wave energy in the shallow-water environment. We suggest that this occurred during the onset of a transgression, flooding the land surface and reworking earlier deposits. Therefore, in this section, the Templet Member (S0) is separated from the overlying Vøringen Member (S1) by a disconformity (SB). At the other localities, this surface (SB) is marked by subaerial exposure and a paraconformity related to non-deposition instead of the erosional surface.
The shallowing-upward trend in S1 is characterized by the successive deposition of coarse-grained, silicified, bioclastic limestones (MFTs–7, 8 and 9). The occurrence of fine-grained, bioclastic limestones at the top of this succession records a renewed deepening of the depositional setting at the transition towards the overlying sequence. In all measured sections the thickness of S1 is ~7.5 m.

Parasequence S2

S2 in the Kapp Starostin Formation records a deepening in a cold-water setting, which is inferred from the occurrence of widespread, bedded cherts with shale partings (MFTs–12 and 13; Fig. 2.5). These basal sediments pass over into massive cherts and, to a lesser extent, into heterozoan carbonates (MFTs–10 and 11) with an outer mid-ramp signature. S2 is the thickest cycle ranging from 71 m in section Kapp Fleur de Lys to 37 m in section Tålmodryggen.

Parasequences S3and S4

The third and fourth shoaling-upward parasequences show a similar microfacies arrangement (Fig. 2.5). In S3, the basal deep-water microfacies comprising clay horizons and chert units shift progressively to shallower microfacies, bryozoan and echinoderm limestones (MFT–10 and 11). The top of S4 is only exposed in section Kapp Fleur de Lys (Stensiöfjellet Member) in which cherts are overlain by brachiopod limestones and glauconitic sandstones (MFTs–7 and 14). The succession in S4 reveals a decrease in sea level and an overall shallowing of the depositional area from an outer- to an inner-ramp setting.

The thickness of S3 varies between 12 m in section Idodalen and 34 m in section Tålmodryggen. S4 displays thickness variations ranging from 20 m (section Tålmodryggen) to 30 m (section Kapp Fleur de Lys).

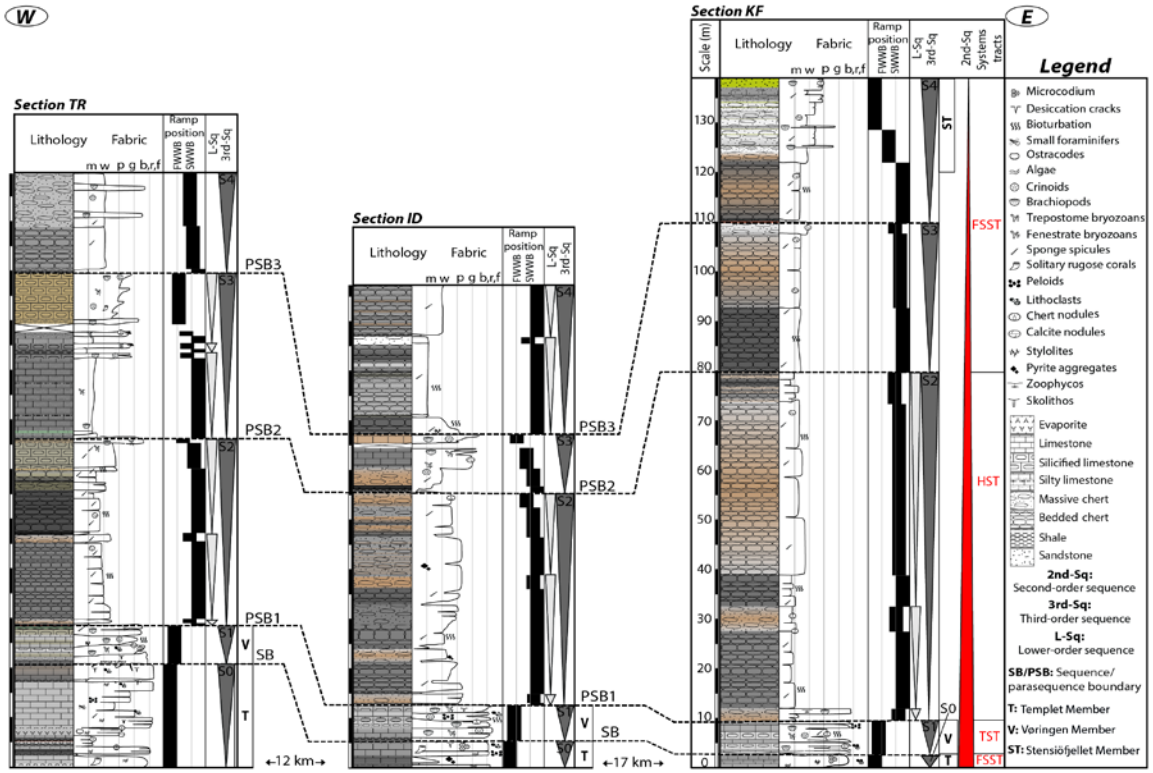

Fig. 2.5 Simplified section correlation (Tålmodryggen (TR), Idodalen (ID), Kapp Fleur de Lys (KF); Fig. 2.1 for section locations), showing thickness, main lithology and fossils, depositional environments, second-order (red cone), third-order (parasequences; dark-grey cones) and lower-order (light-grey cones) depositional cycles and systems tracts. Colours represent bedrock colours. Symbols show the main components of the sediments. Fabric classification for carbonates: m=mudstone; w=wackestone; p=packstone; g=grainstone; b, r, f = bindstone, rud-, floatstone. The dashed lines represent sequence and parasequence boundaries

Second-order cyclicity

The overall Permian succession represents a second-order cycle, with a duration exceeding 16 Myr. It can be subdivided into several systems tracts (Fig. 2.5). An overall shoaling trend approaching the Permo–Triassic boundary is reflected by systematic changes in cycle thickness (thinning up), and by changes in the proportion of outer-ramp and inner-ramp microfacies (the latter increases) of the individual parasequences when moving upwards in the succession. This finding is in line with the global sea-level curve compiled by Haq and Schutter (2008) which displays a general shallowing trend during the Late Permian.

Falling stage systems tract (FSST)

The first falling stage systems tract comprises the strata of S0 with the upper subaerial sequence boundary (SB) marking the lowest position in relative sea level in the study area. The shoaling-upward trend reflects a reduction in the creation of accommodation space relative to sediment supply, resulting from a forced regression or a sea-level fall (Nichols, 1999).

Transgressive systems tract (TST)

S1 represents the stratigraphic succession between the lower sequence boundary (SB) and the maximum flooding surface (shale) and is interpreted as a component of the transgressive systems tract (Fig. 2.5). The coarse-grained, bioclastic limestones show an upward deepening into fine-grained, bioclastic limestones indicative of a retrogradational pattern. The depositional trends indicate that the creation of accommodation space during transgressions out-paced sediment supply.

Highstand systems tract (HST)

The maximum flooding surface (black shale) separates carbonate-dominated, inner ramp deposits of the Vøringen Member (S1) from the deep-water spiculitic cherts of the Kapp Starostin Formation (S2) (Fig. 2.5). It reflects the termination of shallow-marine sedimentation and sediment starvation on the outer part of the ramp system. Deposition beyond the maximum flooding surface, S2, is considered to be part of the highstand systems tract. During the long-lived, highstand systems tract, the rate of sea-level rise slowed down, and cold, silica-rich, deeper waters were brought in via upwelling and created an environment favouring extensive biogenic silica production. The sedimentary succession shows an aggradational to slightly progradational pattern which is reflected by a shift from bedded to massive cherts and, to a lesser extent, to bioclastic limestones.

Falling stage systems tract (FSST)

The second falling stage systems tract is made up of S3 and S4 that record a higher portion of shallow-water microfacies (carbonates and sandstones) with respect to the parasequence below. Hence, these parasequences show a trend of becoming shallower up through the succession. The deposits indicate that the shoreline has moved seawards at the transition to the sediments of the Triassic Sassendalen Group when, during the latest Permian, the climatic conditions changed dramatically leading to a drop in sea level (Haq and Schutter, 2008).

2.6.3 Correlation in central Spitsbergen

The Spitsbergen cross-section, correlating three sections, is oriented west-east and covers the proximal and distal part of the Permian ramp system (Fig. 2.5). A proximal setting is situated in the west of the cross-section, in section Tålmodryggen. This setting is marked by (i) the presence of shallower microfacies such as the sabkha evaporates that occur in the Templet Member (S0), (ii) the extraclasts and sandy deposits in the Vøringen Member (S1), and (iii) the higher portion of limestones in the Kapp Starostin Formation (S2, S3 and S4). Section Tålmodryggen is located on the Nordfjorden High, which was a persistent positive feature (horst block) during the Carboniferous–Permian. This also explains why the sedimentary successions record shallower-water conditions in comparison with other sections (Steel and Worsley, 1984; Ehrenberg et al., 2001). During the deposition of the Kapp Starostin strata (S2, S3 and S4), the main depocentre was located near section Kapp Fleur de Lys that contains a thick succession of deep-water microfacies such as bedded cherts (MFT–12).

In all studied sections in central Spitsbergen, the dominance of bedded cherts in the Kapp Starostin Formation (S2, S3 and S4) suggests that the environment was one of low hydrodynamic energy. However, the presence of wave-generated sedimentary structures indicates periodic disturbances by storms.

2.6.4 Correlation with other sections on Svalbard

The analysed outcrop sections are compared with sections (i) described by Ehrenberg et al. (2001), who worked in southwestern (at Akseløya; section AK) and central Spitsbergen (at Dickson Land, section D–L), and (ii) those of Blomeier et al. (2013) who documented four sections in northeast Svalbard (sections E, H, S and Z) (Fig. 2.6). On Spitsbergen and northeastern Svalbard, Ehrenberg et al. (2001) and Blomeier et al. (2013) reported that the successions of the Kapp Starostin Formation were deposited as a result of third-order sea-level fluctuations. They stated that the overall stacking pattern is characterised by long-term regression, which can be interpreted as a

second-order cycle. These findings are in line with the results of the present study.

S0

In central Spitsbergen, the Templet Member (S0) comprises photozoan elements and some evaporates indicating arid and tropical conditions. At the same time, a minor part of the sedimentary record in northeast Svalbard is marked by heterozoan elements. The majority of the carbonate deposits, however, are characterised by a photozoan biotic assemblage. Such a mix of biota is also known from tropical environments of Mauritania, Panama and the Galapagos Islands (Michel et al., 2011; Reijmer et al., 2012; Reymond et al., 2016). The higher siliciclastic input observed in northeast Svalbard results from the uplift of a terrestrial source area as well as an increased runoff rich in dissolved silica, due to more humid subtropical environments (Blomeier et al., 2011).

S1

The transgression that flooded the ramp during the Artinskian covered the entire Svalbard region (SW to NE). The Vøringen Member (S1) that is present in all sections shows that the whole area was covered by carbonates with a predominance of heterozoan biotic assemblages (Fig. 2.6). Blomeier et al. (2011, 2013) stated that at the base of the Vøringen Member in northeast Svalbard, in situ bryozoan build-ups occurred on the hardgrounds and the condensed surface substrate. The bryozoans do not occur in the Vøringen Member in central and southwestern Spitsbergen. Instead, brachiopod fragments are present in the basal beds. The deeper environment of northeast Svalbard during this time interval (S1) can be explained by a local higher subsidence rate, which possibly linked to the reactivation of the Carboniferous Lomfjorden trough, a smaller graben east of the Lomfjorden–Agardhbukta Fault Zone (Blomeier et al., 2009).

S2, S3, S4

The deepening trend recorded in the Kapp Starostin succession is characterised by spiculitic cherts, which occur in the whole area (S2, S3 and S4) (Fig. 2.6). In northeast Svalbard and on the Finnmark Platform (Norwegian Barents Sea), occurrences of whole sponges have been reported from the outer-ramp to the outer-mid ramp boundary (Ehrenberg et al., 2001; Blomeier et al., 2013). In northeast Svalbard, the presence of massive cherts, as the main lithology, mixed with shallow-water sandstones and limestones strongly suggests a shoreward transport of spiculitic sediment by wave action and periodic storm events.

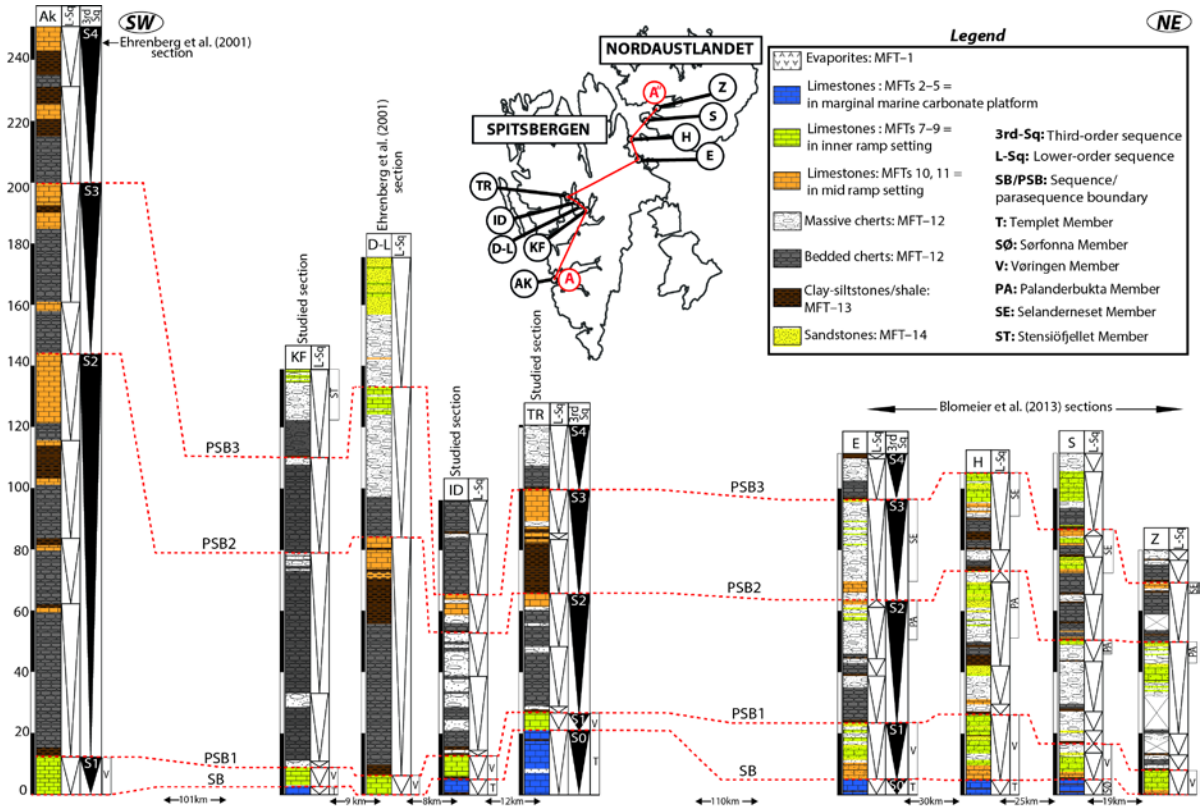

Fig. 2.6 Simplified correlation of the sections located in central (sections TR, ID, D–L and KF) and SW (section AK) Spitsbergen, and NE Svalbard (sections E, H, S and Z). A–A" on the outline map of Svalbard indicates the cross-section used for correlation. Lithologies correspond to the main microfacies, which are assigned to specific depositional settings. Third-order cycles (black cones) are subdivided into a number of shallowing-upward cycles (lower-order cycle; white cones). The dashed lines represent sequence and parasequence boundaries.

In southwestern and central Spitsbergen, dark-coloured, bedded cherts are the dominant microfacies (S2, S3 and S4), resulting in low accumulation rates in the distal and deeper ramp zones. Shallow-water limestone (brachiopod-rich) intervals and sandstones in northeast Svalbard correlate with deep-water limestones (bryozoan and echinoderm-rich) or massive cherts in southwestern and central Spitsbergen. However, the presence of finegrained, clastic sediments in the southwest could be related to erosion of the Sørkapp–Hornsund High, which remained exposed until the end of the Permian (Dallmann et al., 1999).

The sequence-stratigraphic model (Fig. 2.6) shows that the Templet (S0) and Vøringen (S1) members reflect deep-water sedimentation in northeast Svalbard. During the deposition of the Kapp Starostin Formation (S2, S3 and S4), the main sediment depocentre was located in the southwest of Spitsbergen (at Akseløya) which is suggested by the thicker parasequences and the higher proportion of deeper microfacies (e.g., bedded cherts). At the same time, NE Svalbard was located in the most proximal setting, as shown by the thinner sequence and shallower microfacies, e.g., more sandstones and bioclastic limestones. The microfacies distribution patterns show an inclination of the ramp towards the southwest (Fig. 2.6). The Permian is characterised by a period of tectonic quiescence on Svalbard (Steel and Worsley, 1984; Dallmann et al., 1999). The local differences in accommodation space and facies may be linked to the older, pre-existing, structural elements, inherited from the reactivation of the main tectonic lineaments throughout the Carboniferous (Ehrenberg et al., 2001; Blomeier et al., 2013).

From northeast to southwest Svalbard, some of the smaller-scale, lower-order cycles within the individual parasequences become amalgamated (Fig. 2.6). The seaward pinch-out of shallower intervals including single limestone beds and sandstones or the temporary change from bedded into massive cherts, resulted in a decrease in the number of shallowing-upward cycles. The lateral facies distribution indicates an increase in hydrodynamic energy with shallowing water depths across the more subdued relief ramp environment.

2.6.5 Comparison with other time and facies equivalent systems on Arctic and sub-Arctic parts of the Northern Hemisphere

Templet Member

The cold-water carbonates of the lower part of unit L–8 in the Finnmark Platform and heterozoan carbonates with minor photozoan elements of the Great Bear Cape Formation in the Sverdrup Basin (Arctic Canada), are known as offshore equivalents of the Templet Member on Spitsbergen (Larssen et al., 2002; Bensing et al., 2008). The variations in the distribution of the biota

(heterozoan and photozoan) indicate that subtropical and cooler climatic conditions were dominant in the deeper depositional areas of the Pangaean shelf. This depositional setting is characterised by the absence of light and the presence of cold, nutrient-rich water related to upwelling leading to the shutdown of the photozoan carbonate producers. In contrast, warm and tropical climatic conditions, represented by the photozoan association, prevailed over structural highs such as the Fafner succession on the Loppa High (SW Barents Sea; Ahlborn et al., 2014) and along the margins of the Franklinian shelf like Spitsbergen.

The Late Sakmarian–Early Artinskian uplift along the shelf margin and over structural highs led to subaerial exposure and karstification at the top of the Fafner and Gipshuken formations indicating a very proximal setting during the sea-level fall (Groen, 2010; Ahlborn et al., 2014). Contemporaneously, a period of non-deposition and sea-floor exposure is indicated by the occurrence of silty shale with pyrite cementation and a glauconite-enriched surface within the Finnmark Platform (Ehrenberg et al., 2001; Stemmerik and Worsley, 2005). Towards the Nordkapp Basin, sediments consist mainly of cool-water carbonates and bryozoan build-ups.

Vøringen and Kapp Starostin strata

During the Mid/Late Artinskian, a major transgression flooded the shelf margins and structural highs resulting in the deposition of extensive carbonates along the northern margin of Pangea (Steel and Worsley, 1984; Blomeier et al., 2011). The upper parts of unit L–8 (Isbjørn Formation) of the Finnmark Platform and the Great Bear Cape Formation within the Sverdrup Basin are considered to correlate with the Vøringen Member on Spitsbergen (Stemmerik and Worsley, 2005). They are characterised by crinoid, bryozoan and brachiopod-rich limestones deposited in inner-shelf environments. However, in the Sverdrup Basin, elements of the subtropical biota such as fusulinids and colonial corals are present in the shallowest near-shore microfacies (Larssen et al., 2002; Reid et al., 2007). In this locality, evidence of subaerial exposure at the top of the Great Bear Cape Formation and succeeding deltaic deposits of the Sabine Bay Formation might relate to compressional tectonic events during the Kungurian–Melvillian. This tectonic activity caused uplift of the Sverdrup basin margins (Reid et al., 2007). During the remainder of Permian time, the Sverdrup Basin records the onset of passive subsidence, except for a localised uplift of the Tanquary High in the northeast (Reid et al., 2007; Bensing et al., 2008).

On the Finnmark Platform, an unconformity or subaerial exposure surface is also recorded on the topmost part of unit L–8 just below the overlying unit L–9 (Stemmerik and Worsley, 2005; Rafaelsen et al., 2008). This uplift was linked

to the Kungurian tectonic event in the western Barents Sea resulting from the rejuvenation of older lineaments (Stemmerik and Worsley, 2005; Ahlborn et al., 2014). However, on Svalbard, the transition between the Vøringen Member and the overlying Kapp Starostin Formation is conformable.

A deepening of the basin and cold-water climatic conditions during deposition of the spiculitic cherts of the Kapp Starostin Formation have also been recorded in the Lindstrom Formation situated at the margin of Sverdrup Basin and in unit L–9 in the Finnmark Platform (Gates et al., 2004). In the Lindstrom Formation, light-coloured, massive cherts are marked by large spicules and cold-water carbonate biofragments, which show hummocky cross-stratification. These sediments were deposited in an outer- to inner-ramp setting (Gates et al., 2004). An overall increase in spicule size with decreasing bathymetry suggests shoreward transport of spicules during periodic storm events. The presence of concavedown brachiopods along bedding planes suggests hydrodynamic sorting and sediment transport (Gates et al., 2004). Accordingly, Late Permian spiculites in the Sverdrup Basin accumulated in shallower depths than those in central Spitsbergen, which can be interpreted either as a general stormier setting or might be due to a low-relief ramp-type morphology with restricted biological diversity (Gates et al., 2004). Similarly, on the Finnmark Platform, larger spicules, a reduced matrix, and the presence of vuggy fractures in light-coloured spiculites (upper cycle of unit L–9) reflect a higherenergy environment than those recorded in Spitsbergen (Ehrenberg et al., 2001; Seidler et al., 2004; Stemmerik and Worsley, 2005). A secondary porosity present might have developed during the break at the Permian–Triassic transition as a result of rifting events in the Norwegian– Greenland Sea area (Ehrenberg et al., 2001; Seidler et al., 2004; Stemmerik and Worsley, 2005).

2.7 Conclusions

The Templet Member and the Kapp Starostin Formation on Spitsbergen accumulated during a time of prolonged sea-level fall (second-order) and oceanic cooling. The sedimentary successions can be subdivided into a series of systems tracts and third-order sea-level cycles (five parasequences):

S0 (Templet Member): At the marginal marine environment, algal limestones and mudstones grade into lithoclastic rudstones and *Microcodium*-bearing sediments suggesting periods of subaerial exposure. The top of this regressive cycle represents a hiatus and is defined as the sequence boundary (SB). This parasequence is a component of the falling stage systems tract.

S1 (Vøringen Member): At an inner to proximal mid-ramp setting, storm-influenced, silicified brachiopod limestones occur showing an upward deepening into fine-grained, heterozoan limestones during transgression. This parasequence represents a transgressive systems tract.

S2, S3 and S4 (Kapp Starostin Formation): These parasequences are predominantly characterised by widespread spiculitic cherts deposited in an outer-ramp setting. These deep-water deposits shift up-section increasingly into bioclastic limestones and sandstones, which represent a highstand systems tract (S2) and falling stage systems tract (S3 and S4).

The correlation of the sections in central Spitsbergen indicates that the proximal areas of the ramp setting are located in the west. The main sediment depocentre is situated in the region near section Kapp Fleur de Lys in the east and is characterized by a thick succession of deep-water bedded cherts.

The stratigraphic correlation along different locations in Svalbard shows that during the deposition of the Templet and Vøringen members, northeast Svalbard recorded deeper-water microfacies than in central Spitsbergen. This can be explained by high local subsidence rates related to the reactivation of Carboniferous structural elements. During the latest Permian, the main sediment depocentre was located in the southwest of Spitsbergen at Akseløya, which displays thicker parasequences and a higher proportion of bedded cherts than at other locations. These deposits are slightly shallower towards central Spitsbergen, and display a significant shallowing towards northeastern Svalbard.

2.8 Acknowledgements

We acknowledge the Vrije Universiteit Amsterdam, Bremen University and the Norwegian Polar Institute for their financial support. We thank MSc. students Mahtab Mozafari and Jan Schneider of the Vrije Universiteit Amsterdam for their contributions; and Bouke Lacet and Wynanda Koot for preparing the thin-sections and plugs at the Vrije Universiteit Amsterdam. We thank the College of Petroleum Engineering and Geosciences for their support during the final stages of the manuscript. Finally, an anonymous reviewer and NJG editor Trond Slagstad (Geological Survey of Norway) are thanked for their very constructive comments and suggestions that significantly improved the paper. This is CPG – Carbonate Sedimentology Group – contribution no. 4.

Chapter 3

Rock properties of a Carboniferous-Permian mixed carbonate and non-carbonate depositional system

E. Jafarian
L. M. Kleipool
C. Scheibner
D.P.G. Blomeier
J.J.G. Reijmer

Chapter based on: (2017) Variations in petrophysical properties of Upper Palaeozoic mixed carbonate and non-carbonate deposits, Spitsbergen, Svalbard Archipelago. Journal of Petroleum Geology 40, 59-83.

3.1 Abstract

The Late Carboniferous – Early Permian Gipsdalen Group and the Early to Late Permian Templefjorden Group are known hydrocarbon plays in the Arctic region, e.g. on the Finnmark Platform, Loppa High and Sverdrup Basin. Time-equivalent deposits crop out on the island of Spitsbergen and consist of mixed carbonate and non-carbonate (primarily siliciclastic, siliceous, organic-carbon rich and clayey) sediments deposited in continental to deep-marine settings.
In rock samples (n = 73) collected from five outcrop locations on Spitsbergen, thin-section analysis showed the presence of ten microfacies types ranging from claystones and spiculitic cherts to rudstones and dolostones. Petrophysical and textural properties of the samples were measured to evaluate the link with the acoustic (P- and S-wave) velocities of these generally tight rocks, which have an average porosity of about 2%.
Variations in acoustic velocity measurements primarily depend on variations in mineralogical composition (silica versus carbonate) and, to a lesser extent, on variations in porosity and bulk density. Pore networks in the sediments are dominated by microporosity and (micro-) cracks, followed by interparticle porosity. Recrystallization effects and pore shape variations show a lesser effect on the P-wave velocity. Clay content does not exceed 12.7% and also has a secondary impact on the acoustic velocities.
Defining which textural and physical parameters control the acoustic properties of these carbonate and non-carbonate sedimentary rocks will help with the interpretation of the seismic response of equivalent deposits in the subsurface.

3.2 Introduction

Establishing a reliable correlation between acoustic velocities and other petrophysical parameters such as porosity or lithology is critical for identifying the origin of seismic reflections (Anselmetti and Eberli, 1993). A number of properties control seismic velocities and elastic moduli in sedimentary rocks including mineralogy, pore-network geometry, the shape and spatial arrangement of grains and crystals, pore-filling fluid composition, and pore and confining pressures (Wang, 2001; Fournier and Borgomano, 2009). Early studies of the acoustic properties of sedimentary rocks concentrated on siliciclastic sediments because of their importance in petroleum exploration (Christensen and Szymanski, 1991; Vernik and Nur, 1992). Research on the petrophysical properties of carbonate rocks has been limited by comparison,

because carbonates have a wide range of facies, porosity and fabrics (Kenter et al., 2007).

Velocity transforms, e.g. the Wyllie et al. (1956) time-average equation and the Raymer et al. (1980) and Gardner et al. (1974) empirical relations, have been applied for the prediction of porosity, density and lithology from acoustic velocity in both siliciclastic and carbonate rocks (Kenter et al., 1997b). In carbonate systems, diagenetic processes considerably alter the pore network and the mineralogy of the primary sediments, thus affecting their elastic properties. These processes among others are responsible for the wide scatter of values in velocity–porosity transforms in carbonate rocks (Anselmetti and Eberli, 1993).

This study focuses on Upper Palaeozoic sedimentary rocks from Spitsbergen (NW Barents Sea, Arctic Norway: Fig. 3.1), namely: the Gipsdalen Group (Early Carboniferous to Early Permian), which comprises shallow-marine carbonates to continental deposits; and the overlying Tempelfjorden Group (Early to Late Permian), which includes shallow- to deep-marine silicified carbonates and cherts. Late Palaeozoic carbonates and siliceous deposits are reservoir rocks for hydrocarbons at the Gohta and Alta fields on the Loppa High in the western Barents Sea (e.g. Lerch et al., 2016). Mesozoic and Palaeozoic bitumen-stained sediments in Central Spitsbergen have been tested for hydrocarbon flows and migration (Elvevold, 2015; Abay et al., 2017). Similar reservoir rock facies are present in the Sverdrup Basin (Canadian Arctic) and the Permian Basin of West Texas (Saller et al., 1991; Ruppel and Hovorka, 1995; Montgomery, 1998). Since subsurface data for these hydrocarbon reservoir rocks are scarce, a series of outcrop analogues on Spitsbergen were selected for investigation. The study of these continuous exposures will help to understand bed-scale heterogeneities and the spatial distribution of textural and petrophysical properties.

The objective of this paper is to relate the acoustic properties of the mixed carbonate and non-carbonate deposits studied to petrophysical and textural parameters. The following methods were used: outcrop observations combined with plug and thin-section analyses; studies of mineralogical composition, grain size and grain distribution; analysis of density/porosity; and acoustic velocity measurements at various effective pressures. The results are compared with data from time- and facies-equivalent reservoir rocks. The study is intended to help determine the reservoir potential and petroleum geological significance of mixed (carbonate and non-carbonate) reservoir successions.

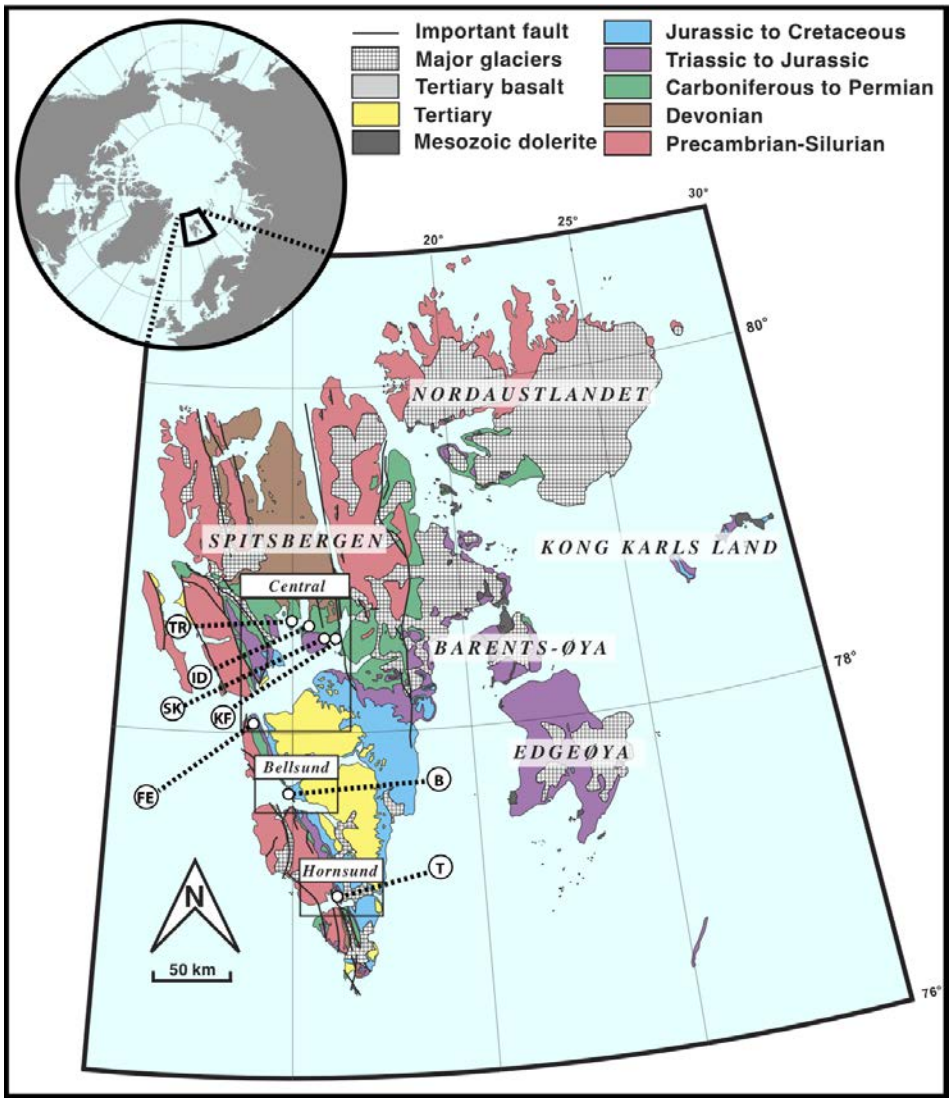

Fig. 3.1 Geological map of the Svalbard archipelago. Strata investigated for this study are of Carboniferous and Permian ages, indicated by the green-shaded areas on the map and in the legend. Black box in upper-left map shows the regional location of the study area. Measured outcrop sections indicated on the main map are: Tålmodryggen (TR); Idodalen (ID); Skansen (SK); Kapp Fleur de Lys (KF); Festningen (FE); Wordiekammen (B); and Treskelodden (T). Modified from http://npolar.no/geonet/itemsgeneral/frame.html.

3.3 Regional setting and lithostratigraphy

Spitsbergen is the largest island in the Svalbard archipelago and is located between 74° and 81°N and 10° and 35°E in the NW Barents Shelf (Fig. 3.1). During the Late Palaeozoic, the Svalbard archipelago was part of an epicontinental shelf at the northern margin of Pangea. The shelf was divided into a series of intracratonic platforms and basins which are exposed at the present day in different circum-Arctic areas such as the Barents Sea (Finnmark Platform, Stappen High), eastern North Greenland (Wandel Sea Basin), Arctic Canada (Sverdrup Basin) and Russia (Timan–Pechora Basin) (Scotese and Langford, 1995; Golonka, 2002).

The Pangea margin moved from approximately 25°N in the Late Carboniferous to around 45°N in the Late Permian (Steel and Worsley, 1984; Scotese and Langford, 1995; Golonka, 2002). The Upper Palaeozoic sedimentary succession of the Svalbard archipelago consists of the Gipsdalen and Tempelfjorden Groups, which have a cumulative thickness of 250-300m in the studied area (Fig. 3.2). In the Gipsdalen Group, the Wordiekammen Formation (lower Moscovian – Sakmarian) is dominated by bioclastic limestones and siliciclastic sediments deposited in open to semi-restricted, shallow subtidal and restricted intertidal to supratidal settings (Blomeier et al., 2009). These sediments are overlain by evaporites and carbonates of the Gipshuken Formation (Blomeier et al., 2009) (Fig. 3.2).

A lateral equivalent of the Wordiekammen Formation, the Treskelodden Formation (Kasimovian – Artinskian) (Fig. 3.2), is divided into two intervals: a siliciclastic-dominated lower interval, which is followed by a cyclic succession of siliciclastic and carbonate rocks dominated by coral horizons (Birkenmajer, 1964). A grey conglomerate marks the boundary between the two intervals. The formation is overlain by the silicified, sandy fossiliferous limestones to skeletal sandstones of the Vøringen Member (Fig. 3.2). The sediments of the Treskelodden Formation were deposited in shallow-marine to lagoonal and alluvial environments, except for the lower alluvial cycle (Birkenmajer, 1984).

The Gipshuken Formation (Sakmarian – Artinskian) is exposed at outcrops throughout Spitsbergen except for the Sørkapp Hornsund High (Fig. 3.2), and is characterized by stacked evaporite/carbonate cycles and carbonate breccias deposited in a warm, semi-arid to arid peritidal environment. The Templet Member forms the uppermost interval of the Gipshuken Formation and shows a decrease in evaporates upwards; however, algal limestones, carbonate breccias and *Microcodium* facies become more abundant, suggesting deposition in a restricted peritidal platform and supratidal sabkha setting (Dallmann et al., 1999; Blomeier et al., 2011).

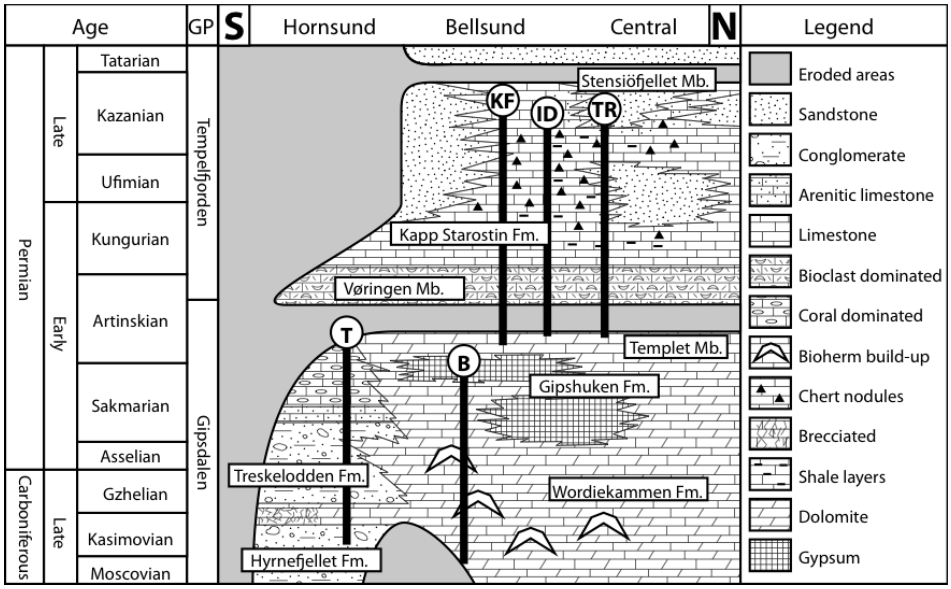

Fig. 3.2 Chronostratigraphic framework and main lithologies in the Late Carboniferous and Permian succession of Svalbard (adapted from Dallmann et al., 1999) with a schematic overview of the stratigraphic positions of the investigated sections and formations. Sections indicated are: Treskelodden (T); Wordiekammen (B); Kapp Fleur de Lys (KF); Idodalen (ID); and Tålmodryggen (TR).

Evidence of subaerial exposure, karstification and collapse of the elevated Gipshuken platform has been recorded in the Early Permian (Sakmarian – Artinskian) indicating a marine regression (Blomeier et al., 2013) (Fig. 3.2). Maximum regression occurred in the Artinskian, resulting in a distinct unconformity that separates the uppermost deposits of the Gipsdalen Group from the lowermost deposits of the overlying Tempelfjorden Group. This hiatus is present throughout Svalbard (Blomeier et al., 2011) and corresponds to a time interval of 1 to 15 Ma according to Ehrenberg et al. (2001).

The boundary between the Gipsdalen and Tempelfjorden Groups is marked by an abrupt facies change and disconformity (or locally a correlative conformity), which resulted from karstification and subsequent reworking of sediments during a widespread transgression in the late Artinskian (Ehrenberg et al., 2001; Blomeier et al., 2011) (Fig. 3.2). The Tempelfjorden Group contains siliceous sponges, brachiopods, bryozoans and crinoids which indicate temperate- to cool-water conditions. At the base of the Group is the Vøringen Member (late Artinskian – early Kungurian), the lowermost part of the Kapp Starostin Formation (late Artinskian – Kazanian / earliest Tatarian), which occurs throughout the Svalbard area. The member comprises coarse-grained silicified, sandy bioclastic limestones to skeletal sandstones

interpreted as shoreface deposits which accumulated on a transgressive, stable marine shelf (Dallmann et al., 1999; Blomeier et al., 2011, 2013). Sediments overlying the Vøringen Member include shales and dark to light-coloured chert horizons at the base, which pass upwards into glauconitic sandstones and silicified, bioclastic limestones (Groen, 2010; Blomeier et al., 2011). These sediments were deposited in a shoreface to deeper storm-dominated, mixed siliceous– carbonate ramp setting (Ehrenberg et al., 2001; Blomeier et al., 2011). The majority of the lithologies are silicified because of the presence of abundant siliceous sponge debris (Groen, 2010).

The uppermost interval of the Kapp Starostin Formation, the Stensiöfjellet Member, is exposed at outcrop in NW and central Spitsbergen, and is characterized by interbedded shallow-marine glauconitic sandstones and spiculitic cherts (Dallmann et al., 1999; Blomeier et al., 2011). The boundary between the Tempelfjorden Group and the overlying Sassendalen Group (Early to Middle Triassic) is sharp and is marked by the abrupt onset of a monotonous succession of dark shales and silt- to sandstones. The base of the Sassendalen Group is characterized by the absence of bioclasts as a result of the Permian-Triassic extinction (Ehrenberg et al., 2001; Blomeier et al., 2011, 2013). However, the stratigraphic location of the Permian/Triassic boundary is still uncertain (Dallmann et al., 1999; Blomeier et al., 2011, 2013).

3.4 Materials and methods

3.4.1 Outcrop studies

During two fieldwork seasons on Spitsbergen, the Carboniferous – Permian successions were described, sampled and logged at five locations (B, T, KF, ID and TR: Fig. 3.1). Data from these sections were complemented by observations from the type-section of the Kapp Starostin Formation at Festningen and with data from Skansen (FE and SK: Fig. 3.1) (Blomeier et al., 2011, 2013).

Two of the sections are located in west and south Spitsbergen (Fig. 3.1): (i) the Bellsund section (section B), which comprises the upper part of the Wordiekammen Formation; and (ii) the Treskelodden section (section T) in the Hornsund area, where the Treskelodden Formation is exposed. A third section (section KF) is located at Kapp Fleur de Lys on the western coast of Billefjorden (Dickson Land). The fourth section studied (section ID) is located at Idodalen, on the eastern coast of Dicksonfjorden. A fifth section (section TR) was measured at Tålmodryggen, on the western coast of Dicksonfjorden (James I Land). The last three sections in central Spitsbergen include the

uppermost part of the Gipshuken Formation and the overlying Kapp Starostin Formation (Fig. 3.2).

3.4.2 Sampling

During the fieldwork, 73 samples were collected (Fig. 3.3) for velocity measurements and associated geochemical and sedimentological analyses. The selected samples cover the entire range of lithofacies (based on colour and lithology) observed in the outcrops. The following samples (n = 39) were obtained from the Gipshuken and Kapp Starostin Formations: Idodalen (ID; n = 8), Kapp Fleur de Lys (KF; n =10), Tålmodryggen (TR; n = 12), Skansen (SK; western coast of Billefjorden; n = 4) and Festningen (FE; Outer Isfjorden; n = 5). Additional samples (n = 34) were selected from the Wordiekammen (Section B; n = 16) and Treskelodden (Section T; n = 18) Formations.

3.4.3 Thermo Gravimetric Analysis (TGA)

TGA was used to define the compositions of the rock samples, and to estimate the total organic carbon (TOC) content, and the carbonate content and residue based on weight loss during heating (Dean, 1974; Earnest, 1988). Sample preparation consisted of grinding the samples to a powder which was subsequently dried in an oven at 60°C for 72 hours; two grams of sample was then loaded into heat-resistant crucibles. In total, 73 samples were measured by TGA on a LECO TGA701 apparatus which measures weight loss during a stepwise heating procedure from 25°C to 1000°C over four hours (Kleipool et al., 2015). The temperature was increased from 25°C to 105°C in an air-filled atmosphere in order to evaporate moisture present, and the residual dry mass was measured and used as a reference weight. Then the temperature was raised to 330°C in a pure oxygen atmosphere to determine the mass fraction of readily oxidizing organic material. The same step was repeated at 550°C. Subsequently the temperature was quickly raised to 615°C in a pure CO2 atmosphere to detect the release of crystallization water or OH-groups present within minerals in the sample material. In a final step, the temperature was raised to 1000°C in a pure CO2 atmosphere to determine the total mass fraction of CaCO3. At each step a constant temperature was maintained until no weight-loss deviations greater than 0.5% were detected. Based on the results of the thermogravimetric analyses, the samples were divided into four groups: non-carbonate sediments (0 20% carbonate); carbonates (80-100% carbonate); mixed lithofacies (20-80% carbonate); and dolostones.

3.4.4 Microfacies analyses

Using thin-section analyses, the four lithofacies types defined by TGA were divided into ten microfacies types based on their lithology, texture, grain size and grain components, and consequently on their depositional environments

(Table 3.1). The siliciclastics and silica-dominated sediments of the mixed group (< 50% carbonate) were categorized according to grain size. Pure carbonates and carbonate-rich sediments (> 50% carbonate) in the mixed group were classified according to Dunham (1962) (Table 3.1).

3.4.5 Fractures and pores

Additional geomechanical information was obtained from plugs and thin sections (Table 3.2). The densities of opened and closed fractures were evaluated and categorised into four classes defined by the number of fractures per unit length (5 cm), namely: none (0 fractures), minimum (0-2 fractures), medium (2-4 fractures) and maximum (> 5 fractures) (see Fig. 3.9).
The pore classification of the samples was based on Xu and Payne (2009) who recognized three general types of pores: (micro-) cracks or elongated pores; interparticle pores ("reference" pores); and moulds or rounded pores. A pore type frequency was assigned to each sample ranging from 0 = absent to 3 = frequent (Table 3.2).

3.4.6 Grain size analysis

A Sympatec HELOS/KR instrument with QUIXEL wet dispersing system was used to determine the grain size distribution of the non-dissolved nonorganic grains. After minor crushing of the samples, hydrogen peroxide (H2O2) was used to remove the organic carbon, and hydrochloric acid (HCl) was used to dissolve the carbonate material present. The diluted samples were slightly heated to accelerate the chemical process. Tetrasodium pyrophosphate decahydrate (Na4P2O7.10H2O) and sodium dithionite (Na2S2O4) were added when rinsing the samples with deionized water. These procedures ensured that only the nonorganic fraction remained for grain size analysis. A sonic bath was used to break up clay-sized particles and non-carbonate cements such as phosphate, pyrite and glauconite. The resulting volume percentage measurements were categorized into the following frequency classes according to the Udden-Wentworth grain-size scale (Wentworth, 1922; McCave et al., 1986; Loizeau et al., 1994): clay (< 8 μm), silt (8–63 μm) and sand (> 63-2000 μm). The clay content of samples with a carbonate content below 7% was obtained by visual assessment of thin sections.

3.4.7 Petrophysical analysis

Acoustic velocity, porosity and density were measured on 73 samples. For these measurements, cylindrical plugs were prepared using a water-cooled 1.5-inch diamond drill. The plugs were dried in an oven at 60C° for at least 72 hours. Plug ends were ground flat and paralleled to within 0.01mm. After sample preparation, plug dimensions and the dry weight of the plugs were measured to calculate the dry bulk density. The grain density was calculated

from the weight and volume, and was determined by a helium pycnometer (Micromeritics AccuPyc 1330). The pycnometer measures the dry grain density. The total porosity was calculated from the dry bulk density and grain density.

Compressional (P-wave) and shear wave (S wave) velocities were measured in dry conditions on plugs in the Petrophysical Laboratory (VU University Amsterdam) in the High-Pressure Measurement System (HPMS) developed by Verde Geoscience. The device measures the propagation time of one compressional signal (P-wave) and two orthogonalpolarized shear waves (S1-wave and S2-wave) along the plug axis. The acoustic velocities were calculated by dividing the sample length by the one-way travel time. The travel time of the first arrival is picked at 3% of the maximum amplitude of the primary three halfcycles of the incoming signal. The system measures acoustic velocities under different effective confining pressures: 2.5, 5, 10, 20 and 40 MPa. The pressure increase causes elastic deformation of the sample by closing flexible microcracks and pores. As a result the sample reaches a velocity plateau or terminal velocity (Bourbié et al., 1987). To generate realistic subsurface conditions, the Gassmann (1951) equation for fluid substitution was used to calculate the saturated compressional wave velocity (Table 3.2).

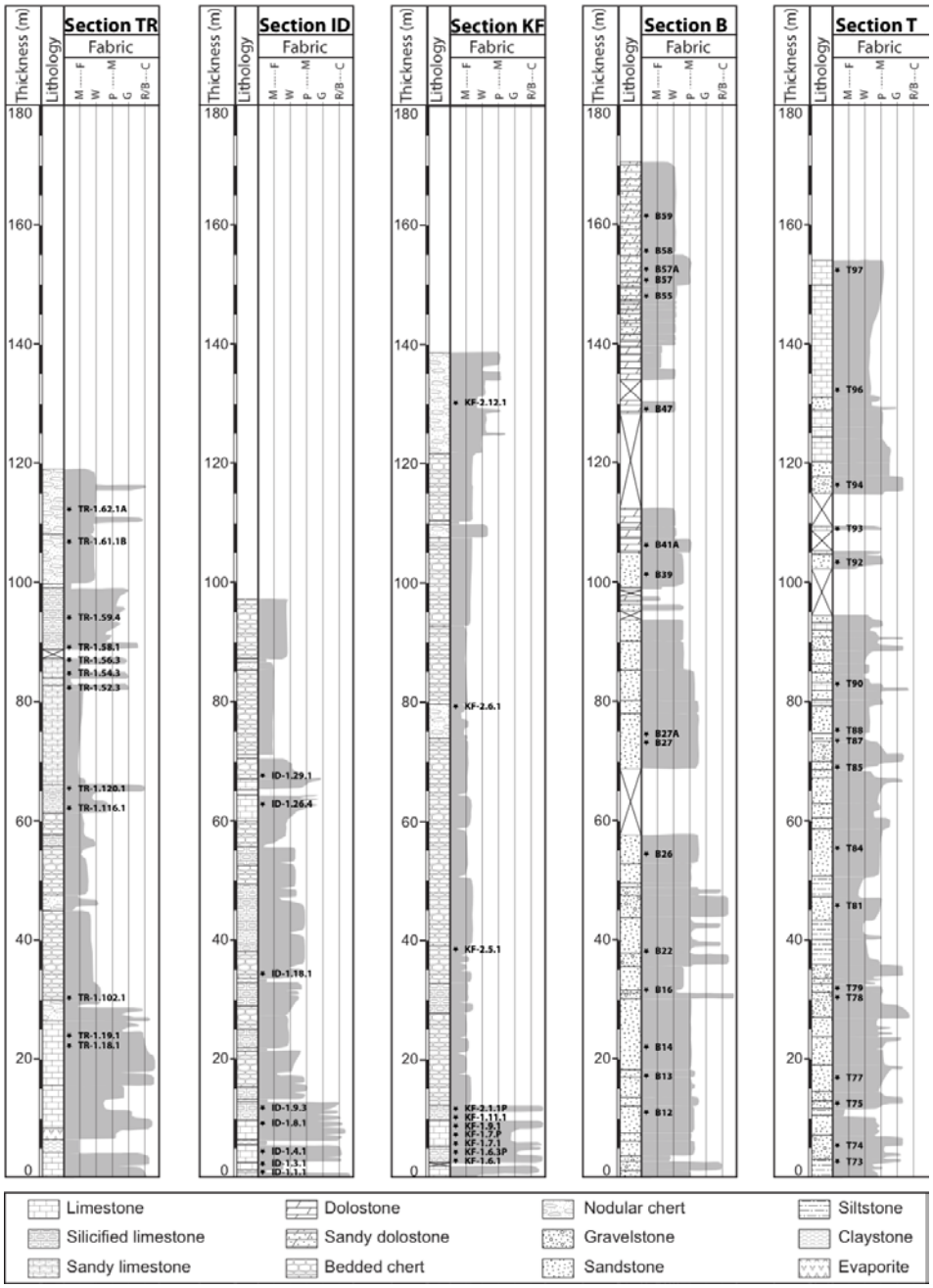

Fig. 3.3 Stratigraphic overview of the section logs. Sample locations are indicated at the tops of the columns. Fabric classifi cation for clastic sediments: F = fi ne sand; M = medium sand; C = coarse sand. Fabric classifi cation for carbonates: M = mudstone; W = wackestone; P = packstone; G = grainstone; R/B = rudstone/boundstone. Thicknesses are in metres.

3.4.8 Multivariate regression analysis

A post-hoc statistical analysis was performed to evaluate the correlation between the acoustic velocities and fourteen textural and petrophysical parameters as follows:

- Rock composition: carbonate content, TOC and non-organic fraction;
- Grain size (of the non-organic fraction): clay, silt and sand fraction and average grain size;
- Volumetric properties: grain density, bulk density and porosity;
- Qualitative data: interparticle pores, mouldic pores/ vugs, fractures and facies types.

The multivariate regression analysis used Stata 13.0 software in order to assess the relationship between predictor factors (textural and petrophysical properties) and the dependent variable (saturated P-wave velocity). For a statistical evaluation of the entire dataset, missing values (grey cells in Table 3.2) were populated using calculated averages for each microfacies which relied on the detailed microfacies analyses.

3.5 Results

3.5.1 Microfacies analyses

Previous sedimentological studies of the Carboniferous – Permian mixed carbonate and non-carbonate deposits of Spitsbergen include those by Ehrenberg et al. (2001) and Blomeier et al. (2009, 2011, 2013), and provided a useful framework within which to define the facies variations. Ten microfacies types (Table 3.1) were defined based on thin-section analyses (Fig. 3.4): MFT-1, clay- to siltstones (n = 1); MFT-2, sandstones (n = 19); MFT-3, conglomerates (n = 3); MFT-4, spiculitic cherts (n = 17); MFT-5, calcareous sandstones (n = 4); MFT-6, mixed bioclastic–siliciclastic rudstones (n = 10); MFT-7, microbial bindstones (n = 3); MFT-8, pack- to grainstones (n = 5); MFT-9, rudstones (n = 5); and MFT-10, dolostones (n = 6). Sandstones (MFT-2), conglomerates (MFT-3) and calcareous sandstones (MFT-5) are interpreted to have been deposited on shoreface to offshore transitions, and occur predominantly within the Wordiekammen and Treskelodden Formations. The dolostones (MFT-10) are restricted to the Wordiekammen Formation (Blomeier et al., 2009; Schneider, 2013). Microbial bindstones (MFT-7) only occur within the Templet Member and are interpreted as low-energy, peritidal flat deposits (Groen, 2010; Blomeier et al., 2011). Spiculitic cherts (MFT-4) with clay- to siltstones (MFT-1) are typical of the Kapp Starostin Formation

and were deposited in low-energy conditions below the storm weather wave base (Ehrenberg et al., 2001). The mixed bioclastic-siliciclastic rudstones (MFT-6), pack- to grainstones (MFT-8) and rudstones (MFT-9) predominantly occur within the Vøringen Member and the Kapp Starostin Formation. They are interpreted as inner to mid-ramp deposits (Blomeier et al., 2011, 2013).
More detailed facies information is presented in Table 3.1.

3.5.2 Section descriptions

Five outcrop sections were studied in different parts of Spitsbergen (see Fig. 3.1). The sections are described below with reference to the measured logs (Fig. 3.3).

Treskelodden section (Section T):

Section T is located in the Hornsund area (Fig. 3.1) and covers the Treskelodden Formation (Figs. 3.2, 3.3). The section measures 154m of which 16m are not exposed. The outcrop succession can be divided into two intervals, which are separated by a grey conglomerate (MFT-3) (Birkenmajer, 1964): a lower siliciclastic interval (MFT-2), and an overlying siliciclastic and carbonate interval (MFT-5, MFT-6 and MFT-8), which contains five coral-dominated bryozoan- and foraminifer-bearing cycles (Fedorowski, 1982; Blazejowski, 2009). The cyclicity is interpreted to result from glaciation and deglaciation events (Birkenmajer, 1964). The lower siliciclastic interval at this section is characterized by multiple fining-upward trends. The overlying mixed siliciclastic – carbonate strata show wavy beds and erosional surfaces.

Bellsund section (Section B):

In section B, the sediments of the Wordiekammen Formation were investigated (Figs. 3.2, 3.3). The lithology of this section is similar to the sequence found in section T and can be divided into three parts. The lower 58m is dominated by low-porosity siliciclastic sediments, composed mainly of sand-sized and heavily sutured quartz grains (MFT-2 and MFT-5). Thin sections show the local presence of fracture porosity. This interval is followed by a 45m thick sediment package which consists of silica-dominated facies (MFT-2, MFT-3 and MFT-5). The siliciclastic-dominated basal interval is overlain by foraminifera and brachiopod-rich carbonates, which have a characteristic light beige to red colour. The uppermost 42m is characterized by carbonate lithologies containing corals; the carbonates are recrystallized and frequently altered by fabric destructive dolomitization (MFT-10).

Table 3.1 Characteristics, occurrence, and environmental reconstruction of the microfacies types (MFTs) from central, west and south Spitsbergen.

MFT-No.	MFT-Name	Characteristics	Components	Occurrence	Depositional environments
1	Clay- to siltstone	Thin beds, dark-colored and laminated	No clear recognizable components, clay and silt-sized fragments have a mixed origin, some calcite filled veins	The Kapp Starostin Formation associated with MFT-4	Forms in quiet environments, typically for the deep marine area of the outer ramp
2	Sandstone	Sand-sized quartz, sub-rounded and moderate-well sorted, locally sutured, some samples show more than 15% of micrite or sparite in their matrix	Sand-sized quartz grains, locally rounded pebble-sized exoclasts, glauconite minerals and fragments of bioclasts	The Treskelodden and Wordiekammen Formations associated with MFT's 3, 5, 6 and 8, and in the Stensiöfjellet Member with MFT's 4 and 6	Represent alluvial to shore face conditions of the inner shelf
3	Conglomerate	Coarse material exceeding sand-sized grains, well-rounded and low sphericity, matrix of the sediment consists of sub-rounded sand/silt-sized grains	Pebble-sized quartz grains embedded in a sandy matrix, minor presence of biota	The Treskelodden and Wordiekammen Formations associated with MFT's 2 and 5	Interpreted as point bars resulting from fluvial deposits
4	Spiculitic chert	Light to dark coloured massive to medium bedded spiculitic cherts in a micrite/microspar matrix, intensively affected by silicification and bioturbation	Accumulations of monaxon spicules, silt- to sand-sized glauconite grains, fragments of ostracods, brachiopods and foraminifers	The Kapp Starostin Formation associated with MFT's 1 and 6	Forms in quiet water, low-energy conditions below the SWWB
5	Calcareous sandstone	Siliciclastic dominated rocks with less than 32% carbonate grains or cement	Sand-sized, moderate-sorted quartz grains with varying degree of roundness, exoclasts ranging from sand- to pebble size	The Treskelodden and Wordiekammen Formations associated with MFT's 2, 3 and 6	Reflect shore face to offshore transition
6	Mixed bioclastic-siliciclastic rudstone	Thin to medium bedded coarse-grained bioclastic-limestones, partly affected by silicification, matrix composed of micrite, microsparite and locally sparite	Mixture of peloids, fragments of bryozoans, echinoderms, brachiopods, siliceous sponge needles, sand-pebble- sized lithoclasts and quartz grains	The Vøringen Member and the Kapp Starostin Formation associated with MFT's 4, 8 and 9, the Treskelodden Formation with MFT's 2, 3, 5 and 8	Reflect the storm-dominated, high-energy conditions within the mid ramp settings around the SWWB
7	Microbial bindstone	Thick to medium sized beds, greyish and brownish fine-grained limestones, distinct horizontal to wavy laminations with alternating sand and micrite	Algal mats with low terrigenous input, few siliceous sponge spicules, fecal pellets, locally Microcodium	The Templet Member associated with MFT-4	Forms in marginal marine areas of a carbonate platform, typically in quiet-water areas of peritidal flats
8	Pack- to grainstone	Medium bedded, partly silicified carbonate deposits, blocky sparite is commonly present	Fragments of bioclasts such as sponge spicules, bryozoans, brachiopods and bivalves, traces of glauconite, peloids and sand-sized detrital grains	The Vøringen Member associated with MFT's 6 and 9, and locally in the Treskelodden Formation	Reflect agitated water condition around the FWWB within the inner ramp setting
9	Rudstone	Medium to thick bedded, coarse-grained bioclasts limestones generally cemented by blocky or syntaxial cements, locally intensively affected by silicification	Fragments of bioclasts such as brachiopods, bivalves, gastropods, bryozoans and echinoderms	The Vøringen Member associated with MFT's 6 and 8	Forms in high-energy conditions (storm events) within shore face to transitional offshore areas of the inner and mid ramp setting
10	Dolostone	Massive to medium bedded crystalline dolomitized sediments	Original components can't be recognized due to fabric destructive recrystallization. The dolomite crystals are well developed	The Wordiekammen Formation associated with MFT's 2, 3 and 5	Originate from previously formed mudstones, extensive dolomitization commonly obliterates the original depositional texture

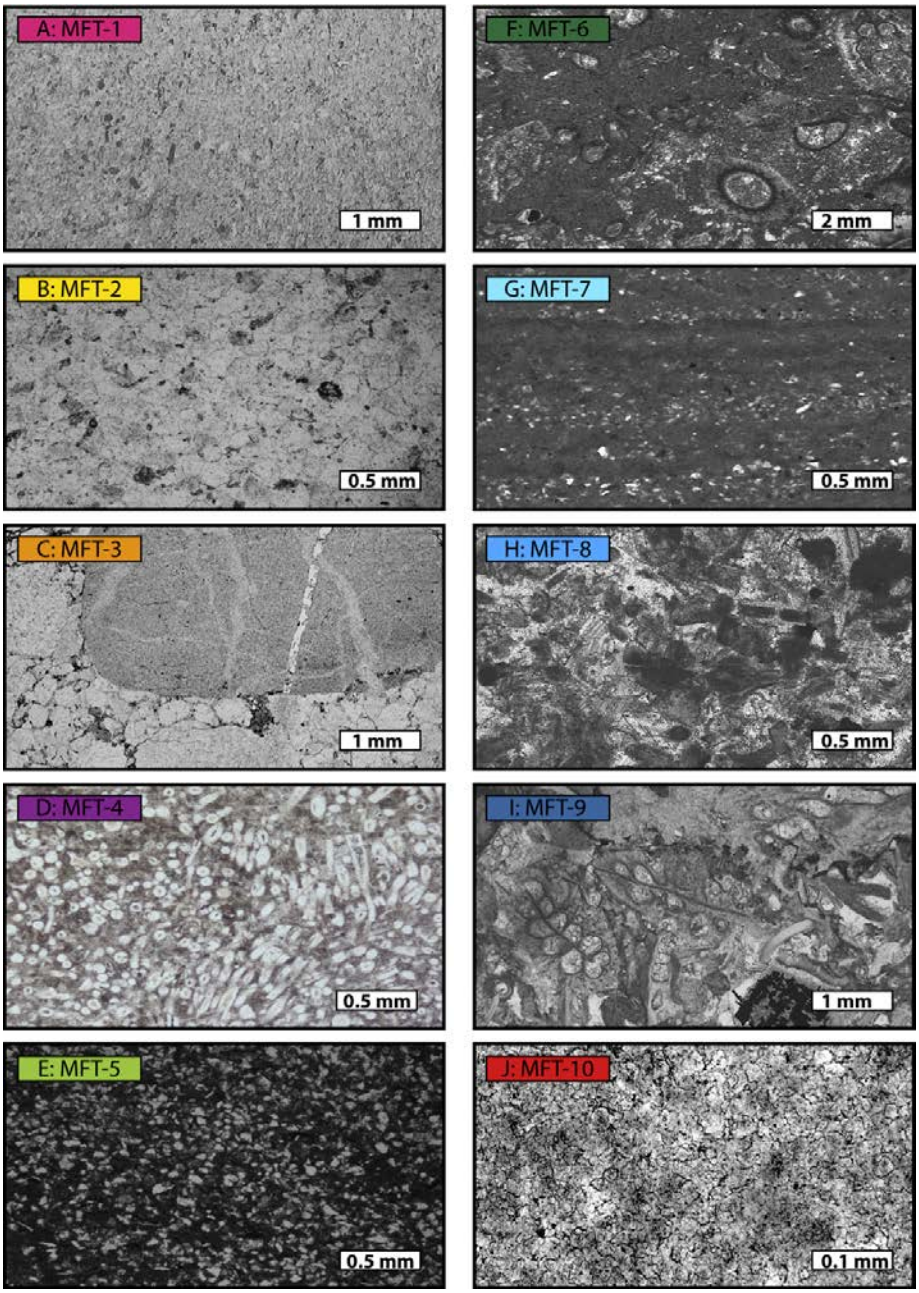

Fig. 3.4 Thin-section photomicrographs of the microfacies which were distinguished; sample number in brackets. (A) MFT-1, clay- to siltstone (FE-1.7.2); (B) MFT-2, sandstone (B12); (C) MFT-3, conglomerate (T94); (D) MFT- 4, spiculitic chert (TR-1.62.1a); (E) MFT-5, calcareous sandstone (B55); (F) MFT-6, mixed bioclastic-siliciclastic rudstone (TR-1-52-3); (G) MFT-7, microbial bindstone (ID-1.1.1); (H) MFT-8, pack- to grainstone (TR-1.18.1); (I) MFT-9, rudstone (TR-1.59.4);v(J) MFT-10, dolostone (B41A).

Kapp Fleur de Lys sections (Section KF):
Kapp Fleur de Lys was studied in two partly overlapping sections (KF) comprising 139m of succession (Figs. 3.2, 3.3). The sections measured correspond to the uppermost 2m of the Gipshuken Formation (Templet Member) and nearly 137m of the Kapp Starostin Formation including the Vøringen Member and part of the Stensiöfjellet Member. The Templet Member consists of grey to dark grey, massive algal limestones and mudstones (MFT-7), which are overlain by a limestone breccia. The boundary between the Templet Member and the overlying Vøringen Member is not exposed. The absence of outcropping strata could suggest a marly or shaley interval with a low sedimentation rate. The Vøringen Member contains 2-3m thick couplets of partly silicified, bioclastic limestones (MFT-8 and MFT-9), which show a fining upward trend and an upward increase in faunal diversity including brachiopods, bivalves, gastropods, bryozoans and echinoderms. The intervals show local bioturbation; stylolites are present throughout the entire member. A monotonous series of generally dark grey, flaser-bedded cherts (MFT-4) with interbedded claystones (MFT-1) characterizes the Kapp Starostin Formation. Trace fossils, Skolithos and Zoophycus "Spreiten" were frequently recorded. The Stensiöfjellet Member consists of a succession of glauconite-rich sandstone horizons (MFT-2) and massive to nodular-bedded cherts (MFT-4) interbedded with partly silicified bioclastic limestones (MFT-8).

Idodalen section (Section ID):
Section ID (Figs. 3.2, 3.3) comprises 6m of the Templet Member, 7m of the Vøringen Member and about 85m of the Kapp Starostin Formation. The sediments of Templet and Vøringen Members and the basal part of the Kapp Starostin Formation are lithologically similar to those encountered in section KF. At 60m from the base of the section, the chert succession (MFT-4) of the Kapp Starostin Formation is interrupted by a series of coarsening upward silicified, bioclastic limestones (MFT-6) containing bryozoans, brachiopods and crinoids. The uppermost 25m of the section are characterized by massive to nodular-bedded cherts (MFT-4). The top of the Kapp Starostin Formation is not exposed.

Tålmodryggen section (Section TR):
Section TR (Figs. 3.2, 3.3) contains a little over 20m of the uppermost strata of the Templet Member, 8m of the Vøringen Member, and 90m of the overlying Kapp Starostin Formation. The Templet Member is marked by an alternation of evaporates (gypsum, anhydrite) and laminated algal limestones. The top of this member is lithologically similar to the successions in KF and ID, where dense algal limestones (MFT-7) overlie carbonate breccia. The Vøringen Member has

a different appearance compared to sections KF and ID. The base of the member is characterized by a grey to light brown lithoclastic rudstone (MFT-6), overlain by grey interbedded lenses of limestone breccia and thin to medium bedded mudstones. Above this, couplets of coarse-grained brachiopod-rich horizons (MFT-9) alternate with fine-grained cherty limestones (MFT-8) characterized by abundant Skolithos burrows. At this locality several lenses and horizons of pebbles show signs of borings, which contrasts with sections KF and ID. Sandy intervals occur in the uppermost chert horizon of the Vøringen Member. The Kapp Starostin Formation continues with cherts (MFT-4) and dark claystone partings (MFT-1). At 60m from the base of the section, intervals of silicified, bioclastic carbonates (bryozoans, brachiopods, corals and siliceous sponges) were observed (MFT-6). Above this, the section continues with platy shales.

About 86m from the base of the section, another succession of silicified coarsening upward carbonate beds (MFT-6 and MFT-9) is present. Rocks in this 14m thick sequence include abundant bryozoan, crinoid and brachiopod fossils, as well as solitary rugose corals and peloids. Above this succession, two massive chert horizons (MFT-4) occur, which together have a total thickness of 20m.

3.5.3 Results of Thermo Gravimetric Analysis

Results of TGA show that the carbonate content of the samples ranges between 0.2% and 99% (Table 3.2), and non-carbonate samples (n = 32), mixed samples (n = 22) and carbonate samples (n = 13) could be differentiated. Dolostone (n = 6) and limestone samples were distinguished based on thin-section analyses. Thin-section analyses showed that the residual nonorganic fraction primarily consisted of siliciclastic and siliceous materials. The total organic carbon (TOC) content ranged between 0 and 2%. In the dolostone samples, the TOC did not exceed 1%; within the clastic samples, it ranged between 0.2 and 1.7%; the mixed samples had a TOC of 0.2 -1.9%; in the limestones, the TOC was < 0.8%.

3.5.4 Grain size

Clay occurs in all the sections measured and reaches a maximum of 12.7% (T90, Treskelodden section); the silt content does not exceed 57.4% (T73, Treskelodden section), and the sand content varies between 0.3% (ID-1.4.1, Idodalen section) and 97% (B26, Bellsund section) (Table 3.2). The average grain size of the non-organic sediment fraction ranges from very finegrained silt to medium-grained sand, 7.8 and 1.4 (Table 3.2) on the Wentworth (1922) scale.

3.5.5 Porosity and elastic properties

Sample selection for sonic velocity measurements attempted to capture the full variety of facies and corresponding rock properties. To determine the impact of pressure on the P- and S-waves in mixed carbonate and non-carbonate rocks, the acoustic velocities of 73 samples were measured at different effective pressures (Table 3.2). S-wave velocities at 2.5 MPa range between 1.908 and 3.478 km/s, and increase to 2.294 – 3.651 km/s at 40 MPa (Fig. 3.5A). P-wave velocities vary between 3.011 and 6.233 km/s at 2.5 MPa confining pressure, and increase to 3.760 – 6.884 km/s at 40 MPa confining pressure (Fig. 3.5B).

The porosity of the samples ranged between 0.1% and 20.7% (Table 3.2). Acoustic velocities decrease with increasing porosity (Fig. 3.6A). P-waves show a variation of ~2 km/s for a given porosity; for S waves, this variation is ~1 km/s.

The measured bulk density of the samples ranged between 2.084 and 2.831 g/cm3, with a peak value between 2.5 and 2.7 g/cm3. P- and S-wave velocity-density transforms demonstrate non-linear behaviour; the overall trend indicates increasing P-wave velocities correspond to increasing bulk density values (Fig. 3.6B). Carbonate content, which is related to facies, shows a linear relationship with P-wave velocity (Figs. 3.7A, 3.8A). Sediments with high carbonate contents tend to have higher P-wave velocities compared to silica-rich and/or clay-rich sediments, as shown by the arrows in Fig. 3.8.

The porosity of the dataset ranges between 0.1% and 20.7% with an average of 2.2%. Only six samples have porosities exceeding 5% (Table 3.2; Figs. 3.7B, 3.8B). Table 3.2 shows the fracture intensities and the dominant pore types of the thin sections and plugs based on their visual appearance. Three pore types were identified according to the defiition in Xu and Payne (2009): (i) cracks and fractures, (ii) “reference” pores (interparticle and intercrystalline pores); and (iii) “stiff pores” (vuggy and mouldic pores). The lithofacies cover the wide range of fracture occurrences based on the predefined groups. Due to the low porosity of the sediments, the pore types were not always identifiable.

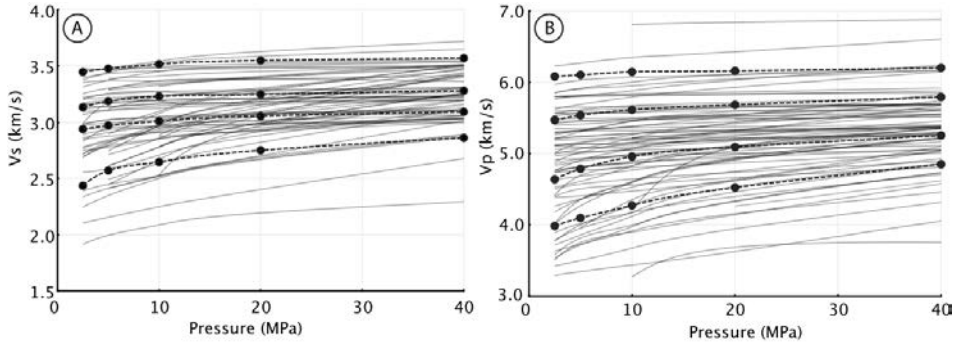

Fig. 3.5 Cross-plots of S-wave **(A)** and P-wave **(B)** velocities versus changes along the pre-defined pressure path. The solid black lines represent the velocity paths of the individual samples. The dashed lines show the typical behaviour during pressure increase and rising velocity (selected samples). The velocity difference between the initial measurement (2.5 MPa) and the final measurement (40 MPa) is higher for samples with a low initial velocity measured at 2.5 MPa. In addition, the lines show asymptotic curvature towards the horizontal which is reached at around 10 to 20 MPa and which is considered to be the terminal velocity (Bourbié et al., 1987)

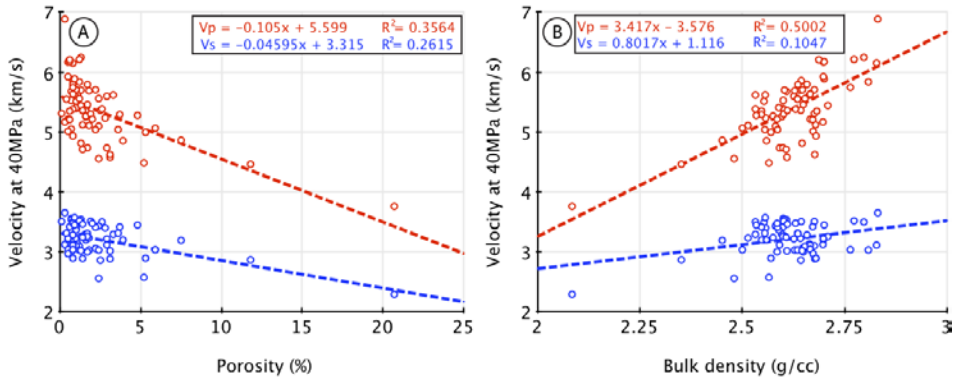

Fig. 3.6 Cross-plots of P-wave (blue dots) and S- wave velocity (red dots) versus porosity **(A)** and bulk density **(B)**. The corresponding trend lines (dashed) have the same colours. The clustering of the data-points between 0 to 5% (porosity) and 2.5 to 2.75 g/cm3 (bulk density) has resulted in low correlation coefficients.

3.5.6 Multivariate regression analysis

The first test that was made before running the multivariate regression model assessed the normal distribution of the data. The skewness and kurtosis

distributions of all predictor factors vary between −1.0 and +1.0, and hence are consistent with a normal distribution (Table 3.4).

The next test was related to the multi-colinearity of the predictors which occurs when more than two predictor variables are linearly associated, or in other words, are dependent on other predictors. Thus for example, Facies represents a combination of other factors such as carbonate content, grain size and nonorganic fraction.

The variance inflation factors (VIF) were calculated to measure the degree of multi-colinearity between predictors (O'brien, 2007). These factors should be less than 10 and optimally less than 5. A step-wise approach was used to eliminate the highly correlative factors from the dataset. After multiple iterations, the grain density, non organic material, facies, and sand fraction showed high correlative factors and were therefore removed from the final run.

After running the multivariate regression model, the R2 had a value of 0.79, which indicates that 79% of the variations in saturated P-wave velocity can be explained by the textural and petrophysical factors which passed the VIF < 10 selection – in this case carbonate content, porosity, bulk density, clay content and others (see Table 3.4).

The coefficient values (Table 3.4) represent the mean change in the saturated P-wave velocity for one unit of change in the predictor factor, while holding other predictors in the model constant. The positive and negative regression coefficients show that for every unit increase in the predictor factors, an increase or a decrease is expected in the coefficient value of the saturated P-wave velocity, respectively.

The significance of the relationship between the predictor factor and saturated P wave velocity is shown by the t value of the factors' coefficient. The t values of about 1.65, 1.96, and 2.58 reflect confidence levels of 90%, 95% and 99% respectively. A confidence level refers to the percentage of all possible samples, which are positioned close to the mean (Table 3.4).

The analysed textural and petrophysical factors do not vary at the same scale; a standardized coefficient (beta) was introduced to enable a comparison of the factors influencing the saturated P-wave velocity (Schroeder et al., 1986). The predictor factors are arranged by their order of impact on the saturated P-wave velocity (beta), with carbonate content, porosity, bulk density and clay content being the most important factors (Table 3.4).

Table 3.2 Summary of the sample information, textural characteristics and petrophysical measurements. The grey cells do not contain measured values; instead, these cells are populated with calculated averages based on microfacies analysis and petrophysical measurements. The calculated averages have been used to perform the full dataset statistical analysis. These values have not been used in the graphs.

Sample Information			Visible pore-types			Density-porosity			Elastic properties			Mineral composition			Non-organic textural properties			
Sample name	Facies	Fractures	Cracks	Reference	Stiff	Bulk density	Grain density	Porosity	P-wave (40MPa)	S-wave (40MPa)	Saturated P-wave	TOC	Carbonate	Non-organic	Grain-size	Clay	Silt	Sand
#	#	#	#	#	#	g/cc	g/cc	%	km/s	km/s	km/s	%	%	%	phi	%	%	%
FE-1.101.1	4	3	2	0	0	2.600	2.618	0.7	5.527	3.559	5.566	0.7	4.8	94.5	2.1	4.5	20	70
FE-1.102.1	4	3	0	0	1	2.608	2.627	0.7	5.678	3.537	5.711	0.5	17.5	82.0	1.4	1.4	3.1	77.5
FE-1.103.1	4	2	0	0	0	2.644	2.666	0.8	5.857	3.506	5.952	0.7	45.2	54.1	2.2	3.0	6.7	44.5
FE-1.104.1	4	2	1	0	2	2.603	2.637	1.3	5.700	3.543	5.725	0.9	19.7	79.4	1.4	2.1	4.1	73.3
FE-1.7.2	1	2	2	0	0	2.599	2.625	1.0	5.392	3.414	5.442	1.4	6.8	91.8	8.0	6.8	80	5
ID-1.1.1	7	1	0	0	0	2.626	2.704	2.9	5.596	3.218	5.848	0.7	88.1	11.2	7.3	6.7	3.8	0.6
ID-1.18.1	4	1	0	0	0	2.596	2.639	1.6	5.257	3.298	5.502	1.3	30.4	68.3	1.8	3.2	5.4	59.8
ID-1.26.4	6	2	2	0	0	2.642	2.670	1.0	5.697	3.226	5.922	0.5	69.0	30.5	4.5	4.7	10.9	15.0
ID-1.29.1	4	1	0	0	0	2.589	2.617	1.0	5.409	3.365	5.543	1.0	20.6	78.4	1.7	3.2	5.2	70.0
ID-1.3.1	7	1	0	0	1	2.679	2.718	1.4	5.121	2.892	5.627	0.8	82.1	17.1	7.4	10.4	5.9	0.7
ID-1.4.1	7	1	0	0	1	2.570	2.715	5.3	4.995	2.896	5.315	0.7	85.7	13.6	7.8	9.0	4.4	0.3
ID-1.8.1	9	0	0	0	0	2.628	2.675	1.8	5.689	3.031	5.892	0.4	87.3	12.3	3.1	1.8	1.3	9.3
ID-1.9.3	4	1	0	0	0	2.603	2.641	1.4	5.376	3.265	5.481	1.1	24.2	74.7	2.2	5.3	6.0	63.5
KF-1.11.1	4	1	0	1	1	2.553	2.580	1.0	5.514	3.492	5.694	0.8	24.0	75.2	1.6	3.4	4.8	66.9
KF-1.6.1	8	2	2	0	0	2.565	2.706	5.2	4.486	2.576	4.966	0.3	86.2	13.5	4.7	0.4	9.7	3.5
KF-1.6.3P	8	1	0	0	0	2.647	2.707	2.2	5.706	3.057	5.884	0.2	89.5	10.3	5.5	4	0.3	6
KF-1.7.1	9	1	0	0	0	2.664	2.694	1.1	5.614	3.133	5.983	0.3	89.6	10.1	3.9	2.5	1.1	6.5
KF-1.7.P	8	0	0	0	0	2.649	2.695	1.7	5.459	3.001	5.802	0.3	89.6	10.1	5.5	3	4	3.1
KF-1.9.1	9	2	1	0	1	2.635	2.699	2.4	5.560	3.031	5.808	0.2	90.9	8.9	6.3	3.1	4.6	1.2
KF-2.1.1P	4	3	1	0	0	2.547	2.589	1.6	5.351	3.200	5.465	1.2	25.9	72.9	2.5	7.1	9.8	55.9
KF-2.12.1	4	3	2	0	1	2.084	2.627	20.7	3.760	2.294	4.001	1.1	8.5	90.4	3.3	7.7	19.4	63.3
KF-2.5.1	4	0	0	0	1	2.480	2.542	2.4	4.556	2.559	4.785	1.7	16.4	81.9	1.9	3.8	6.4	71.6
KF-2.6.1	4	0	0	0	1	2.585	2.604	0.7	5.051	3.003	5.456	1.3	37.5	61.2	4.3	11.4	16.1	33.8
SK-1.15.1	6	1	0	0	0	2.500	2.656	5.9	5.063	3.036	5.219	0.5	37.9	61.6	2.3	3.6	7.4	50.6
SK-1.18.1	9	3	3	0	0	2.643	2.710	2.5	5.362	2.862	5.655	0.4	93.1	6.5	4.2	0.5	1	5
SK-1.24.1	4	2	0	0	0	2.514	2.561	1.8	5.111	3.233	5.252	1.1	7.4	91.5	1.6	2.7	4.9	83.9
SK-1.41.1	2	0	0	2	0	2.351	2.666	11.8	4.463	2.868	4.605	0.5	0.4	99.1	2.9	1.1	8	90
TR-1.102.1	4	1	0	0	0	2.575	2.617	1.6	5.267	3.240	5.519	0.7	34.3	65.0	2.3	5.2	8.4	51.3
TR-1.116.1	4	3	2	0	0	2.556	2.580	0.9	5.618	3.571	5.638	0.8	7.6	91.6	1.6	1.9	4.5	85.3
TR-1.120.1	6	2	1	0	0	2.635	2.646	0.4	5.548	3.310	5.794	0.8	42.1	57.1	1.8	2.3	3.5	51.2
TR-1.18.1	8	2	0	0	0	2.698	2.711	0.5	6.168	3.196	6.306	0.1	97.6	2.3	5.5	0.3	1	1
TR-1.19.1	6	2	0	2	0	2.709	2.744	1.3	5.443	3.257	5.854	1.9	76.1	22.0	6.9	11.2	8.0	2.8
TR-1.52.3	6	2	2	0	0	2.653	2.685	1.2	5.559	3.093	5.750	0.9	63.6	35.5	3.9	6.2	6.6	22.8
TR-1.54.3	6	2	0	0	0	2.676	2.703	1.0	5.707	3.100	5.892	0.7	74.7	24.6	5.2	7.6	7.1	9.8
TR-1.56.3	6	1	0	0	0	2.636	2.682	1.7	5.793	3.305	5.940	0.5	68.8	30.7	4.3	5.0	9.2	16.5
TR-1.58.1	6	1	0	0	0	2.666	2.689	0.8	5.635	3.110	5.839	0.8	67.1	32.1	4.6	7.2	6.4	18.5
TR-1.59.4	9	0	0	0	0	2.658	2.678	0.8	5.797	3.282	6.154	0.4	87.3	12.3	3.7	1.0	5.0	6.3
TR-1.61.1B	4	3	3	0	0	2.532	2.600	2.6	5.384	3.501	5.469	0.9	8.0	91.1	1.9	3.4	6.4	81.4
TR-1.62.1A	4	3	3	0	0	2.532	2.618	3.3	5.617	3.293	5.657	0.6	6.5	92.9	1.8	3.1	6.3	83.5

Sample Information			Visible pore-types			Density-porosity			Elastic properties			Mineral composition			Non-organic textural properties			
Sample name	Facies	Fractures	Cracks	Reference	Stiff	Bulk density	Grain density	Porosity	P-wave (40MPa)	S-wave (40MPa)	Saturated P-wave	TOC	Carbonate	Non-organic	Grain-size	Clay	Silt	Sand
#	#	#	#	#	#	g/cc	g/cc	%	km/s	km/s	km/s	%	%	%	phi	%	%	%
B12	2	2	2	1	0	2.601	2.653	1.9	5.299	3.512	5.402	0.4	2.7	96.9	2.9	2.0	8.0	86.9
B13	2	1	0	1	0	2.609	2.693	3.1	4.579	3.017	4.946	0.5	16.5	83.0	3.0	3.8	8.4	70.8
B14	2	0	0	1	0	2.557	2.631	2.8	5.234	3.399	5.296	0.3	0.3	99.4	3.0	1.0	2.4	96.0
B16	3	2	2	2	0	2.451	2.649	7.5	4.865	3.194	4.979	0.2	0.6	99.2	3.0	1.0	2.2	96.0
B22	2	0	0	2	0	2.581	2.646	2.4	5.100	3.431	5.263	0.4	0.7	98.9	3.0	0.0	1.9	97.0
B26	2	0	0	2	0	2.547	2.645	3.7	5.291	3.416	5.329	0.2	0.7	99.1	3.0	1.0	1.1	97.0
B27	2	0	0	2	0	2.559	2.662	3.9	4.856	3.200	5.071	0.7	10.0	89.3	2.3	3.4	6.7	79.2
B27A	2	0	0	2	0	2.591	2.670	2.9	4.736	3.118	5.042	0.5	13.4	86.1	2.3	3.5	5.9	76.6
B39	5	2	3	1	0	2.666	2.680	0.5	5.214	3.045	5.320	0.4	21.1	78.5	2.4	3.7	8.9	65.9
B41A	10	2	1	0	0	2.828	2.851	0.8	6.150	3.113	6.451	0.4	99.5	0.0	6.0	0	0	0.0
B47	10	3	1	0	0	2.797	2.834	1.3	6.245	3.499	6.573	0.9	99.0	0.1	6.0	0	0	0.1
B55	5	3	3	0	0	2.677	2.762	3.1	4.623	2.886	5.245	0.8	54.8	44.5	2.9	4.5	10	30
B57	10	2	1	0	0	2.773	2.806	1.2	6.212	3.519	6.621	0.0	99.7	0.3	6.0	0	0	0.3
B57A	10	0	0	0	0	2.764	2.785	0.8	5.746	3.037	6.381	0.0	99.6	0.4	6.0	0	0	0.4
B58	10	3	3	0	0	2.808	2.842	1.2	5.839	3.032	6.253	0.4	98.6	1.0	6.0	0	0	1.0
B59	10	2	2	0	0	2.831	2.841	0.3	6.884	3.651	7.005	0.6	99.3	0.9	6.0	0	0	0.9
T0	2	3	0	0	0	2.555	2.651	3.6	5.041	3.313	5.149	0.7	0.3	99.0	1.9	2.8	6.8	89.4
T73	2	3	3	0	0	2.697	2.705	0.3	5.169	3.123	5.272	0.8	12.6	86.6	5.1	10.3	57.4	18.9
T74	3	0	0	1	0	2.676	2.680	0.1	5.309	3.507	5.543	0.9	6.9	92.2	3.0	2.0	10.0	80.2
T75	2	0	0	1	0	2.599	2.644	1.7	4.738	3.259	5.104	0.4	0.4	99.2	3.0	0.5	5.0	93.7
T77	2	0	0	0	0	2.672	2.687	0.6	5.207	3.420	5.530	0.7	17.2	82.1	3.0	4.0	30.0	48.2
T78	2	0	0	1	0	2.586	2.645	2.2	5.040	3.411	5.241	0.8	1.2	98.0	3.0	2.5	3.5	92.0
T79	2	0	0	1	0	2.610	2.646	1.4	5.359	3.463	5.395	0.5	0.2	99.3	3.0	2.0	3.2	94.0
T81	2	1	1	1	0	2.607	2.645	1.4	4.710	3.245	5.126	0.4	2.1	97.5	3.0	1.5	2.0	94.0
T84	2	0	0	3	0	2.630	2.651	0.8	5.382	3.479	5.571	0.4	15.6	84.0	2.2	3.1	5.4	75.5
T85	2	0	0	1	0	2.673	2.687	0.5	5.012	2.971	5.168	1.2	15.4	83.4	3.5	10.0	19.3	54.1
T87	2	0	0	2	0	2.585	2.639	2.0	5.216	3.476	5.336	0.4	0.2	99.4	3.0	2.0	1.4	96.0
T88	5	1	0	0	0	2.680	2.700	0.8	4.935	2.895	5.204	0.9	26.5	72.6	3.4	6.4	16.0	50.2
T90	6	0	0	0	0	2.700	2.726	0.9	5.887	3.447	5.906	0.7	43.2	56.1	4.3	12.7	13.4	30.1
T92	2	0	0	0	0	2.646	2.681	1.3	4.815	3.021	5.062	0.9	10.7	88.4	3.6	11.1	17.0	60.3
T93	5	0	0	0	0	2.682	2.699	0.6	5.349	ND	ND	1.1	32.1	66.8	2.9	6.8	20	40
T94	3	2	1	2	0	2.534	2.662	4.8	5.278	3.447	5.322	0.6	0.6	98.8	3.0	2.5	10.0	86.3
T96	8	2	0	0	0	2.687	2.703	0.6	6.206	ND	ND	0.2	84.5	15.3	6.4	6.7	4.3	4.3
T97	6	1	0	0	0	2.698	2.711	0.5	5.924	3.223	6.085	0.2	76.8	23.0	2.2	1.5	2.0	19.5

3.6 Discussion

The acoustic properties of sedimentary rocks depend on a variety of interacting parameters (Wang, 2001). The influence of textural and petrophysical factors affecting acoustic properties is reviewed in the following paragraphs, with a brief comparison with similar carbonate–siliciclastic successions known from outcrops in New Mexico, Argentina, Spain and northern France. The Carboniferous – Permian succession on Svalbard is then related to time- and facies-equivalents units in the subsurface which are hydrocarbon producing reservoir rocks.

3.6.1 Porosity and pore types

The standard time average equations of Wyllie et al. (1956) and Raymer et al. (1980) show that acoustic velocities and variations in porosity are directly related. Subsequent studies, however, demonstrated that porosity (and therefore the bulk - grain density ratio) primarily controls acoustic velocities and impedance contrasts (Braaksma et al., 2003; Hossain and Zhou, 2015). The average porosity of the rocks analysed in this study is low (2.2%); therefore the impact of other factors controlling acoustic velocities can be better assessed. Neither of the time-average equations address changes in porosity as a result of diagenetic processes affecting the original depositional fabric. In sandstones, diagenetic processes including silica cementation modify the original permeability, texture and mineralogical composition, changing the elastic properties of the sediments (Hossain and Zhou, 2015). In carbonates, the occlusion of pore space by carbonate cements together with recrystallization and dolomitization processes will result in changes to porosity and pore types, and to the associated acoustic impedance (Fournier and Borgomano, 2007).

The samples analysed show a declining velocity trend with increasing porosity. This trend is clear for the relative high porosity samples (porosity > 5%); in the low porosity domain, this trend is also present but is less evident. The amount of porosity is not considered to be the most important parameter but it still plays an important role. Over-estimation of the Wyllie time-average equation for quartz and calcite (WTA; Figs. 3.7, 3.8) may be the result of mineralogical effects, diagenetic modification or microfracture development. The pore type variation, which is often considered to be an important factor influencing the elastic properties in carbonate sediments, plays a minor role in the samples analysed due to the absence of high porosity samples (Anselmetti and Eberli, 1993; Baechle et al., 2008; Weger et al., 2009; Soete et al., 2015).

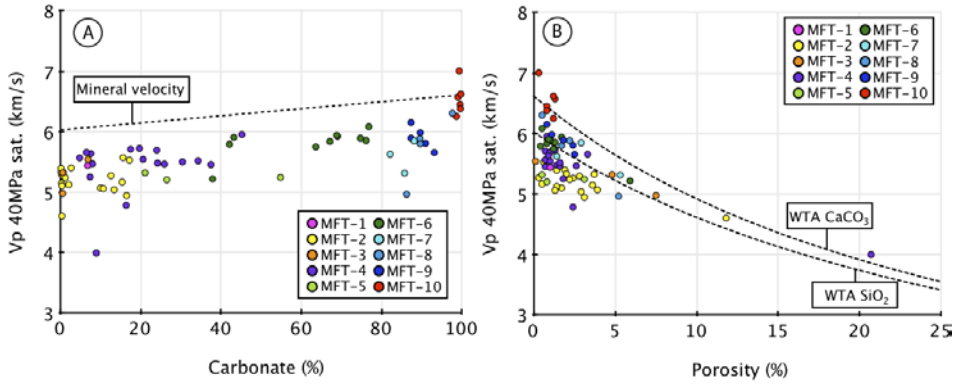

Fig. 3.7 Plots of Gassmann saturated P-wave velocity versus carbonate content **(A)** and porosity **(B),** with facies types superimposed (see Table 3.1). The mineral velocity line **(A)** displays the theoretical maximum velocity (Mavko et al., 2009) for SiO2 (left) and CaCO3 (right). The Wyllie time average equation (WTA) is applied for the pure mineralogies **(B)**.

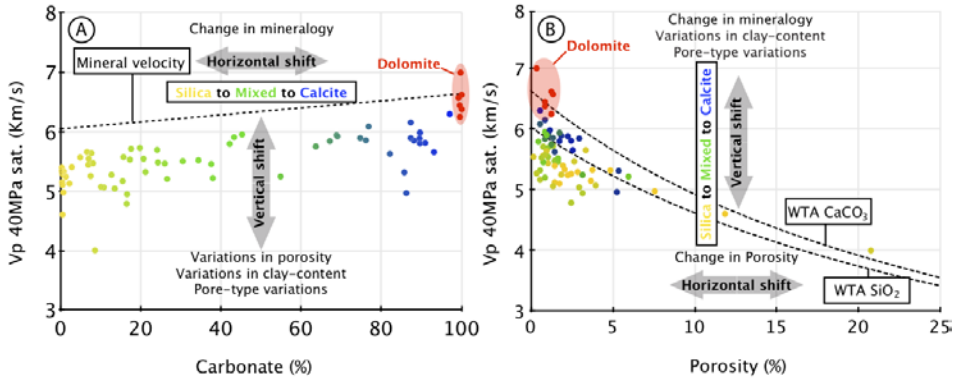

Fig. 3.8 Plots of Gassmann saturated P-wave velocity versus carbonate content **(A)** and porosity **(B)**; the mineral composition based on carbonate content is superimposed. The mineral velocity line **(A)** shows the theoretical maximum velocity (Mavko et al., 2009; Table 3.3) for SiO2 (left) and CaCO3 (right). The Wyllie time average equation (WTA) is applied for these pure mineralogies **(B)**.

Xu and Payne (2009) distinguished three pore types based on pore aspect ratio, namely: micropores and cracks (with low aspect ratio); interparticle and intercrystalline pores (intermediate aspect ratio); and moulds and vugs (high aspect ratio). This pore-type model implies that a decrease in aspect ratio results in a velocity decrease for a given porosity. The results of the pore-type

analysis show that the samples analysed are dominated by microporosity and cracks (i.e. elongated pores). The majority of the samples show P-wave velocities that fall within the crack domain below the reference line that separates the "stiff pore" domain (i.e. vuggy and mouldic pores with high aspect ratios) from the crack domain (Fig. 3.9). The observed trend is lithology independent, as shown in Fig. 3.9.

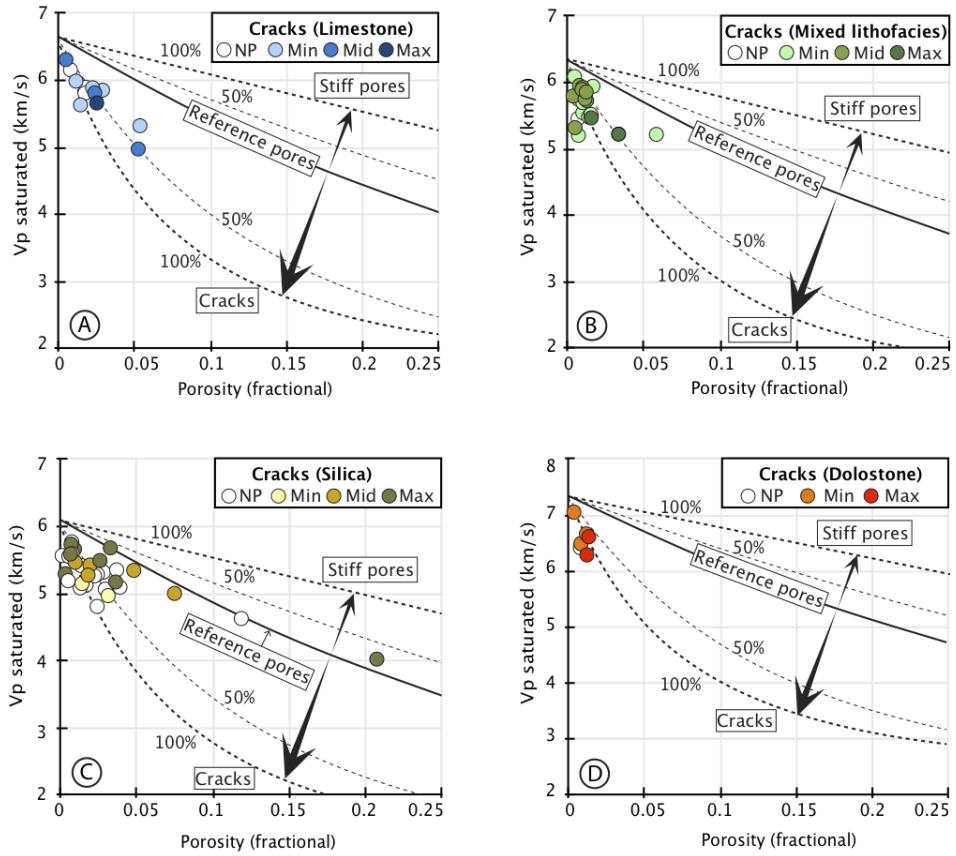

Fig. 3.9 Plots of Gassmann saturated P-wave velocity versus fractional porosity. The data selected for the separate plots are based on mineral composition: limestones with a carbonate content > 80% **(A)**; sediments with a mixed mineralogy **(B)**; siliceous sediments with a carbonate content < 20% **(C)**; and dolostones **(D)**. For each plot, the dark colours represent high fracture intensities and the light colours represent low fracture intensities.

3.6.2 Mineralogy

The studied Late Carboniferous to Permian sediments have a mixed mineralogical composition including silica (quartz, sponge spicules), calcite

and dolomite, and to a lesser extent clay (< 12.7%). Carbonate and siliciclastic rocks show some overlap of elastic properties when their original granular fabric is preserved (Kenter et al., 2007). However, when diagenetic processes such as recrystallization, dolomitization or chertification have modified the original fabric, the elastic properties will be affected (Braaksma et al., 2003; Kenter et al., 2007; Hossain and Zhou, 2015). In a re-evaluation of data from outcrops (Verwer et al., 2008, 2011) and cores (Ehrenberg et al., 2004; Fournier and Borgomano, 2007; Weger et al., 2009), Kittridge (2015) showed that mineralogy (calcite and dolomite) may exert a significant, first-order control on elastic properties. If mineralogy is not taken into account, velocity variations for a given porosity could be misinterpreted as pore shape variations (Kittridge, 2015).

The samples analysed in this study show distinct variations in mineralogy, with a wide range in carbonate content. An increase in acoustic velocity was observed between siliciclastic – siliceous rocks (MFT-1, MFT-2, MFT-3 and MFT-4; ~5.3 km/s) and limestones (MFT-7, MFT-8 and MFT-9; ~5.8 km/s). Dolostones (MFT-10) display even higher velocities as a consequence of their recrystallized character and grain density (Anselmetti and Eberli, 2001) (Figs. 3.7, 3.8).

Table 3.3 Theoretical mineral properties of water, quartz, calcite, and dolomite (Mavko et al., 2009).

Mineral	Density g/cc	P-wave velocity km/s	S-wave velocity km/s
Water	1.04	1.50	-
Quartz	2.65	6.05	4.09
Calcite	2.71	6.64	3.44
Dolomite	2.87	7.34	3.96

This mineralogical relationship is consistent with the data of Anselmetti and Eberli (1993) and Kenter et al. (1997b), who showed that, for a specified porosity, carbonates have higher velocities than siliciclastics. Theoretical velocity values (Table 3.3) for pure mineralogies are consistent with these results (Mavko et al., 2009).

The clay content of the Permian and Carboniferous samples analysed did not exceed 12.7% (Fig. 3.10). Braaksma et al. (2003) proposed that there is a strong velocity decrease with clay contents up to 12% followed by fairly constant velocity values with higher clay contents. However, the clear negative relationship described by Braaksma et al. (2003) was not observed in the samples analysed. The multivariate regression analysis shows that only a

minor relationship exists between the clay content and the P-wave velocity (Table 3.4).

Han et al. (1986) showed that clay content (by volume) reduces P-wave velocities, and proposed that these values are independent of pressure. This contrasts with Hossain and Zhou (2015), who measured a velocity increase with increasing clay content up to a threshold of 15% followed by a slight decrease. However in the samples analysed in this study, the P-wave velocity remained the same with an increasing clay fraction from 0% to 12.7% (Fig. 3.10). The absence of this trend can be explained by the impact of more important factors (Table 3.4) such as carbonate content and porosity which might obscure the negative effect of the clay content on the P-wave velocity.

3.6.3 Texture and fabric

In siliciclastics rocks, the main parameters determining the velocity-density relationship are sediment sorting and composition (Vernik and Nur, 1992; Braaksma et al., 2003). In the present study, the texture of the siliciclastic and siliceous sediments was described according to grain shape, size and distribution. The texture of carbonate sediments was described using the Dunham (1962) classification.

The mean grain size of the non-organic sediment fraction in the samples analysed ranged from very fine-grained silt to medium-grained sand (8 to 1 on the Wentworth scale: Wentworth, 1922). In the silica-dominated samples (non-organic fraction > 80%) saturated P-wave values range from 4.605 to 5.711 km/s; sample KF-2.12.1 falls outside of this range due to its high porosity. The narrow range in P-wave values partly relates to the clay and silt contents, with a maximum clay fraction of 12.7% (Fig. 3.10A) and a maximum silt fraction of 57.4% (Fig. 3.10B). An increase of the sand fraction is related to a decrease in P-wave velocity (Fig. 3.10C). This increase in sand fraction corresponds to a decreasing proportion of carbonate, and thus a decrease in velocity. Finally, the mean grain size, according to the Wentworth scale, does not show any relation to P-wave velocity (Fig. 3.10D). Diagenetic alterations can change the texture and mineralogy of sedimentary rocks (e.g. from aragonite to calcite to dolomite) (Eberli et al., 2003). The dolomitized samples show relatively high velocities (Figs. 3.7, 3.8). Seismic velocities in dolomitized rocks may vary depending on the dolomitization process affecting the sediments. For a constant porosity, fabric-destructive dolomitization results in a slight increase in velocities, while fabric-preserving dolomitization will result in a significant increase in velocities (Anselmetti and Eberli, 2001). The dolomitized samples analysed (MFT-10) show higher velocity values compared to the non-dolomitized samples, but values are not close to the

theoretical velocity of the dolomite mineral (Table 3.3). Verwer et al. (2008) proposed that in granular carbonate rocks, the depositional grains are the principal medium for acoustic-wave propagation. By contrast, in crystalline rocks this medium is provided by the framework of interlocking crystals formed during diagenetic modification.

Some samples analysed were chertified, resulting in an increase in acoustic velocities (Hossain and Zhou, 2015). With a few exceptions due to high porosities, the siliceous (MFT-4) and mixed sediments (MFT-4 and MFT-6) as well as partly silicified limestones (MFT-9) show consistent velocities. These measured velocities are slightly higher compared to their non-silicified counterparts (Fig. 3.7).

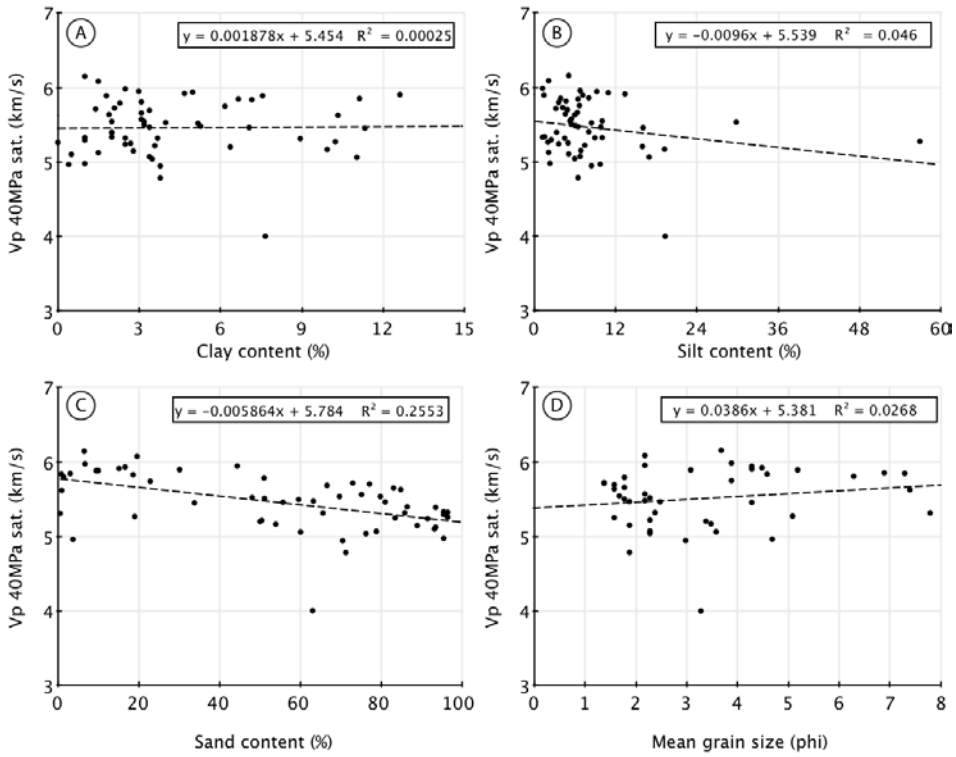

Fig. 3.10 Plots of Gassmann saturated P-wave velocity versus clay content (A), silt content (B), sand content (C) and mean grain size (D). The dashed trend lines in black show low correlation coefficients for all the cross-plots.

Hossain and Zhou (2015) demonstrated that an increase in cement was accompanied by a decrease in porosity but an increase in velocity. Blocky sparite was common in the pack- to grainstones facies (MFT-8), which show higher acoustic velocities than the microbial bindstones (MFT-7) (Fig. 3.7).

These observations are in agreement with the results of Kleipool et al. (2015), who showed that sediments with the same quartz-calcite ratio may differ in acoustic properties, and that cemented sediments show higher acoustic velocity values than micrite-supported sediments.

3.6.4 Pressure

At low effective pressures (2.5–10 MPa), most of the measured samples show a non-linear increase in acoustic velocities (Fig. 3.5), which could be attributed to improved grain contact and closure of cracks and pores (Gardner et al., 1974; Vernik and Nur, 1992). At effective pressures of 10–40 MPa, the majority of the samples display a linear relationship between pressure and velocity, indicating that at pressures of about 10 MPa most of the fractures and pores are closed (Bourbié et al., 1987); above this value, the terminal velocity, porosity reduction from pore closure is very minor (Vernik and Nur, 1992). No decreases in velocity during increasing pressures were observed, suggesting that stress-induced cracking and fracturing did not occur during the experiment.

At 40 MPa, the range in dry P-wave velocities (3.760 - 6.884 km/s) is primarily caused by variations in mineralogy and to a lesser extent by the amount and type of porosity. Since the dataset covers a low-porosity domain, the effect of compaction on the acoustic properties is minor. The acoustic velocities of datasets with high porosity domains may have a bigger chance of being affected by an increase in pressure (Anselmetti and Eberli, 1993).

3.6.5 P- to S-wave ratio

The P- to S-wave ratio can be used as a proxy in defining the mineral composition of low porosity mixed siliciclastics and limestones (e.g. Kleipool et al., 2015). Theoretical P- and S-wave values can be modelled for a wide spectrum of calcite quartz ratios and for varying porosity (Castagna, 1993).

The measured P- to S-wave ratios in the samples analysed fall within the ranges of the modelled lines obtained using the Castagna (1993) models (Fig. 3.11). In Fig. 3.11A, the carbonate content matches the colour-coding of the modelled lines, with the exception of the dolostone samples which lie outside of these ranges. These out-of-range measurements are in accordance with Castagna (1993) who indicated a unique P- to S-wave ratio for dolomite. Overall, P-wave velocities show a positive relationship with increasing carbonate content while S-wave velocities illustrate a negative trend.

Other colour-codings were used for porosity (Fig. 3.11B), clay content (Fig. 3.11C) and the average grain size (Fig. 3.11D). Since the majority of the measured porosities range from 0% to 5%, it is difficult to quantify the porosity-effect on the P- to S-wave ratio. The clay content and grain size

distribution show a slight colour separation. Blue-coloured data points that are linked to low-clay content (Fig. 3.11C) and high mean grain sizes (low phi-values; Fig. 3.11D) show lower P- to S-wave ratios.

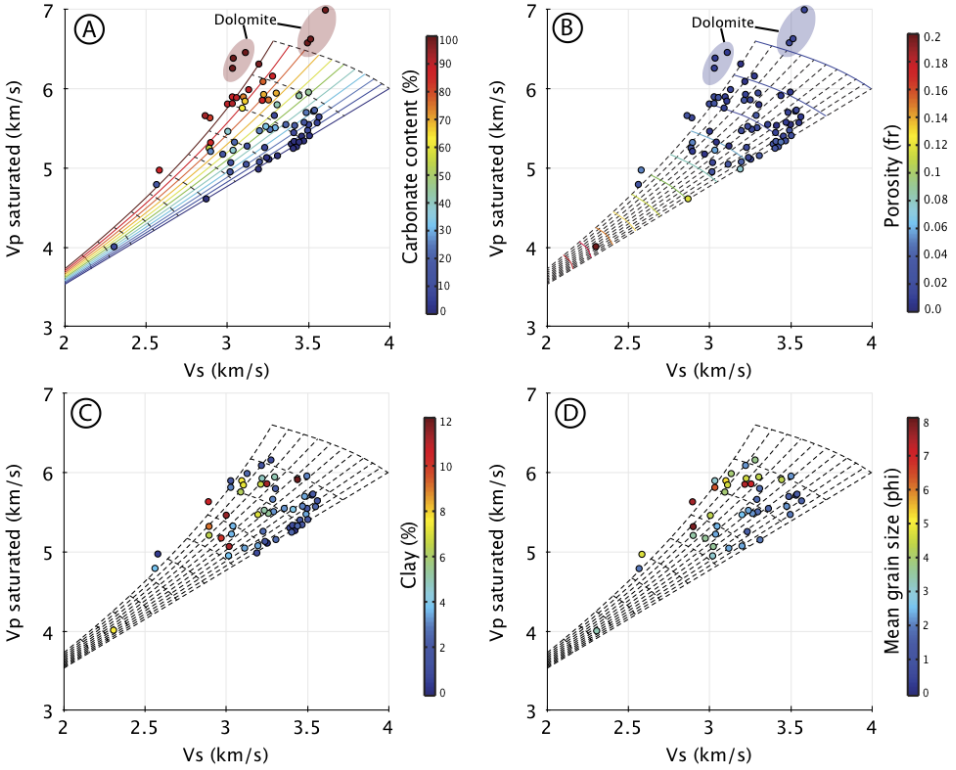

Fig. 3.11 Plots of Gassmann saturated P-wave velocity versus S-wave velocity at 40 MPa. The superimposed colour schemes respectively display carbonate content **(A)**, porosity **(B)**, clay content **(C)**, and mean grain size **(D)**. The modelled lines are derived from Castagna (1993) and the Wyllie time average equation (WTA) (Table 3.3), and in combination can be used to predict the P- and S-wave velocities for a given porosity and carbonate content**.**

3.6.6 Multivariate regression analysis

The statistical analysis confirms the discussion above, and shows that carbonate content has the highest impact on the saturated P-wave velocity. The amount of porosity and bulk density also play an important role when predicting the saturated P-wave velocity; however, porosity has a negative effect (Table 3.4).

Clay content is the fourth important factor, showing a negative relation with the saturated P-wave velocity. The amount of fractures (open /closed) is the

final important factor. The remainder factors are statistically less significant, and have minor effects on saturated P-wave velocity.

Table 3.4 Results of the multivariate regression analysis. The predictor factors are arranged by their impact on the saturated P-wave velocity; the Carbonate fraction has the highest impact, and Mouldic/Vug pores the lowest. The grain density, non-organic fraction, facies, and sand fraction are not displayed in this overview because their correlative factors were too high after multiple iterations. Skewness and Kurtosis display the geometry of the data distribution. The variance inflation factors (VIF) show the degree of multi-colinearity between predictors. The coefficient value (Coefficient) represents the mean change in the saturated P-wave velocity for one unit of change in the predictor factor, keeping the other predictors in the model constant. The significance of the relationship between the predictor factor and saturated P-wave velocity is displayed by the t value. The standardized coefficient (Beta) enables a comparison of the factors influencing the saturated P wave velocity.

Predictor factors	Skewness	Kurtosis	VIF	Coef.	t value	Beta
Carbonate content	0.11	0.00	4.21	0.005	3.510	0.411
Porosity	0.00	0.00	5.43	-0.050	-2.250	-0.299
Bulk density	0.00	0.00	7.87	1.252	1.690	0.270
Clay content	0.00	0.46	2.10	-0.029	-2.360	-0.195
Fracture (open/close)	0.53	0.00	1.39	0.050	1.720	0.115
Silt content	0.00	0.00	2.05	-0.002	-0.820	-0.067
Grain size	0.00	0.66	3.60	0.015	0.510	0.054
Inter particle pores	0.00	0.64	1.60	-0.022	-0.470	-0.033
TOC	0.00	0.08	1.80	0.024	0.250	0.018
Moldic/Vug pores	0.00	0.01	1.22	0.004	0.090	0.005
Dependent variable:	P-wave velocity (40MPa)					
Number of samples:	73					
R-squared:	0.79					

3.6.7 Summary

The data show that the petrophysical properties agree well with the microfacies classification (Table 3.1; Figs. 3.7, 3.12). Siliciclastic and siliceous microfacies (clay- to siltstones, sandstones, conglomerates and some spiculitic cherts; MFT 1-4) show the lowest P-wave velocities. Limestone microfacies (microbial bindstones, pack- to grainstones and rudstones; MFT 7-9) and tight recrystallized dolostones (MFT-10) have the highest velocities in combination with fairly low porosities (Fig. 3.12).

The multivariate analysis demonstrates that within low-porous mixed microfacies (0-5%), the carbonate - silica ratio is the most important factor determining the variations in acoustic properties (Figs. 3.7, 3.8; Table 3.4).

Due to the narrow porosity range of the bulk dataset, the impact of porosity on the acoustic velocities is obscured. The six high porosity samples (porosity > 5%), however, show lower acoustic velocities.

Pore types were difficult to determine due to the scarcity of visible pores. The Xu and Payne (2009) model implies that most porosity occurs as non-visible micropores and cracks reducing P-wave velocity (Fig. 3.9). The multivariate regression analysis shows that the amount of visible fractures, which are predominantly filled by calcite cement, has a positive impact on velocity.

The dataset shows that diagenetic processes (dissolution, cementation, dolomitization and chertification) affect the mineralogical composition and the amount and type of porosity. The acoustic velocities of the mixed (MFT-4-6) and carbonate-dominated microfacies (MFT-7-9) were significantly affected by velocity-enhancing diagenetic modification e.g. dolomitization, chertification and cementation. However, this qualitative effect is not reflected in multivariate statistical analysis (Figs. 3.7, 3.8; Table 3.4).

The rock texture is partly defined by the grain size analysis, which quantifies the amount of clay fragments based on their size and occurrence, while clay fragments are also defined as a different type of mineral. The multivariate regression analysis shows that clay content plays a negative role controlling the saturated P-wave velocity. This negative effect is not present in the cross-plot (Fig. 3.10A). This inconsistency might result from the composite effect of other factors such as carbonate content and porosity.

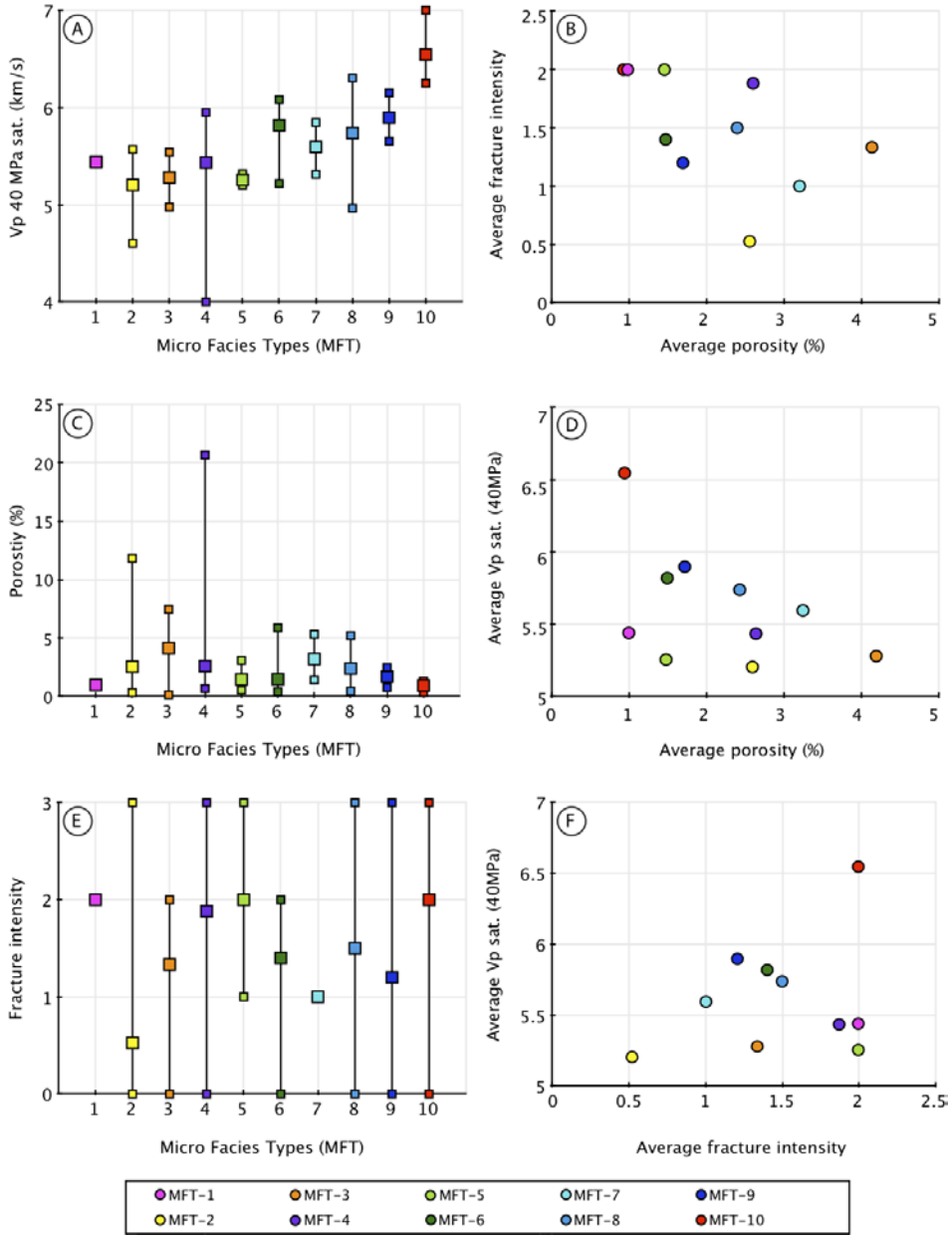

Fig. 3.12 P-wave velocity **(A)**, porosity **(C)** and fracture intensity **(E)** domains are arranged by microfacies type (MFT). The small squares indicate the maximum and minimum values measured; the large squares relate to the average value of the specific MFT. The average porosity of each MFT is plotted against the average

fracture intensity **(B)** and average P-wave velocity **(D)** measured. In **(F)**, the average P-wave velocity is plotted against the average fracture intensity.

3.6.8 Comparison with other mixed carbonate and non-carbonate deposits

Previous studies of mixed carbonate and non-carbonate successions focused on sediments with moderate to high porosities. A study of carbonates with variable porosity (9 to 56%) in the subsurface of Florida (Anselmetti et al., 1997) demonstrated that porosity, primary pore type, and quartz and dolomite content were the main controls on seismic velocities.

Kenter et al. (1997b) investigated Permian shelf-margin mixed sediments in the upper San Andres Formation, New Mexico, which had porosities up to 23%. They found that observed variations in sonic velocity were related to pore type (mouldic, vuggy, fractures) and to the carbonate-siliciclastic ratio.

Braaksma et al. (2003, 2006) studied a Jurassic ramp system (Boulonnais, northern France) including coastal plain sand- and mudstones, shallow-marine sandstones and shelf mudstones, and found that the acoustic properties of the sediments were mainly controlled by porosity and to a lesser extent by carbonate or clay content.

Zeller et al. (2015a, 2015b) distinguished three lithological groups (carbonates, sandstones and shales) in a mixed shelf succession in the Neuquén Basin (Argentina). These lithologies had different petrophysical signatures which were used for synthetic seismic modelling. Measured porosities ranged from 0 to 20% with a peak around 5%, which is relatively similar to the range of the samples analysed in the present study.

Consistent with the results of the present study, the discriminating factor dividing the Neuquén dataset of Zeller et al. (2015a, 2015b) was mineralogy (lithological variation). The petrophysical properties of carbonates, sandstones and shales occupy slightly overlapping domains in a P-wave velocity versus porosity cross-plot with low porosities (which had a small range) and high acoustic velocities for carbonates, an intermediate spread in acoustic velocities and porosities for sandstones, and low velocities and variable porosities for shales (see Fig. 3.10 of Zeller et al., 2015a).

Finally, Kleipool et al. (2015) investigated an Upper Jurassic mixed siliciclastic-carbonate ramp system in Ricla (NE Spain), and showed the dominant influence of the siliciclastic – carbonate ratio on the acoustic properties of the rocks.

3.6.9 Spiculitic chert reservoir analogues

Bio-siliceous sediments composed of skeletons and spicules of silica-secreting organisms can be reservoir and source rocks for hydrocarbons (Rogers and Longman, 2001) or may host base metals (Iijima et al., 1983). Porous spiculitic

cherts form reservoir rocks in unit L-9 of the Tempelfjorden Group of the Finnmark
Platform (Norwegian Barents Sea; Ehrenberg et al., 2001) which is time-equivalent to the Kapp Starostin Formation studied at outcrop in Spitsbergen; and also in the Lower Devonian Thirtyone Formation in west Texas (Saller et al., 1991; Ruppel and Hovorka, 1995; Montgomery, 1998).
In the samples analysed in this study, light-coloured spiculitic cherts (MFT-4) are characterized by macrospicules embedded in micrite/microspar matrix, which are altered by complex early diagenetic processes including spicule dissolution and reprecipitation as chalcedony/chert cement. In the Thirtyone Formation, a similar facies is interpreted as a gravity-flow deposit, which accumulated in the upper slope and in topographic lows. In unit L-9 and the Kapp Starostin Formation, the facies is interpreted to have been deposited in well-oxygenated waters around and just below the storm wave base.
In unit L-9 and the Thirtyone Formation, spiculitic cherts show high porosity values (10–30%) with multiple pore types (mouldic, vuggy, fracture, interparticle and intercrystalline) with a wide range of permeabilities. In the present study, the average porosity of the spiculitic chert facies (MFT-4) is 2.6% (Table 3.2). Cracks and micropores are the dominant pore types. Silicification and cementation of the primary pore system combined with the high micrite content of the sediments resulted in low porosity values and high acoustic velocities (Figs. 3.7, 3.8). One sample shows a high porosity (20.7%; KF-2.12.1), possibly due to porosity-enhancing diagenetic processes or fracturing.
Porosity has a major effect on acoustic velocities; therefore a porosity increase usually leads to a velocity decrease (Anselmetti and Eberli, 2001). A combination of silicification and poor grain-sorting resulted in loss of porosity and therefore an increase in acoustic velocity. It seems that the sorting of the spiculites is better in unit L-9 and the Thirtyone Formation than in our dataset, and has resulted in high porosity and therefore low velocity. In addition, fracturing and geochemical alteration such as meteoric and marinephreatic diagenesis enhanced the porosity in both formations.

3.6.10 Carbonate reservoir analogues

In the Upper Carboniferous to upper Lower Permian of the Sverdrup Basin (Canadian Arctic Archipelago) and the Hammerfest Basin (Norwegian Arctic Shelf), reefal build-ups occur along the margins of the carbonate platforms. The majority of the mud-rich and tightly cemented reefal carbonates underwent porosity-enhancing dolomitization and developed into potential reservoir rocks (Beauchamp et al., 2010). Stemmerik et al. (1999) described porosity ranges of 0% to 5% for the tight limestones and 5% to 30% for the

dolomitized inner shelf facies which developed on the Finnmark Platform. Low matrix permeabilities were recorded, but intense fracturing resulted in high permeabilities.
The Wordiekammen Formation in the present study area comprises a diversity of in situ reefal build-ups and bioclastic intervals with fragments of corals and bryozoans (Blomeier et al., 2009). The nature of the dolomitization process and the associated pore characteristics determine the acoustic velocity of carbonates (Anselmetti and Eberli, 2001). The high-velocity, low-porosity dolostones (MFT-10) in the samples analysed show an average porosity of 0.9% and hence cannot be considered as potential reservoir rocks. Replacement dolomitization produced interlocking crystals and converted the limestones into dense dolostones. This contrasts with the reefal carbonate build-ups in the Sverdrup Basin, which also show fabric-destructive dolomitization. However, little recrystallization occurred and dolomitization resulted in porosity enhancement (Beauchamp and Desrochers, 1997; Stemmerik et al., 1999; Beauchamp and Olchowy, 2003) resulting in lower velocities. The difference in alteration processes causes a petrophyscial contrast between the present data from Spitsbergen (Figs. 3.7, 3.8) and the carbonate build-ups from the Sverdrup Basin.

3.7 Conclusions

The analysed Late Carboniferous – Late Permian mixed carbonate and non-carbonate sediments are characterized by a low average porosity of 2.2%, although the dataset ranges from 0.1 to 20.7%. The measured saturated P-wave velocities range from 4.001 to 7.005 km/s. Multivariate regression analyses suggests that these variations in acoustic properties are primarily caused by the mineralogical composition of the samples, followed by the porosity and bulk density. The clay fraction and the presence of fractures are of secondary importance, while the pore type, average grain size, silt fraction and TOC only show a minor effect on the saturated P-wave velocities. Other factors such as grain density, non-organic fraction, type of facies, and sand fraction are highly correlative and could not therefore be integrated in the statistical analysis.
The results of this study are consistent with previous outcrop studies of mixed siliciclastic – carbonate systems, including in the Neuquén Basin (Argentina) and the Upper Jurassic Ricla ramp system (NE Spain).
The studied mixed carbonate and non-carbonate sediments show similar facies patterns to subsurface reservoir rocks in the Permian Basin (West Texas), the

Sverdrup Basin (Canadian Arctic), the Finnmark Platform and the Hammerfest Basin (Norwegian Barents Sea). The physical properties of the rocks, however, show some differences. The porosity in the studied dolostones was reduced due to dolomitization processes, while porosity in the dolostones in the Sverdrup and Hammerfest Basins was enhanced as a result of dolomitization. The poor sorting of spiculite facies analyed in the present study, in combination with diagenetic alteration, has resulted in low porosities. This contrasts with the spiculites facies in the Permian Basin and Finnmark Platform (Norwegian Barents Sea), in which porosity is controlled by depositional facies, fracturing and diagenetic processes.

3.8 Acknowledgements

We acknowledge the VU University Amsterdam, Bremen University and the Norwegian Polar Institute for their financial support. We thank MSc. Students Ralph Groen, Mahtab Mozafari and Jan Schneider of the VU University Amsterdam for their contributions; and Bouke Lacet and Wynanda Koot for preparing the thin-sections and plugs at the VU University Amsterdam. Koos de Jong is thanked for an extensive quality check of the petrophysical measurements. Finally, Michael Zeller (Statoil), an anonymous reviewer and Christopher Tiratsoo (JPG) are thanked for their constructive comments and suggestions which significantly improved the paper.

Chapter 4

Synthetic seismic model of a Permian biosiliceous carbonate–carbonate depositional system

E. Jafarian
K. De Jong
L. M. Kleipool
C. Scheibner
D.P.G. Blomeier
J.J.G. Reijmer

Chapter based on: (Final revision) Synthetic seismic model of a Permian biosiliceous carbonate – carbonate depositional system (Spitsbergen, Svalbard Archipelago). Manuscript submitted to "Marine and Petroleum Geology".

4.1 Abstract

The non-unique correspondence between seismic and subsurface geology is a fundamental problem when interpreting seismic data sets. Synthetic seismic models of outcrop analogs are commonly constructed to cover the gap between the small-scale outcrop observations in the field and low-resolution seismic data.
The Permian biosiliceous carbonate – carbonate sediments on Spitsbergen are characterized by a wide variability in lithologies and microfacies determining the petrophysical properties (e.g., porosity, acoustic properties) that consequently complicate seismic interpretation. This study uses 1D and 2D synthetic seismic modelling techniques (at different resolutions) to gain an understanding of how seismic reflectors are expressed with respect to the sediment distribution, aiming to facilitate real seismic interpretation.
In the study area, nine microfacies were defined that were used to produce a geological model (GM) displaying small-scale microfacies variations within a well-defined sequence stratigraphic framework. Laboratory derived petrophysical properties (Vp, ρBulk and AI) were assigned to each predefined microfacies body in the geological models in order to construct acoustic impedance models that were used to produce synthetic seismograms.
The appearance of the seismic reflectors in the synthetic seismic profiles is primarily controlled by changes in mineral composition and link to spatial microfacies distributions within the depositional sequences. Differences in acoustic impedance and the origin of synthetic seismic reflections within a single microfacies type are mainly caused by porosity contrasts (varying between 5 and 20%) and diagenetic modifications such as chertification and cementation. This detailed information cannot be derived from the low-frequency seismograms (25 to 100 Hz) resulting in changes in seismic expression when seismic resolution diminishes.
Comparison with time equivalent, real and synthetic seismic data of the Finnmark Platform reveals similarities with the synthetic seismic reflection patterns of Spitsbergen. In both areas, the pronounced seismic traces follow abrupt microfacies transitions, which are coherent with cycle boundaries and timelines.

4.2 Introduction

Field-based studies are fundamental for understanding sedimentary systems e.g., geometry, the lateral and vertical heterogeneity of the sediments.

Continuous exposures allow for observations at all scales (mm to km) and provide insights into the small-scale heterogeneities within a sequence stratigraphic framework (Janson et al., 2007; Schwab et al., 2007; Zeller et al., 2014). An outcrop-based analysis is the most convenient method to identify the best exploration and production techniques in the hydrocarbon industry. Synthetic seismic models derived from outcrop studies can be of use for comparison with seismic datasets (Zeller et al., 2014, 2015a).

Accurate interpretation of low-resolution seismic data is one of the main factors of successful hydrocarbon exploration programs (Bacon et al., 2007). However, indirect measurements of seismic data and mostly incorrect prediction of subsurface geology are the fundamental potential problems in seismic interpretation (May and Hron, 1978; Alves et al., 2014). A method to calibrate and ground-truth seismic analysis is to construct synthetic seismic models resulting from a predefined geological framework and associated petrophysical data obtained from outcrops. These models can not only fill the gap between high-resolution outcrop observations and low-resolution seismic data, but can also answer questions related to the origin of the seismic reflectors (Bracco Gartner, 2000; Kenter et al., 2001; Janson et al., 2007; Schwab et al., 2007; Falivene et al., 2010; Kleipool et al., 2015; Zeller et al., 2015a).

1D synthetic seismic traces provide the direct comparison of the seismic response and the associated rock properties. 2D synthetic seismic profiles resulting from a sequence stratigraphic framework allows for comparison with real seismic data (Hodgetts and Howell, 2000).

The usability of the seismic outcrop modelling is validated by a comparison with real seismic data of comparable sedimentary systems. This analogy can help to understand to what extent subsurface and outcrop are similar, and how much information from the outcrop can be used for reservoir models. (Ravenne and Vially, 1988; Jacquin et al., 1991; Bracco Gartner, 2000; Schwab et al., 2007; Falivene et al., 2010).

This study focuses on three selected outcrops, sections Kapp Fleur de Lys (KF); Idodalen (ID); and Tålmodryggen (TR), on Spitsbergen (Svalbard Archipelago, Norway). The outcrops cover the Permian biosiliceous carbonate-to-carbonate succession of the Gipshuken and Kapp Starostin Formations representing two different carbonate factories. From bottom to top they are: (i) a tropical factory (T-factory, Schlager, 2005) with a photozoan microfacies association e.g., green algae and benthic foraminifera; and (ii) a cool and cold-water factory (C-factory, Schlager, 2005) with associated heterozoan biota, e.g., brachiopods, bryozoans, echinoderms, and siliceous sponges. The carbonates formed by the T-factory show a flat-topped platform geometry with a shallow-water lagoon and steep slopes. The carbonates associated with the C-factory lack platform

rims and tend to form seaward sloping profiles in equilibrium with wave action, resulting in a ramp-type morphology with spiculitic mound structures.
The petrophysical properties, depositional setting and sequence stratigraphy of the investigated area have been studied in detail (Ehrenberg et al., 2001; Blomeier et al., 2011, 2013; Jafarian et al., 2017b) and were used as primary input for the synthetic seismic analysis. The seismic models were produced using multiple frequencies (25, 35, 50, 100, 200, and 400 Hz). The output is compared with the microfacies, rock property distribution and the general stratigraphic framework exposed in the outcrop. This comparison is used to examine the ability of seismic frequencies to resolve outcrop observations and will help to explain how much of the lithologic information ideally can be obtained from seismic data (Janson et al., 2007; Kleipool et al., 2017).
The biosiliceous and carbonate sediments researched are marked by a wide variability of petrophysical properties (porosity, density, and acoustic properties), which complicate seismic interpretations (Jafarian et al., 2017a). These deposits are reservoir rocks in various basins, e.g., the Permian Basin (West Texas; Montgomery, 1998) and the Finnmark Platform (Norwegian Barents Sea; Ehrenberg et al., 2001; Colpaert et al., 2007). Therefore, this study will be of benefit in understanding the seismic expression of the biosiliceous carbonate – carbonate succession and, the link between the sedimentological and petrophysical properties to seismic data in reservoir analogues.

4.3 Geological Setting

During the Upper Palaeozoic, the Franklinian epicontinental shelf was situated at the northern rim of Pangea. It was arranged into a series of platforms and basins, e.g., Svalbard, the Finnmark Platform, and Stappen High (Barents Sea), the Wandel Sea Basin (eastern North Greenland), the Sverdrup Basin (Arctic Canada) and the Timan-Pechora Basin (Russia). This platform-basin configuration gradually moved from nearly low-latitude position at 25°N in the Upper Carboniferous to a more northern position at approximately 45°N in the Upper Permian (Scotese and Langford, 1995; Golonka, 2002).
Spitsbergen is the main island of the Svalbard archipelago (Fig. 4.1A) and shows a well-exposed upper Palaeozoic sedimentary succession comprising: the Early Carboniferous to Early Permian Gipsdalen Group and the Early to Late Permian Tempelfjorden Group (Fig. 4.1B) (Nakrem et al., 1992).
The Templet Member is the top part of the Gipshuken Formation (upper formation of the Gipsdalen Group) in central Spitsbergen and shows the deposition of evaporite/carbonate cycles indicating restricted, peritidal platform settings and sabkha (Dallmann et al., 1999). Lower Permian

(Artinskian) sediments related to the regressive phase are observed in the Templet Member tops and are marked by intensely altered intraformational clasts embedded in fine-grained sediment or blocky sparite representing an exposure surface (Fig. 4.1B) (Ehrenberg et al., 2001; Groen, 2010; Blomeier et al., 2011).

The Tempelfjorden Group comprises the Kapp Starostin Formation in central and NE Spitsbergen as well as Nordaustlandet (Fig. 4.1B). It starts with the Vøringen Member (except the Brøggerhalvøya) that is marked by heterozoan limestones (brachiopods, echinoderms, bryozoans) accumulating in cool-water conditions of a nearshore setting during a marine transgression (Blomeier et al., 2011, 2013). The member is succeeded by spiculitic cherts representing cold and deep-water environments, which are associated with a number of palaeogeographic (closure of the Ural Ocean) and palaeoceanographic variations (upwelling of cold, nutrient-rich deep waters) (Stemmerik and Worsley, 1989; Beauchamp, 1994; Blomeier et al., 2011, 2013).

In central Spitsbergen, the upper part of the Kapp Starostin strata is described as the Stensiöfjellet Member which is composed of glauconitic sandstones, limestones and spiculitic cherts representing nearshore deposition (Fig. 4.1B) (Dallmann et al., 1999). The transition of the Stensiöfjellet deposits to the overlying Sassendalen Group (Triassic) is characterized by a rapid shift to marine siliciclastics (shales, siltstones and to a lesser extent sandstones) (Dallmann et al., 1999; Blomeier et al., 2011).

4.4 Methods

4.4.1 Input parameter

Previous work on Svalbard comprised detailed field and laboratory analyses to study the Templet strata and the Kapp Starostin successions (Ehrenberg et al., 2001; Blomeier et al., 2011, 2013; Jafarian et al., 2017a, b). Geological parameters such as microfacies characteristics, stratigraphic framework, and petrophysical properties (sonic velocity, porosity, and bulk density) were acquired from sections described during earlier studies. This information was used as input to construct a geological model (GM), an acoustic impedance model (AIM) and resulting 1D and 2D synthetic seismic models.

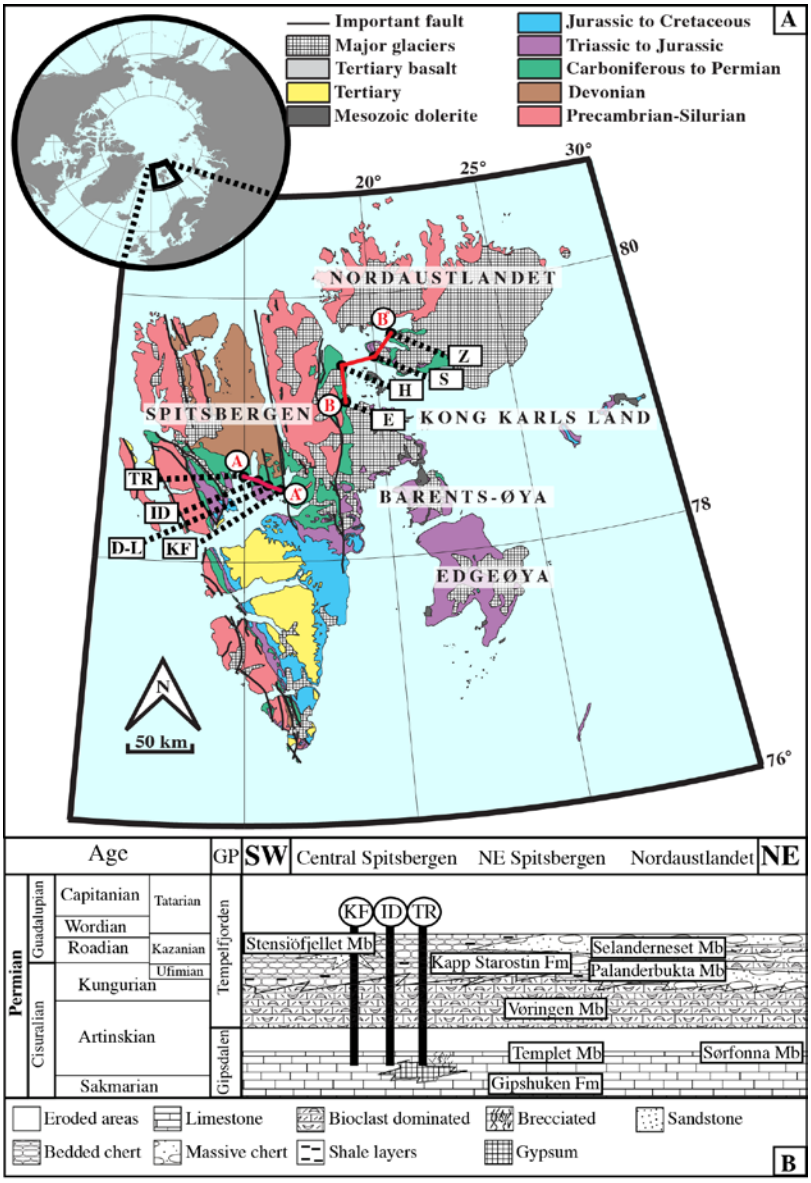

Fig. 4.1 A) Geological map of the Svalbard archipelago. Strata studied for this paper are of the Permian age indicated with the green shaded parts on the map. Sections location on central Spitsbergen (Kapp Fleur de Lys (KF); Idodalen (ID); Tålmodryggen (TR): present study; and Dickson Land (D-L): Ehrenberg et al., 2001) and NE Svalbard (Eremitten (E); Hódbreen (H); Selanderneset (S); Zeipelfjella (Z): Blomeier et al., 2011, 2013) are indicated. A-A" and B-B" indicate cross-sections used for the geological profiles in figs. 4.4 and 4.5. (Modified from http: //npolar.no/geonet/items general/frame.html). B) Chronostratigraphic framework and main lithologies in the Permian succession of Svalbard (adapted from Dallmann et al., 1999) with a schematic overview of the stratigraphic positions of the studied sections and formations.

4.4.2 Geological framework

During fieldwork in central Spitsbergen, three sections, Kapp Fleur de Lys (KF); Idodalen (ID); and Tålmodryggen (TR), have been measured (e.g., lithology, components, sedimentary structures, and colour) that ranging in thickness from 97m to 139m. Based on thermogravimetric analysis (TGA) and thin section analyses (texture and composition) on 39 samples collected from the sections, nine different microfacies were distinguished covering a proximal and distal part of the depositional system. Individual samples were used to characterize the vertical microfacies distribution in three stratigraphic sections from central Spitsbergen and provide a geological framework for 1D synthetic seismic logs.

The environmental microfacies interpretation was used to identify the relative water depth during deposition and to develop a sequence stratigraphic model for the measured sections. Based on the sedimentological observations (Bed-scale to outcrop-scale) and sequence stratigraphic correlations, the microfacies distribution panel over central Spitsbergen (section D-L: Ehrenberg et al., 2001; sections KF, ID, and TR: Jafarian et al., 2017b) and NE Svalbard outcrops (sections E, H, S, and Z: Blomeier et al., 2011, 2013) was established, which represents the geological model (GM).

The defined microfacies in the GM model were vertically extrapolated to reach an equal height, thus filling the eroded zones of the upper portion of the sections. Without the extrapolation, some areas would remain unfilled and seismic artefacts could show up (Kleipool et al., 2017). This model was used during the 2D synthetic seismic modelling and allowed comparison with real seismic data (Hodgetts and Howell, 2000).

4.4.3 Acoustic impedance model (AIM)

In order to construct synthetic seismic logs and profiles of outcrops, it is important to understand the petrophysical characteristics of the individual microfacies. The product of compressional velocity (Vp) and bulk density (ρBulk) is the acoustic impedance (AI) which is the key property controlling the seismic response (Stafleu, 1994).

Velocity values were measured under realistic subsurface confining pressure (40 MPa: representing around 1,5 km depth) to ensure that the terminal velocity of each sample is reached (Bourbié et al., 1987). In the subsurface, rocks are saturated with brine in nearly all settings. The Gassmann fluid substitution (Gassmann, 1951) predicts saturated compressional wave velocities. It assumes that shear moduli remain constant during fluid substitutions while many carbonate rocks show shear weakening or shear strengthening (Baechle et al., 2005; Adam et al., 2006). Due to this limitation of

the Gassmann theory we used dry P-wave velocities. Besides that, due to generally low porosity, fluids or gasses which can fill intergranular space within sedimentary rocks, are excluded. Thus, the dominant intergranular space is assigned to cement or micrite.

This biosiliceous – carbonate depositional system is marked by a wide variability in microfacies types. Hence, the average values of the dry P-wave velocity (at 40 MPa) and dry bulk density (ρBulk) of each defined microfacies were multiplied to calculate acoustic impedances (Eq. (1)).

(1) $AI = Vp * \rho Bulk$

Calculated averages of porosity, dry bulk density (ρBulk), dry P-wave velocity, and the acoustic impedance of each microfacies were assigned to the individual microfacies bodies in the GM to show the spatial distribution of petrophysical properties within sections. In some microfacies (MFTs-1, 2 and 6), only one sample was accessible. The acoustic impedance model (AIM) was used to create 2D synthetic seismic profiles.

To construct 1D synthetic seismic logs, vertical microfacies transitions in the sections (KF, ID, and TR) were used. The acoustic impedance values of each sample of the individual microfacies were calculated and assigned to the corresponding layers in the sections. Sampling gaps in the sections were populated with calculated impedance values based on their microfacies characteristics (colour, texture, grain size, components) provided by the detailed stratigraphic field logs.

4.4.4 Synthetic seismic modelling

Vertical changes in acoustic impedance are used to calculate the reflection coefficients (R) (Eq. (2)) (Stafleu et al., 1994). To create a link between the rock properties and real analogue seismic data, the vertical reflection coefficients (R) were convoluted to seismic traces using a zero-phase Ricker wavelet (Ricker, 1953) at various frequencies (25, 35, 50, 100, 200, and 400 Hz). The output was imported into SeisLab, an application written in MATLAB® (MathWorks, Natick, Massachusetts, USA) visualizing seismic models. To generate a continuous 2D seismic profile a series of 250 shotpoints are interpolated, the 1D synthetic seismic log is created from a single shotpoint.

(2) $R = \frac{AI2 - AI1}{AI2 + AI1}$

Zero-phase wavelets were selected because they have higher resolution than minimum phase wavelets and the peaks of Ricker wavelets are centred at the reflecting boundaries (Schoenberger, 1974).

In 1D and 2D seismic models, the increment in acoustic impedance is represented by hard-kick signals (positive peak; red) and decrease in acoustic impedance is characterized by soft-kick signals (negative peak; blue).

The vertical resolution of the high-frequency seismic signal was approximated at 3.5m (quarter wavelength criterion assuming 400 Hz peak frequency and 5500 m/s average velocity; (Eq. (3)), which decreased to about 55m when lowering the wavelet frequency to 25 Hz). The 25 to 50 Hz frequencies are commonly used in E&P industry, since they may reach potential hydrocarbon depths (Stafleu et al., 1994). The low-frequency synthetic seismic models are used for comparison with subsurface seismic data. The high-frequency wavelets (100 to 400 Hz) do not reach that depth but emphasize which features of the depositional setting such as microfacies distribution and geometry were overlooked with decreasing wavelet frequency.

$$(3) \qquad Wavelength\ (\lambda) = \frac{Velocity\ \left(\frac{m}{s}\right)}{Frequency\ (Hz)}$$

4.5 Results

4.5.1 Microfacies analyses

The studied succession covers a large variety of microfacies types. Nine microfacies types were recognized according to their lithology, texture, grain size, main components and consequently their depositional environment (Fig. 4.2). The following microfacies types were defined: MFT-1: Sandstones, MFT-2: Clay- to siltstones, MFT-3: Spiculitic massive cherts, MFT-4: Spiculitic bedded cherts, MFT-5: Coarse-grained, bryozoan limestones, MFT-6: Lithoclastic rudstones (carbonate breccias), MFT-7: Fine-grained, mixed-bioclastic limestones, MFT-8: Microbial limestones, MFT-9: Coarse-grained, brachiopod limestones. Table 4.1 provides more detailed information of the individual microfacies types, e.g., porosity, mineralogy, acoustic impedance. An extensive description of the microfacies can be found in Jafarian et al. (2017b).

4.5.2 Sections

Kapp Fleur de Lys section (Section KF):

At this location (Figs. 4.1 and 4.3), the Templet Member is marked by an alternation of microbial limestones and mudstones (MFT-8) that are succeeded by lithoclastic rudstones (carbonate breccias; MFT-6). It shows an increase in thickness when moving from Kapp Fleur de Lys section to Tålmodryggen section (Fig. 4.3). The contact of the Templet and the overlying Vøringen Members is not exposed (Groen, 2010; Jafarian et al., 2017b). The succeeding Vøringen Member comprises silicified, bioclastic limestones

(MFTs-7 and 9), which show a fining-upward trend. A monotonous series of bedded and massive cherts (MFTs-3 and 4) with claystone partings (MFT-2) characterizes the Kapp Starostin Formation. The uppermost part of this section shows a succession of chert units (MFTs-3 and 4) grading into silicified, bioclastic limestones (MFT-9) and glauconite-rich sandstones (MFT-1) constituting the Stensiöfjellet Member.

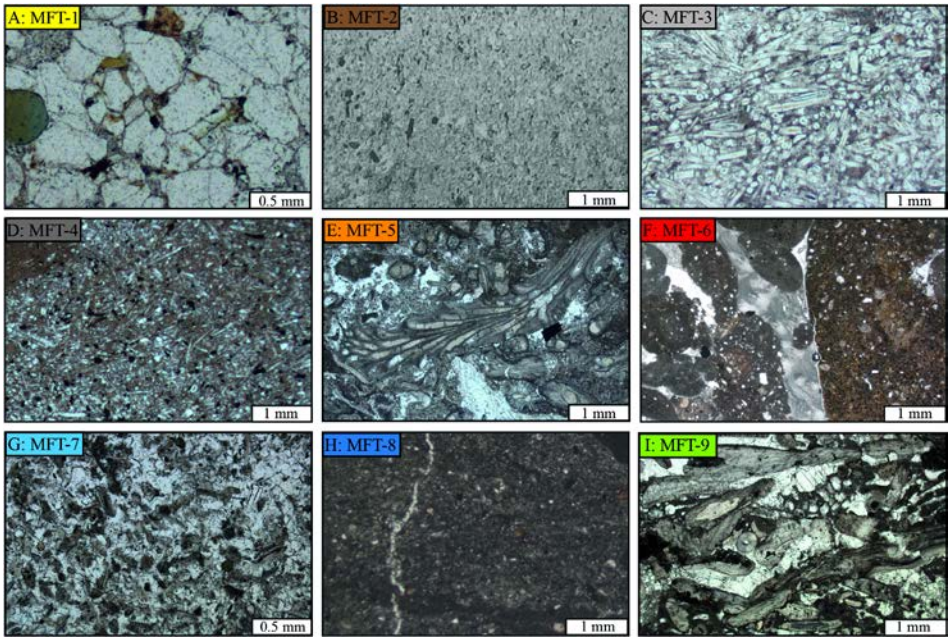

Fig. 4.2 Thin section photographs of each distinguished microfacies: A: MFT-1, Sandstones (Sk-1.41.1); B: MFT-2, Clay- to siltstones (FE-1.7.2); C: MFT-3, Spiculitic massive cherts (TR-1.62.1a); D: MFT-4, Spiculitic bedded cherts (TR-1.18.1); E: MFT-5, Coarse-grained, bryozoan limestones (ID-1.26.4); F: MFT-6, Lithoclastic rudstones (carbonate breccias) (TR-1.19.1); G: MFT-7, Fine-grained, mixed-bioclastic limestones (TR-1.18.1); H: MFT-8, Microbial limestones (ID-1.3.1); and I: MFT-9, Coarse-grained, brachiopod limestones (KF-1.9.1).

Table 4.1 Characteristics, occurrence, and environmental reconstruction of the microfacies types of central Spitsbergen.

MFT.No	MFT-Name	Carbonate range (%)	Porosity range (%)	Bulk density range (g/cc)	Vp (40MPa) (km/s)	Acoustic impedance range (Nsm^{-3})	Dominant pore type	Texture	Components	Occurrence	Depositional environments
MFT-1	Sandstones	0.4	11.8	2.35	4.46	10.5	Reference	Sandstone	Well-sorted, edge-rounded to rounded, sand-sized quartz grains, less than 5% glauconite minerals	Kapp Starostin Fm.	Represent alluvial to shore face conditions of the inner shelf
MFT-2	Clay- to siltstones	6.8	1.0	2.59	5.39	14.0	Crack	Clay- to siltstone	Components are not clear recognizable due to obliteration of primarily origin	Kapp Starostin Fm.	Reflect quiet environments, typically for the deep marine area of the outer ramp
MFT-3	Spiculitic massive cherts	6.5–25.9	0.7–20.7	2.08–2.61	3.76–5.70	7.83–14.83	Crack	Packstone to wackestone	Abundant megaspicules, arenitic to ruditic skeletal fragments (often heterozoan). Sediments are intensively silicified	Kapp Starostin Fm.	Form around and below the SWWB
MFT-4	Spiculitic bedded cherts	4.8–45.2	0.7–2.6	2.48–2.64	4.55–5.85	11.30–15.48	Crack	Packstone to wackestone	Abundance microspicules and burrows in micritic matrix. The deposits are affected by silicification	Kapp Starostin Fm.	Form in quiet water, low-energy conditions below the SWWB
MFT-5	Coarse-grained, bryozoan limestones	42.1–87.3	0.4–1.7	2.63–2.68	5.54–5.79	14.61–15.40	Crack	Floatstone to rudstone	Poorly sorted debris of bryozoans, echinoderms, occasional brachiopods and spicules of sponge. Matrix is composed of micrite/microsparite. Sparry-filled inter- and intraparticle voids present	Kapp Starostin Fm.	Form in distal mid ramp around the SWWB
MFT-6	Lithoclastic rudstones (carbonate breccias)	76.1	1.3	2.70	5.44	14.70	Reference	Rudstone	Abundant angular to well-rounded intraformational clasts embedded in micritic/microsparitic matrix. Locally blocky or sytaxial sparite cemens are present	Templet Mb., Vøringen Mb.	Within sabkha environments, the former deposits are influenced by erosion, reworking and redeposition in diverse degrees
MFT-7	Fine-grained, mixed-bioclastic limestones	37.9–97.6	0.5–5.9	2.50–2.69	4.48–6.16	11.50–16.64	Crack	Grainstone	Mainly fine to medium brachiopod shell debris and sometimes sponge spicules are cemented by blocky sparite	Vøringen Mb.	Form in agitated water conditions around the FWWB
MFT-8	Microbial limestones	82.1–88.1	1.4–5.3	2.57–2.68	4.99–5.59	12.80–14.70	Crack	Bindstone	Abundant Algal mats, dense micritic peloids and sand-sized, quartz grains in micritic matrix	Templet Mb.	Reflect marginal-marine, tidal flats of a warm-water carbonate platform
MFT-9	Coarse-grained, brachiopod limestones	87.3–93.1	1.1–2.5	2.63–2.66	5.36–5.68	14.17–14.95	Crack	Rudstone	Abundant coarse grained, well to poorly sorted, thick-shelled brachiopods, rare debris of bivalves, gastropods, trepostome bryozoans and echinoderms. Components mainly are cemented by sparite	Vøringen Mb.	Reflect high-energy, periodic storm events, during which the skeletal material was reworked and accumulated across the inner ramp (above FWWB)

Idodalen section (Section ID) and Tålmodryggen section (Section TR):
In sections ID and TR, the deposits of the Templet and Vøringen Members are lithological analogous to those outcropping in section KF (Figs. 4.1 and 4.3). However, in section TR, the Vøringen Member starts with a basal limestone breccia (MFT-6), which is absent in sections KF and ID (Fig. 4.3). This basal part is overlain by bioclastic cherty limestones (MFTs-7 and 9) and sandy horizons (MFT-1). In both localities (sections ID and TR), the deposits of the Kapp Starostin Formation continue with chert units (MFTs-3 and 4) and dark claystone horizons (MFT-2). The succession gradually shifts into silicified, heterozoan carbonates (MFT-5) which are less developed within section ID and not exposed at section KF.

4.5.3 Sequence stratigraphy

Based on the interpretations of depositional environments, the herein-defined microfacies are arranged in cyclic patterns developed by fluctuations of relative sea level (Fig. 4.3).
The Early to Late Permian (Artinskian to Kazanian) biosiliceous – carbonate succession on Spitsbergen shows a second-order cycle with a duration exceeding twenty Myr (Nichols, 1999), which can be subdivided into five third-order sequences (Jafarian et al., 2017b) (Fig. 4.3). The third-order parasequences (S0, S1, S2, S3, and S4) are packages of beds that demonstrate a progradational pattern with a thickness of several tens of meters and a range of one to ten Myr (Nichols, 1999). The boundaries of the parasequences (PSB1, PSB2, and PSB3) are marked by an abrupt rise in relative sea level followed by a sudden shift from shallow (e.g., carbonates and sandstones) to deep marine microfacies (e.g., claystones and cherts). The top of the shallowest unit is interpreted as the parasequence boundary. However, SB shows the boundary between the Templet (S0) and Vøringen (S1) Members, which is characterized by the lowest base level in the studied area and representing periods of subaerial exposure. This surface is interpreted as the sequence boundary and indicates a hiatus. PSB1 separates the Vøringen Member from the Kapp Starostin Formation (S2) and, PSB2 and PSB3 are positioned between the shallowest and deepest units within the Kapp Starostin strata.
The following parasequences were defined:

- (S0): This cycle comprises Templet Member developing in a marginal marine environment. It shows a progradational pattern, which is marked by microbial limestones (MFT-8) topped by carbonate breccias (MFT-6) and *Microcodium* bearing sediments suggesting periods of subaerial exposure (Fig. 4.3). Hence, the upper part of this regressive cycle is interpreted as an unconformity boundary (SB).

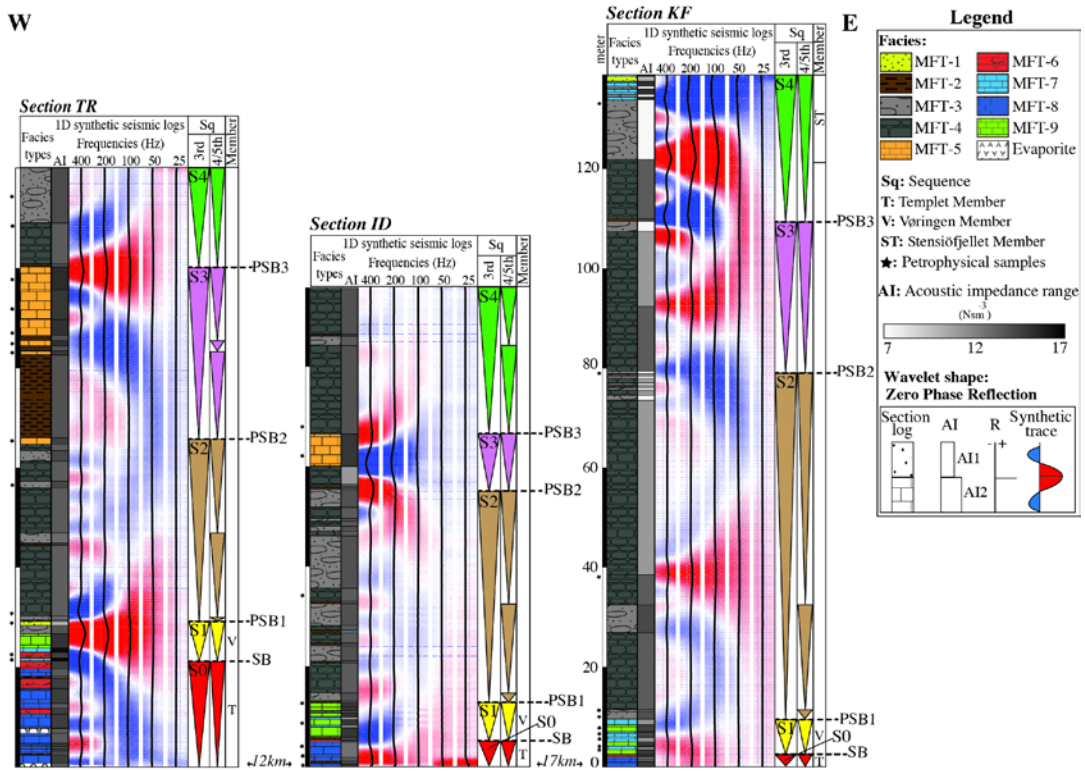

Fig. 4.3 A detailed overview of sedimentological sections (TR, ID, and KF) in central Spitsbergen showing thickness, main lithology, depositional cycles (third, fourth/fifth-orders) and sequence/parasequence boundaries (SB, PSB1, PSB2, and PSB3). Besides, acoustic impedance variations and 1D synthetic seismic traces are added. A Ricker wavelet (Ricker, 1953) is used with an array of different frequencies (25, 50, 100, 200, and 400 Hz). The red colours are positive signals (hard-kick) and blue colours are negative signals (soft-kick).

- (S1): This parasequence contains the Vøringen Member. At section ID (not exposed in section KF) this cycle is started with claystone horizon (MFT-2) that represents a substantial relative rise in sea level (Fig. 4.3). In section TR, heavily altered extraclasts (MFT-6) of older strata within the lower part of the Vøringen Member, indicate erosion of earlier deposits through high wave energy (during transgression) in the shallow-water area. The shallowing-upward trend is marked by coarse-grained, bioclastic limestones (MFT-9) (Groen, 2010; Blomeier et al., 2011). The occurrence of fine-grained, heterozoan limestones (MFT-7) at the top of this succession might record a renewed deepening of the depositional environment at the transition into the overlying parasequence.
- (S2, S3, and S4): Cycles S2, S3 and S4 in the Kapp Starostin Formation show a similar microfacies arrangement, from basal claystone horizon and bedded cherts (MFTs-2 and 4) to massive chert (MFT- 3). These deposits locally followed by a coarsening and shallowing-upward trend into bioclastic limestones (MFT-5) (Fig. 4.3).

Lower-order sea-level variations (fourth and fifth-order cycles) or high-energy storms locally disturb parasequences (S2, S3, and S4) and subdivide them into a number of temporally shoaling-upward cycles (Jafarian et al., 2017b) (Fig. 4.3).

4.5.4 Geological model (GM)

Lateral modelling of sedimentary facies provides a better understanding of the microfacies variability during sedimentation. Based on the microfacies distribution and defined sequence/parasequence boundaries, third-order sequences and associated microfacies in central Spitsbergen and NE Svalbard are laterally correlated to produce a geological model (GM) (Figs. 4.4 and 4.5) (Jafarian et al., 2017b). The latter shows that section TR (central Spitsbergen) is positioned in a proximal shallow-water setting marking by a higher input of extraclasts and sand content in the Vøringen Member and a greater portion of shallow-water microfacies (limestones) in the Kapp Starostin Formation (Fig. 4.4). Towards section KF, limestones gradually become thinner while deep-water bedded cherts (MFT-4) increase in thickness. There is an overall limited lateral microfacies variation, and comparable sedimentation patterns occur along NE Svalbard up to central Spitsbergen (Figs. 4.4 and 4.5). The geological models (GM) suggest that NE Svalbard is positioned at a low accommodation locality as shown by the thinner sequences and shallower microfacies (massive cherts, sandstones, and bioclastic limestones) of the Kapp Starostin Formation. However, the Vøringen Member shows deeper-water sedimentation (bryozoan limestones) in this area compared with central Spitsbergen (Figs. 4.4 and 4.5).

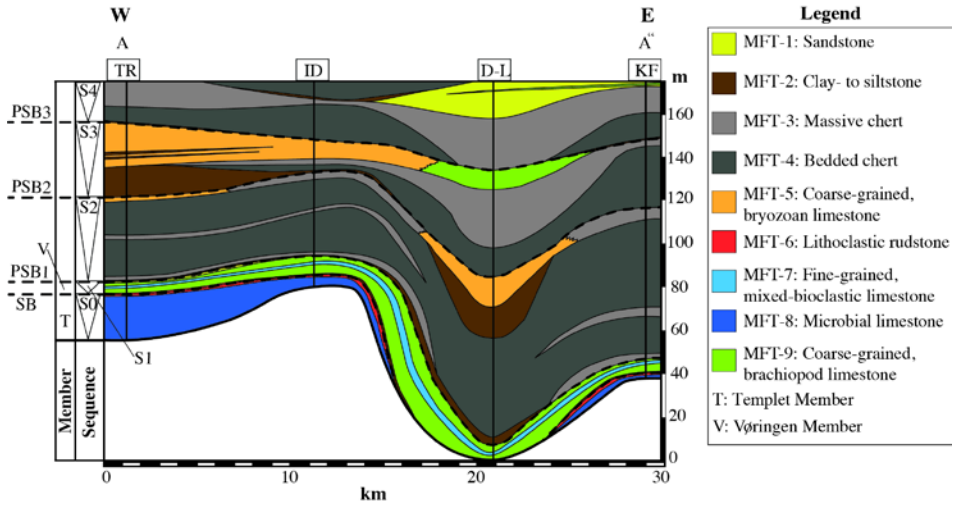

Fig. 4.4 The geological model of central Spitsbergen based on the sequence stratigraphy correlation showing lateral microfacies changes. Section locations (TR, ID, D-L, and KF), third-order sequences (S0, S1, S2, S3, and S4), and sequence/parasequence boundaries (SB, PSB1, PSB2, and PSB3) are added.

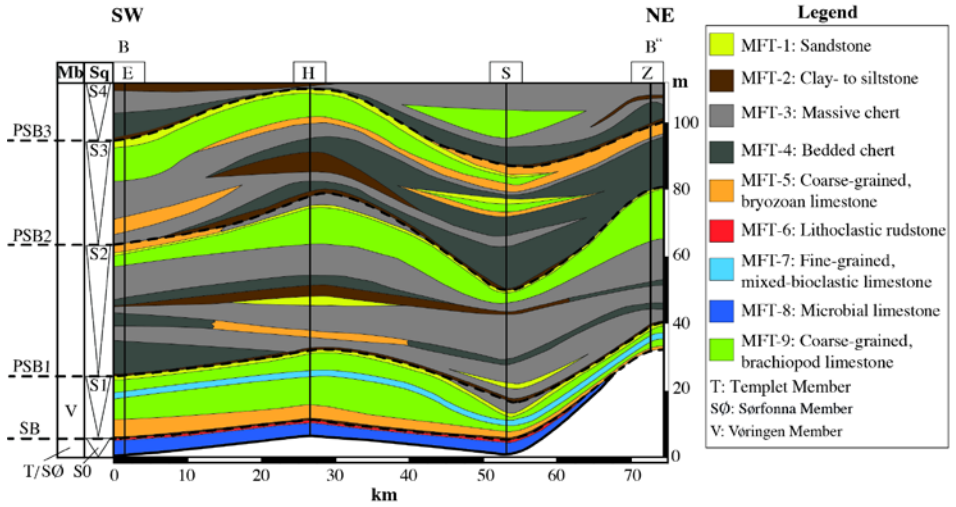

Fig. 4.5 The geological model of central Spitsbergen based on the sequence stratigraphy correlation showing lateral microfacies changes. Section locations (TR, ID, D-L, and KF), third-order sequences (S0, S1, S2, S3, and S4), and sequence/parasequence boundaries (SB, PSB1, PSB2, and PSB3) are added.

4.5.5 Petrophysical properties

The 39 samples that were used for modelling represent a wide variety of petrophysical properties (Table 4.1; Fig. 4.6).

The mineralogical composition of the sediments covers a broad range of carbonate contents from 0.4% to 97.6%. The carbonate content decreases from the Templet Member to the Kapp Starostin Formation while biogenic silica (spicules) content increases (Table 4.1).

Each microfacies type is characterized by different amounts of porosity and an almost certain mineralogical composition. Porosity values fall between 0.4% and 5.9% except for two porous samples with 11.8% (sandstones) and 20.7% (spiculitic massive cherts) porosity. Since variability of porosity within the studied samples is generally low, the porosity has been considered constant (average) for a given microfacies in the petrophysical input models. Thus, lateral and vertical porosity changes within each microfacies body are not incorporated in the 2D models while they are considered as 1D synthetic seismic logs.

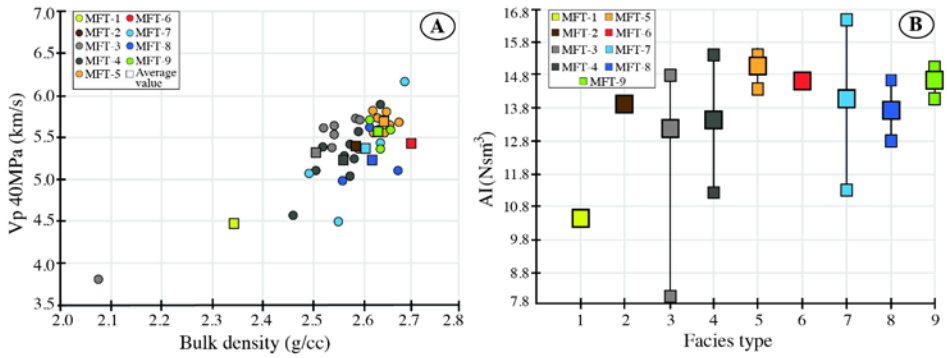

Fig. 4.6 A) Cross plot of measured dry P-wave velocity and bulk density for each measured sample coded by microfacies. Circle symbols indicate the measured value of one sample for each microfacies, whereas square symbols indicate the average values for each microfacies. B) The acoustic impedance domains are arranged by microfacies type (MFT). The small squares indicate the maximum and minimum values measured; the large square relates to the average value of the specific MFT.

The bulk density distribution shows that the lowest bulk density value 2.08 g/cc occurs in the spiculitic massive cherts microfacies (MFT-3), and lithoclastic rudstones microfacies (MFT-6) have the highest bulk density value, 2.70 g/cc (Table 4.1; Fig. 4.6A). At a pressure of 40 MPa, compressional velocities of the mixed facies vary from 3.76 to 6.16 km/s. The acoustic impedance values range between 7.83 and 16.64 Nsm^{-3} and are generally higher in the carbonate-rich microfacies (MFTs- 5 to 9) (Table 4.1; Fig. 4.6B).

Petrophysical input models (Figs. 4.7 and 4.8) illustrate that the highest average porosity (11.8%) and lowest average bulk density (2.35 g/cc) is covered by sandstone microfacies. Hence the lowest average velocity (4.46 km/s) and acoustic impedance (10.49 Nsm^{-3}) occurs in this microfacies. The highest averages of Vp (5.68 km/s) and acoustic impedance (15.06 Nsm^{-3}) are measured in the coarse-grained, bryozoan limestone microfacies (MFT-5) in combination with the lowest average porosity (0.99%).

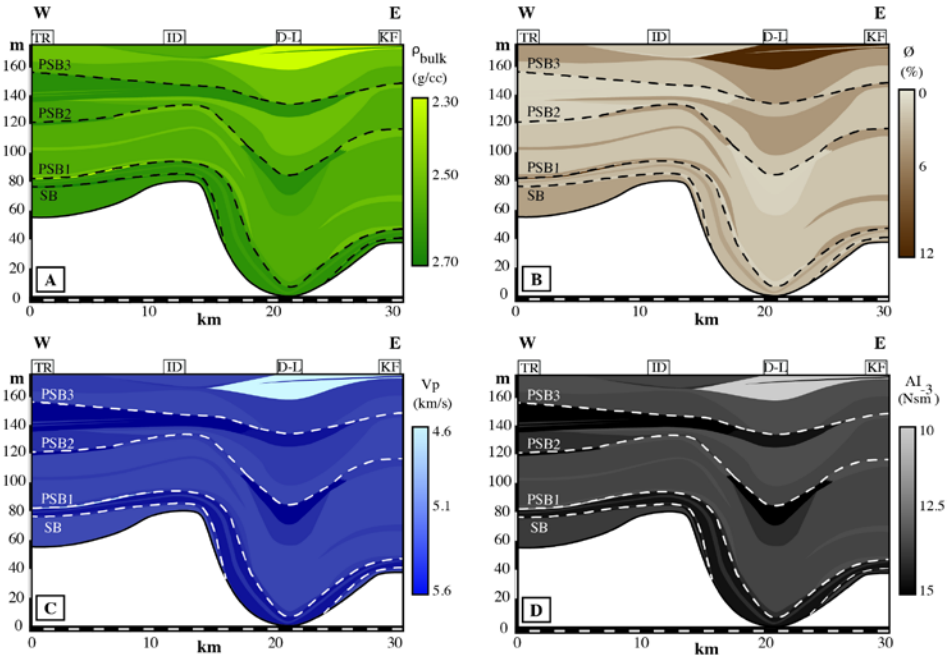

Fig. 4.7 Petrophysical input models: the distribution of bulk densities (A), porosities (B), pressure wave velocities (C) and the calculated acoustic impedances (D) are superimposed on the geological models of central Spitsbergen. Sections location and sequence/parasequence boundaries (SB, PSB1, PSB2, and PSB3) are added.

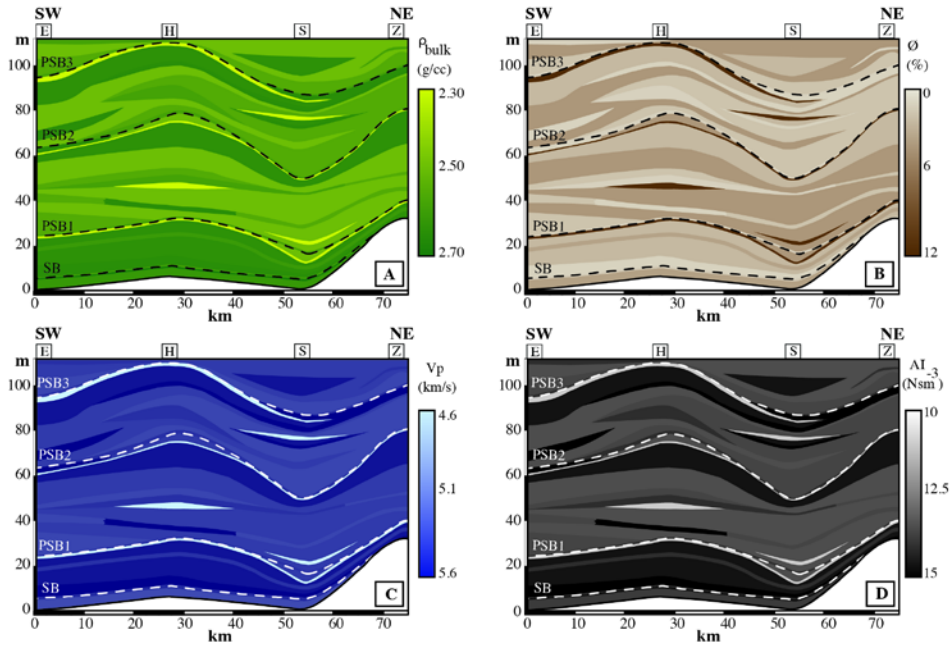

Fig. 4.8 Petrophysical input models: the distribution of bulk densities (A), porosities (B), pressure wave velocities (C) and the calculated acoustic impedances (D) are superimposed on the geological models of NE Svalbard. Sections location and sequence/parasequence boundaries (SB, PSB1, PSB2, and PSB3) are added.

4.5.6 Synthetic seismic logs (1D)

The observed outcrop microfacies distributions on central Spitsbergen have been translated into synthetic seismic logs at multiple frequencies, e.g., 25, 50, 100, 200 and 400 Hz (Fig. 4.3).

Sequence / parasequence boundary

In sections TR and ID, the sequence boundary (SB) between the Templet and Vøringen Members is marked by a soft-kick signal in the 200 to 400 Hz logs (Fig. 4.3). In a distal realm (section KF), this boundary is not reflected within the synthetic seismograms since the thickness of the Templet Member falls below seismic resolution.

The 200 and 400 Hz logs show that PSB1 in section KF represents the shift from relatively high-porous, fine-grained, mixed-bioclastic limestones (MFT-7) of the Vøringen Member to the overlying silicified cherts (MFT- 3) of the Kapp Starostin Formation (Fig. 4.3). This transition is reflected as a low-amplitude soft-kick signal. In section TR, the upper part of the Vøringen Member is marked by massive cherts, which are lithologically similar to the overlying Kapp Starostin strata (Fig. 4.3). These top chert units show a different

mineralogical composition compared with the lower carbonate sediments (MFT-9). The interface between them is reflected as a pronounced hard-kick signal. Therefore, facies similarity of the top of the Vøringen Member and the overlying Kapp Starostin strata cause a downward shift in the position of PSB1 within the synthetic seismograms. In section ID, the microfacies transition within the Vøringen Member frequently changes on a meter or sub-meter scale resulting in destructive interfering waves.

The 200 and 400 Hz logs display that in section KF, the gradual shift from massive cherts to bedded cherts across PSB2 is expressed as a soft-kick signal (Fig. 4.3). This is in contrast to the pronounced hard-kick signal at this boundary in section ID. PSB2 in section TR is marked by a sharp transition from bryozoan limestones to overlying shales, expected to show a hard-kick signal at this interface (Fig. 4.3). However, this transition is obliterated in the seismic seismograms, which might be due to the limited thickness of carbonate layer falling below seismic detectability.

In section KF, PSB3 separates deep-water shale and bedded cherts from porous massive cherts of the underlying cycle. This transition is expressed as a pronounced soft-kick signal in the 100 to 400 Hz logs (Fig. 4.3). In contrast to section KF, PSB3 shows a distinct hard-kick signal in sections TR and ID representing carbonates overlain by shale and spiculitic cherts (Fig. 4.3).

4.5.7 Synthetic seismic profiles (2D)

Sequence / parasequence boundary

In central Spitsbergen and NE Svalbard, the lithoclastic rudstone (MFT-6) and shale layer (MFT-2) interface marking the sequence boundary (SB), falls below seismic detectability. Hence, SB shows the transition from the microbial limestones (MFT- 8) of the Templet Member to the coarse-grained, heterozoan carbonates (MFTs- 5 and 9) of the Vøringen Member and is reflected as a low-amplitude soft-kick signal in the 400 Hz profiles (Figs. 4.9 and 4.10).

PSB1 displays the transition of carbonate (Vøringen Member) to shale layer and spiculitic chert (Kapp Starostin Formation) and is detected as a continuous hard-kick signal (100 to 400 Hz profiles) along NE Svalbard up to central Spitsbergen (Figs. 4.9 and 4.10). However, at the location of section S in NE Svalbard (Fig. 4.5), the occurrence of massive cherts at the top of the Vøringen strata record a renewed deepening of the sedimentary environment at the transition into the subsequent parasequence. This shift towards the overlying shale and chert layers is reflected as a soft-kick signal in the 400 Hz model (Fig. 4.10). The alternating layers of sandstone and shale across the PSB1 fall below the seismic detectability.

The high-frequency profiles (200 and 400 Hz) show that in both areas (NE Svalbard and central Spitsbergen), PSB2 and PSB3 generally represent the interface between the carbonates on top of the shallowing-upward cycle and, the overlying deep-water cherts. PSB2 and PSB3 are expressed as strong positive seismic signals (Figs. 4.9 and 4.10). The facies change over, e.g., sandstone to shale, across these boundaries thins below seismic resolution.

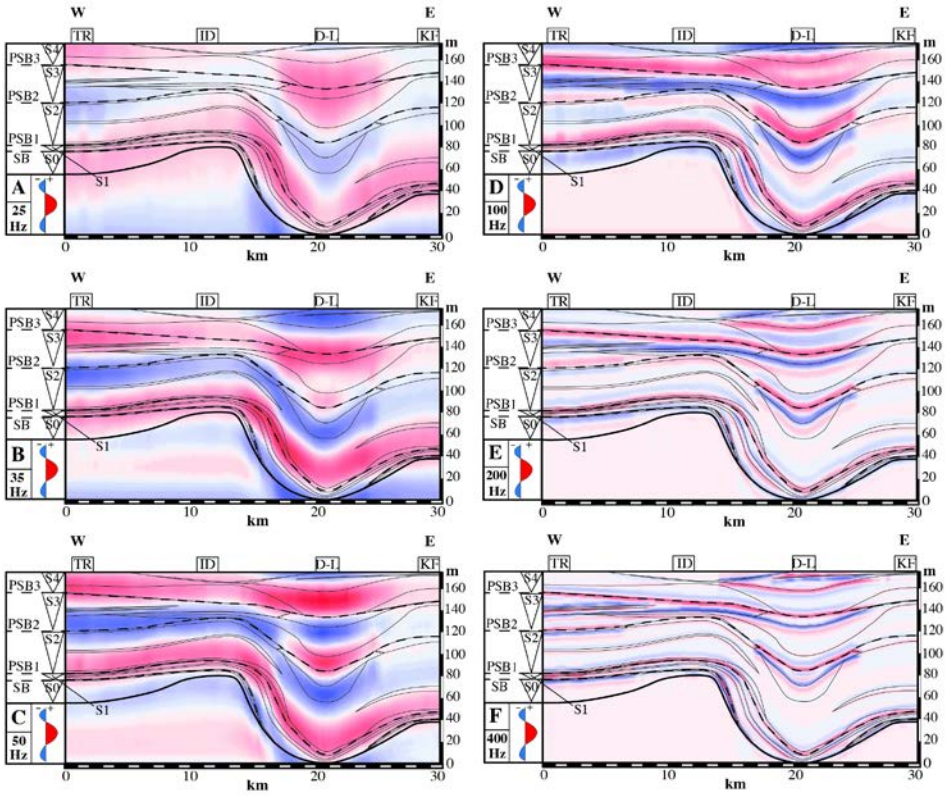

Fig. 4.9 Synthetic seismic profile at multiple frequencies (A: 25 Hz, B: 35 Hz, C: 50 Hz, D: 100 Hz, E: 200 Hz, F: 400 Hz) of central Spitsbergen. Acoustic impedance values were used to calculate the reflection coefficients between the individual unit interfaces. Ricker wavelet (Ricker, 1953) was used for convolution to generate a synthetic seismic profile. The red colours are positive signals (hard-kick) and blue colours are negative signals (soft-kick). Sections location, microfacies transitions, defined third-order sequences (S0, S1, S2, S3, and S4) and sequence/parasequence boundaries (SB, PSB1, PSB2, and PSB3) are superimposed.

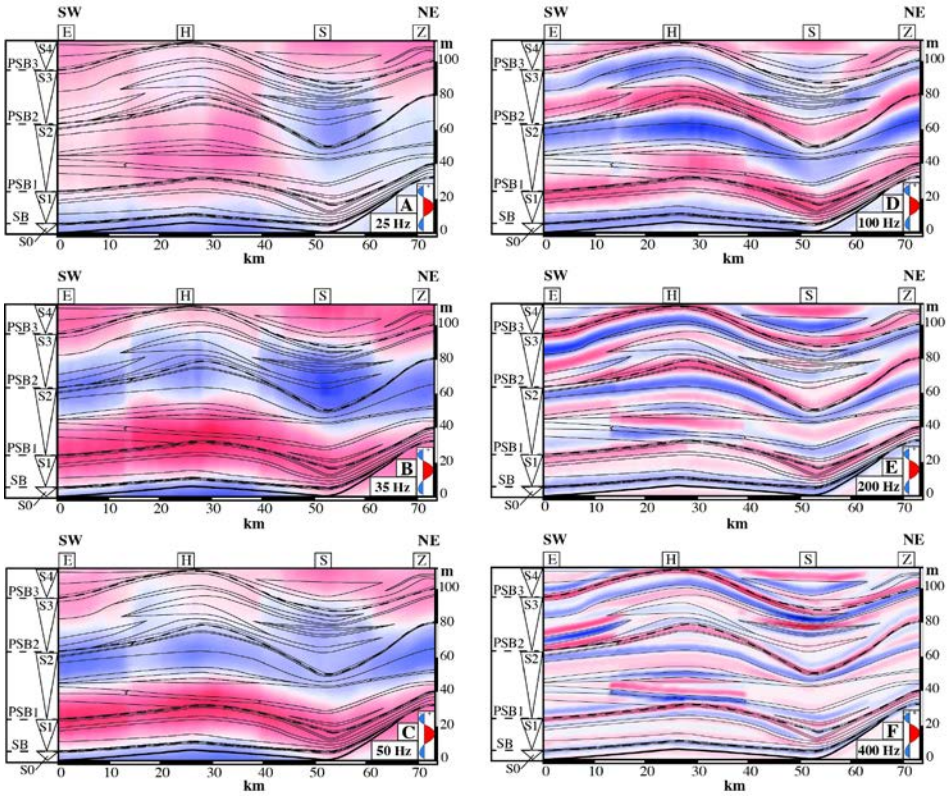

Fig. 4.10 Synthetic seismic profile at multiple frequencies (A: 25 Hz, B: 35 Hz, C: 50 Hz, D: 100 Hz, E: 200 Hz, F: 400 Hz) of NE Svalbard. Acoustic impedance values were used to calculate the reflection coefficients between the individual unit interfaces. Ricker wavelet (Ricker, 1953) was used for convolution to generate a synthetic seismic profile. The red colours are positive signals (hard-kick) and blue colours are negative signals (soft-kick). Sections location, microfacies transitions, defined third-order sequences (S0, S1, S2, S3, and S4) and sequence/parasequence boundaries (SB, PSB1, PSB2, and PSB3) are superimposed.

4.6 Discussion

4.6.1 Interpretation of the synthetic seismic profiles

Structural style and morphology

The shape of the seismic reflectors follows the antecedent topography of the studied areas (Figs. 4.9 and 4.10). Anticline and syncline shapes can be recognized from the seismic reflectors, which imply thickness variations of the Kapp Starostin successions. During the Permian, no main tectonic movement

has been documented on Svalbard. Differences in accommodation space most likely resulted from the distribution and reactivation of pre-existing structural elements, and eustatic sea-level fluctuations (Blomeier et al., 2013; Ehrenberg et al., 2001). The amplitude strength of seismic reflectors varies laterally emphasizing lateral changes in microfacies (Figs. 4.9 and 4.10). For example, at PSB2 in central Spitsbergen, carbonates shift into massive cherts frequently (Figs. 4.4 and 4.9). Moreover, destructive interference patterns as a result of wedge-shaped sediments with microfacies alternating on a meter or sub-meter scale and microfacies pinch outs, cause a decline of amplitude reflectors and discontinuity of them in the studied areas. Continuity of seismic reflections is closely related to continuity of bedding. Seismograms generated with the low-frequency wavelets (25 to 100 Hz) do not show any detailed depositional geometries such as these microfacies pinch-outs and sediment wedges (Figs. 4.9 and 4.10). This holds for NE Svalbard in particular.

Sequence /parasequence boundary

Since sequence/parasequence boundaries are marked by a sudden shift from shallowest to deepest microfacies associated with high petrophysical contrasts, high-amplitude seismic reflectors are expected to occur at these transitions.

In the studied areas, the profound shift in carbonate producers from T-factory (Templet Member) to C-factory (Vøringen Member), see table 4.2, has been associated with large-scale climatic, paleoceanographic and paleogeographic changes linked to the northwards drift of Pangea (Beauchamp, 1994; Beauchamp and Baud, 2002; Reid et al., 2007; Blomeier et al., 2011; Beauchamp and Grasby, 2012). Based on GM models, this carbonate switchover marks the sequence boundary (SB), which is reflected as a low-amplitude soft-kick signal (Figs. 4.3,4. 9 and 4.10).

Stafleu et al. (1994) demonstrated that the acoustic properties of tight limestones of the Vercors (France) might be controlled by grain-size and texture. In the studied synthetic seismic models, the low-amplitude, negative reflectors at SB can be explained by textural differences in carbonates resulting from depositional and diagenetic alterations (Table 4.2). The carbonate content of the micrite-supported sediments from the T-factory varies between 76.1% and 88.1%. These values largely correspond to the fraction of micrite filled interparticle space (MFTs-6 and 8). Sediments produced within the C-factory, on the other hand, are grain-supported. The wide range of carbonate content (37.9% to 97.6%) is related to the type of grains and associated post-depositional processes. Diagenetic modifications such as cementation and recrystallization can change the pore network and texture of sedimentary rocks and to the associated acoustic impedance (Fournier and Borgomano,

2007; Jafarian et al., 2017a). In the investigated areas, bioclastic-dominated limestones associated with the C-factory (S1), which are affected by cementation and chertification, show higher acoustic velocities and impedances compared to the mud-dominated limestones formed by the T-factory (S0) (Jafarian et al., 2017a). The increase in acoustic properties can be explained by the framework of interlocking crystals that were formed during diagenetic processes. These rock modifications may result in higher rock rigidity and lower porosities and thus provide a better framework in conveying seismic signals compared to a more flexible micritic matrix (Jafarian et al., 2017a; Janson and Lucia, 2014) (Figs. 4.3, 4.9 and 4.10).

Table 4.2 Summary of the carbonate producing factories information, averages of petrophysical properties and textural characteristics.

Carbonate producing factories	Dominant MFT	Dominant biota	Dominant diagenetic features	Texture	Average carbonate (%)	Average porosity (%)	Average Vp (40MPa) (km/s)	Average Acoustic impedance (Nsm^{-3})
T-factory carbonates	MFTs- 6, 8	Algal mats, few sponge spicules, foraminifers, ostracods	Micritization	mud-dominated	83.0	2.7	5.2	14.0
C-factory carbonates	MFTs- 5, 7 and 9	Brachiopods, bryozoans, echinoderms, sponge spicules	Chertification, Cementation	Grain-dominated	77.1	1.9	5.5	14.6

In the Kapp Starostin Formation, which is dominated by deeper and cold-water spiculitic chert horizons, the carbonate content increases towards the sequence tops as a result of third-order sea-level variations (Figs. 4.4 and 4.5). The parasequence boundaries PSB1, PSB2, and PSB3 are marked by an abrupt microfacies shift from carbonates to cherts (Figs. 4.4 and 4.5). Jafarian et al. (2017a) reported that an increment in carbonate content results in an increase of acoustic velocities. The carbonate-rich layers have higher bulk densities as well as velocities and consequently acoustic impedances compared to the surrounding chert units. The amplitude strength and polarity of the seismic traces are controlled by the relative difference in the acoustic properties at the transition between two sediment bodies (Nichols, 1999). Thus, independently of seismic frequency, a transition from carbonates to cherts creates the largest acoustic impedance contrasts and the pronounced seismic reflections (Figs. 4.3, 4.9 and 4.10).

These findings are in line with Zeller et al. (2015a) who investigated Upper Jurassic to Lower Cretaceous shelf mixed carbonate – siliciclastic sediments in the Neuquén Basin (Argentina) that had a low-porosity domain (around 5%).

The carbonate-rich sequence tops showed a higher acoustic impedance contrast with the surrounding siltstones and shales, which resulted in strong reflections within the synthetic seismograms.
In both investigated areas, the 200 Hz, 400 Hz and to a lesser extent 100 Hz profiles display an almost one to one relationship between the acoustic impedance models and the seismic events; SB, PSB1, PSB2, and PSB3 are at their true horizontal and vertical positions (Figs. 4.9 and 4.10). PSB1 that separates the outer ramp cherts of the Kapp Starostin Formation and the inner ramp carbonates of the Vøringen Member is the most robust feature that can be observed in all profiles (Figs. 4.9 and 4.10). Toward lower frequencies, 35 to 50 Hz, sequence/parasequence boundaries are obliterated (SB and PSB2) or show a mismatch with the outcrop equivalents (PSB3). The 25 Hz profiles do not provide insightful information on microfacies distribution and associated internal structures (Figs. 4.9 and 4.10).
As expected, the resolution problems and interference patterns decreases by an increment of the frequency (Figs. 4.9 and 4.10). The limited resolution of conventional industrial seismic wavelets precludes a one to one correspondence between the outcrop observations and seismic images. This is because of the wavelength of the seismic waves, which are too large to detect sediment heterogeneities on a meter-scale. In the low-frequency spectrum, higher-amplitude reflections might be caused by the occurrence of interference waves.

4.6.2 Relation to petrophysical properties

Porosity

It is known that porosity has a significant influence on acoustic velocities and impedance variations (Anselmetti and Eberli, 1993; Braaksma et al., 2003; Hossain and Zhou, 2015). Generally, with decreasing porosity and increasing density, velocity, and acoustic impedance increase.
In Miocene carbonates of the Cerro de la Molata platform (SE Spain; Kleipool et al., 2017) and Barremian-Aptian carbonates from the Provence (SE France; Fournier et al., 2014) with a high-porosity domain (0% to max 50%), porosity and pore types exert a significant, first-order control on elastic properties.
The average porosity of the predefined microfacies is < 4%, except for the sandstone microfacies with an average of 11.8%. The acoustic impedance models of this study follow the density and porosity trends (Figs. 4.7 and 4.8). On central Spitsbergen, Jafarian et al. (2017a) demonstrated that a decrease in velocity was accompanied by an increase in porosity. However, this negative trend is more evident for the relative high-porous samples (porosity > 5%;

MFT-1: TR-1.41.1; MFT-3: KF-2.12.1; MFT-7: KF-1.6.1; and MFT-8: ID-1.4.1). This results in a high impedance contrast to surrounding non-porous layers and consequently high-amplitude reflections in the synthetic seismic seismograms (Fig. 4.3). For example, in section KF, PSB2 and PSB3 demonstrate the transition from porous massive cherts to bedded cherts by a strong negative reflection.

The wide scatter of values in velocity–porosity transforms can be caused by the type of pores (e.g., Xu and Payne, 2009; Zhao et al., 2013). Stiff pores, i.e., vuggy and moldic, can increment the pore space considerably without increasing the general elastic compressibility of the sediments. In contrast, a small fraction of crack-like pores results in softening the rock and reducing velocity (Xu and Payne, 2009; Zhao et al., 2013).

In the studied samples, the majority of the porosity is not visible in thin sections suggesting that it primarily occurs as micropores and microcracks. This finding is in agreement with the model of Xu and Payne (2009), which shows that crack-like pores dominate the pore space in this dataset diminishing acoustic velocity (Jafarian et al., 2017a). Hence, even in these relatively low-porous sediments, porosity still plays an important role controlling the acoustic properties, but the influence is less compared to datasets with wider porosity domains.

Mineralogy

The impact of mineralogy on the acoustic properties is well visible in sediments with limited porosity and pore types such as the studied dataset (Jafarian et al., 2017a; Kleipool et al., 2015). In this low-porous, biosiliceous – carbonate deposits, the seismic reflectors created with high-frequency wavelets (200 to 400 Hz) follow the spatial microfacies distribution within the defined parasequences (Figs. 4.9 and 4.10).

Since NE Svalbard is located in shallower depth, lower-order sea-level fluctuations associated with overall stormier, high-energy conditions locally disturb chert-dominated third-order sequences by the deposition of single limestone or sandstone beds (Blomeier et al., 2013; Jafarian et al., 2017b) (Fig. 4.5). Therefore, in this area, the contrast in mineralogy is significant within the individual parasequences, which are expressed as seismic reflectors in the 200 and 400 Hz profiles (Fig. 4.10). However, the seaward pinch-out of shallow-water deposits (limestone or sandstone) results in a momentary transition from bedded into massive cherts in central Spitsbergen (Fig. 4.4). These subtle microfacies changes are marked by minor physical contrasts (Fig. 4.9). The low-resolution profiles (25 to 100 Hz) do not have the ability to resolve these microfacies alternating on a meter or sub-meter scale that occur within the lower-order sequences.

We can infer that the appearance of the seismic reflectors is primarily influenced by the high mineralogical contrasts of the defined facies, which variations are predominantly linked to relative sea-level fluctuations and, to a lesser extent, the sedimentary system. Due to variations in the spatial microfacies distribution, the proximal part displays higher internal amplitude contrasts with respect to the distal part (Figs. 4.3, 4.9 and 4.10). These observations are consistent with the results of Kleipool et al. (2015) who argued that high-amplitude contrasts in a low-porous mixed siliciclastic – carbonate ramp system (Upper Jurassic, Spain) are caused by the abrupt shifts in the type of the sediments. For the mixed carbonate – siliciclastic system of the Sobrarbe delta system (Pyrenees, N-Spain) with a domain porosity between 0% and 5%, De Jong (2015) also documented that the seismic traces follow the spatial microfacies distribution. Nevertheless, sediments of a single microfacies type with an almost given mineralogical composition (chert units in particular) show differences in acoustic impedance (Table 4.1). In the example shown in Fig. 4.3, PSB2 at section ID and KF representing the transition from massive to bedded cherts, however, shows different seismic signatures. This signifies internally non-homogeneous sediments, which most likely can be explained by the impact of visible and non-visible (microcrack) porosity or diagenetic alterations such as chertification and cementation that may enhance the seismic signal.

4.6.3 Seismic timeline and facies

Deposition and transportation of sediments within the C-factory are controlled by waves and currents resulting in a ramp-type morphology with continuous layer distribution. In the studied ramp system with overall limited lateral microfacies variations, significant changes in sediment composition and texture are coherent with the sequence/parasequence boundaries (e.g., carbonates-chert interfaces) (Figs. 4.4 and 4.5). These major transitions are mostly set to coincide with stratigraphic time surfaces. Consequently, the brightest seismic reflectors are coherent with both (Figs. 4.9 and 4.10). This is in line with the main premise in sequence stratigraphy that major stratal surfaces effectively signify geologic time surfaces. The latter is marked by sharp lithological contrast resulting from lateral shifts of the facies tracts (Van Wagoner et al., 1990). For the Bahamian T-Factory carbonate system, Eberli et al. (2001, 2002) showed that seismic reflections had chronostratigraphic significance. Sea-level fluctuations resulted in changes in sediment composition, sedimentation rate and diagenesis, which led to variations in sonic velocities, impedance contrasts and associated hard-kick and soft-kick seismic reflections (Eberli et al., 2001, 2002). Kleipool et al. (2017) proposed a

conceptual model of the microfacies control on seismic reflectors within the C-factory. They noted that when cool-water carbonate factories are active, rapid microfacies shifts as a result of sea-level fluctuation are coherent with timelines and consequently with the main impedance boundaries. In contrast, the shelf carbonate systems are marked by a complex geometry with high lithological and physical differences within a single microfacies tract, whereas lateral microfacies shifts tend to be gradational over large distances. Thus, seismic signatures follow microfacies boundaries instead of geological time surfaces.

In the Permian shelf-margin mixed sediments of the upper San Andres Formation (Last Chance Canyon, New Mexico) Stafleu and Sonnenfeld (1994) proposed two impedance models: (i) one with contrast at time-significant surfaces and, others (ii) with contrast at facies transitions. Comparison between these models and seismic line (placed around 50 km northwest of Last Chance Canyon) suggests that facies shifts, which are oblique to stratal surfaces, may be a prominent origin for seismic reflectors rather than time-significant surfaces. However, the resolution of stratal surfaces and facies shifts is intensely controlled by carbonate-sandstone alternations.

All in all, we can deduce that the type of carbonate factory, which is decisive for the platform morphology and consequently depositional character, controls the seismic reflection pattern.

4.6.4 Synthetic seismic profiles as analogue

The applicability of synthetic seismograms of outcrops and petrophysical data can be tested, if compared to time equivalent subsurface analogs (Bracco Gartner, 2000; Eberli et al., 2004).

The Upper Palaeozoic carbonate to biosiliceous successions of Svalbard occur along the entire Arctic shelf region and are known hydrocarbon plays on the Finnmark Platform, Loppa High and Sverdrup Basin (Ehrenberg et al., 2001; Golonka, 2002; Lerch et al., 2016). These deposits are characterized by a wide variability in petrophysical properties that hence introduce an additional uncertainty into seismic analyses.

The Templet Member analyzed in this study is the microfacies equivalent of the tropical carbonates (foraminifera, algae) of unit L-7, but also time equivalent with the lower part of the overlying unit L-8 at the Finnmark Platform (Norwegian Barents Sea) (Fig. 4.11A). The top of unit L-8 consisting of heterozoan carbonates (e.g., crinoids, bryozoans, brachiopods) correlates with the Vøringen Member researched in this study, and lithological unit L-9 (Templefjorden group) is time and microfacies equivalent to the Kapp Starostin Formation (Jafarian et al., 2017b).

In the Finnmark Platform, Colpaert et al. (2007) studied the seismic sequence stratigraphy of the Upper Palaeozoic deposits by using 3D seismic data, and detailed lithostratigraphic studies resulting from well logs and cores. Based on well log data, synthetic seismic wavelets at 25 Hz frequency were constructed for correlation with the defined seismic sequences.

The thickness of the measured sections on Spitsbergen with at most 139m falls below seismic resolution at real-frequency spectrum of 25 and 35 Hz. Therefore, the high- frequency wavelets (50 to 400 Hz) has been used for comparison with the real and synthetic seismic models of the Finnmark Platform of Colpaert et al. (2007) (Figs. 4.9 and 4.11). One needs to be aware that the continuous data of well logs, with approximately 50cm vertical resolution, are more accurate for generating a seismic model, even at low-frequency wavelets, than data based on a limited number of samples. However, outcrop data do show lateral and vertical heterogeneity of the sediments due to the fine scale, data continuity and their 3D accessibility. Additionally, petrophysical data can be directly linked to sediment samples.

In the Finnmark Platform, the carbonate factory switching from tropical (unit L-7) to cool-water (unit L-8) is recognized by a low-amplitude positive signal in the real and synthetic seismic data (Colpaert et al., 2007) (Fig. 4.11D). On Spitsbergen, this boundary is obliterated at 25 Hz and showed a negative signal toward higher-frequency profiles (50 to 400 Hz) (Figs. 4.9 and 4.11B, C). A low-impedance interval at the basal transgressive sediments of unit L-8 could be related to the reworked lowstand deposits or higher shale content. These deposits are also present at the base of the Vøringen strata but thin out below seismic detectability.

The overlying cool-water grainstones (brachiopods, bryozoans, and echinoderms) of unit L-8 display high acoustic impedance values similar to the seismic expression of heterozoan carbonates in the Vøringen Member. The real seismic of unit L-8 shows mounded bryozoan build-up structures on the deeper-water slopes (Colpaert et al., 2007). These features were not observed on Spitsbergen since the study area was located in the shallower depositional setting during this period (Fig. 4.11B, C).

In the Finnmark Platform, the sharp interface between low-impedance cherts of unit L-9 (Average Vp: 5 km/s) and high-impedance carbonates of unit L-8 (Average Vp: 6 km/s) is marked by a distinct positive reflection in the synthetic and real seismic data (Fig. 4.11D). The seismic expression at this major microfacies shift is matched with the synthetic seismic signature at PSB1 of the present study (Figs. 4.9 and 4.11B, C). Based on subsurface seismic data of unit L-9, spiculites mounds occur along restricted zones that show internal variations in seismic reflections. The seismic behavior of the Kapp Starostin Formation also shows similar heterogeneities which originate from changes in

lithology, porosity or the impact of a secondary process such as chertification (Figs. 4.9 and 4.11) (Colpaert et al., 2007). In the Finnmark Platform, Isolated mounds as well as continuous buildup complexes of different sizes could cause the wavy character of seismic reflectors.

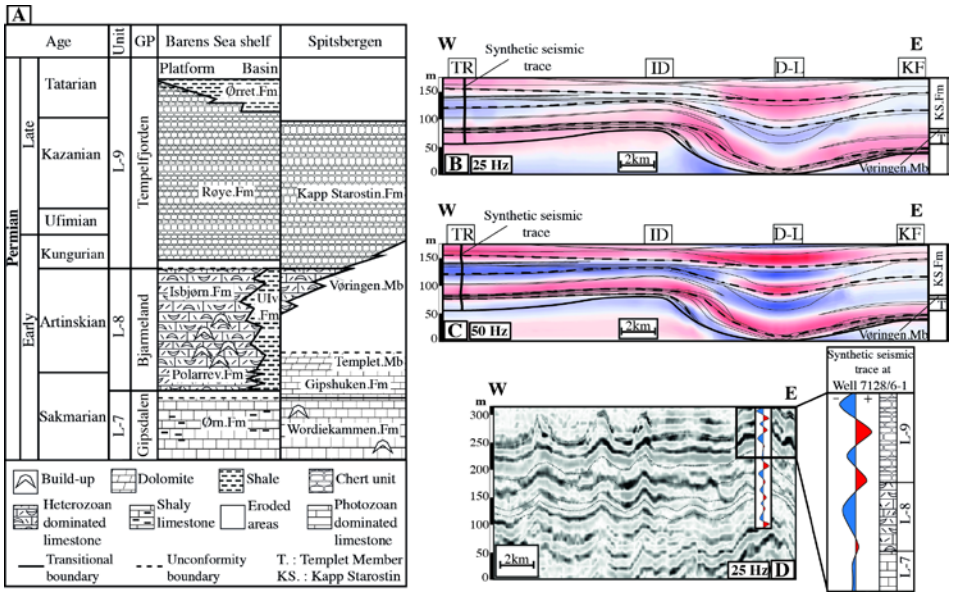

Fig. 4.11 A: The Upper Paleozoic lithostratigraphy of the Barents Sea Shelf and Spitsbergen (Colpaert et al., 2007; Ahlborn et al., 2014). B: the 1D synthetic seismic trace of the section TR (at 25 Hz) is superimposed on the 2D synthetic seismic profile (at 25 Hz) of central Spitsbergen. C: the 1D synthetic seismic trace of section TR (at 50 Hz) is superimposed on the 2D synthetic seismic profile (at 50 Hz) of central Spitsbergen. D: Synthetic seismic log (well 7128/6-1) and real seismic profile (at 25 Hz) of Finnmark platform (Colpaert et al., 2007).

In summary, it can be deduced that there is no big impedance contrasts between the micrite-supported tropical carbonates of unit L-7 (the Gipsdalen Group, Average Vp: 6 km/s) and the grain-supported cool-water carbonates of unit L-8 (the Bjarmeland Group, Average Vp: 6 km/s) (Fig. 4.11D) (Rafaelsen et al., 2008). The distinct seismic events in the synthetic and real seismic data of the Finnmark Platform are caused by major shifts in the type of sediments, which are coherent with the cycle boundaries (e.g., carbonate – non carbonate shifts). These observations are in line with the findings of the present study and are also in agreement with the results of the seismic model of Rudolph et al. (1989). The latter showed that in regions of complex depositional architectures with abrupt microfacies changes, sequence boundaries might

represent a simplified, but still valid version of the actual subsurface stratigraphy.

4.7 Conclusions

The goal of this study was to document the seismic expression of the Permian low-porous, biosiliceous – carbonate sediments, which were studied at several outcrops on Svalbard. The key findings of the transposition of the observed outcrop microfacies variations into synthetic seismograms at multiple frequencies are:

- The sequence stratigraphy documented in the outcrop can be linked to the reflectors in the synthetic seismic profiles produced with high-frequency wavelets (100 to 400 Hz).
- Conventional, low-frequency wavelets (25 to 50 Hz) have a resolution limitation and do not show a clear relationship between the Svalbard outcrop observations and the synthetic seismic profiles. However, some of the key surfaces (sequence/parasequence boundaries) can be identified in the real seismic spectrum but show a mismatch between the seismic reflectors and their outcrop equivalents.
- Abrupt microfacies transitions related to changes in sea level, followed by the amount of porosity and diagenetic effects such as cementation and chertification cause high-amplitude reflections in the synthetic seismic profiles. In the deeper and cold-water spiculites-dominated parasequences, the carbonate-rich sequence tops have strong seismic reflections in the synthetic seismic seismograms. The amount of porosity has the adverse effect on the acoustic velocities whereas carbonate content, cementation and chertification enhance the acoustic velocities and impedances in the present dataset.
- Within the C-carbonate factory, which is marked by lateral homogenous layers, major reflections are coherent with main facies shifts, thus sequence/parasequence boundaries and depositional timelines. In contrary, a facies dependent seismic signature would be expected in T-carbonate factory due to the lateral heterogeneity of the sediment within a single facies tract.
- Rapid changes in lithology and diagenetic overprints cause interference patterns resulting in a poor correlation between the synthetic seismograms and outcrop observations.
- Comparison with real seismic and synthetic seismic traces of the Finnmark Platform, a subsurface analogue with similar lithology,

shows similarities in the seismic reflection patterns. This comparison confirms that major changes in the mineral composition of the sediments as a result of sea-level fluctuations are the main trigger for shifts in amplitude strength and polarity of the seismic traces.

4.8 Acknowledgements

Financial support of the Vrije Universiteit Amsterdam (the Netherlands), University of Bremen (Germany) and the Norwegian Polar Institute (Tromsø, Norway) is greatly acknowledged. Bouke Lacet and Wynanda Koot (Vrije Universiteit Amsterdam) are thanked for preparing the thin-sections and cylindrical plugs. We thank MSc. students Ralph Groen, Mahtab Mozafari and Jan Schneider of the Vrije Universiteit Amsterdam for their contributions. We thank the College of Petroleum Engineering and Geosciences of the King Fahd University of Petroleum and Minerals (Kingdom of Saudi Arabia) for their support during the final stages of the manuscript. The constructive suggestions and comments of an anonymous reviewer contributed to a significant improvement of this paper. Finally Ronald J. Steel is thanked for his support as associate editor. This is CPG-CarbSed contribution no. 5.

Chapter 5

Synthesis

5.1 Sequence stratigraphy

The analyzed outcrops on Spitsbergen contain sediments produced by two different types of carbonate factories. The Gipsdalen Group comprises a photozoan facies association representing a warm tropical factory (T-factory, Schlager, 2005). The Tempelfjorden Group contains heterozoan biota (e.g. brachiopods, bryozoans, echinoderms, and siliceous sponges) indicating a cool and cold water factory (C-factory, Schlager, 2005).

The Early Artinskian to Kazanian successions of the Templet Member and the Kapp Starostin Formation cover a broad variety of facies ranging from shallow-water sandstone to limestones and deep-water cherts. Based on outcrop observations and the environmental microfacies interpretations on Spitsbergen, the studied succession was subdivided into five parasequences that are superimposed on a second-order sea-level fall (Chapter 2).

Each parasequence (S0, S1, S2, S3, and S4) reflects sedimentation from the deepest to the shallowest marine environments; the parasequence boundaries (PSB) are defined at the top of the shallowest unit of each parasequence.

The sediments within parasequence S0 are formed by a tropical carbonate factory; it is marked by mud-rich carbonates. The strata show a coarsening-upward trend into carbonate breccias and *Microcodium*, which suggests a period of subaerial exposure. The top of this regressive cycle represents a hiatus and is defined as a sequence boundary (SB).

Coarse-grained heterozoan limestones characterize Parasequence S1, the Vøringen Member. Parasequences S2, S3 and S4 in the Kapp Starostin Formation show a similar microfacies arrangement, from bedded to massive cherts that locally shift upward into bioclastic limestones and sandstones. Parasequences and associated microfacies are laterally correlated to produce a geological model (GM) that subsequently was used for petrophysical characterization (Chapter 3) and synthetic seismic modelling (Chapter 4).

5.2 Determination of textural and petrophysical properties

To construct synthetic seismic models, we require acoustic impedances, which are the product of acoustic velocities (Vp) and bulk densities (ρBulk). In our dataset, velocity plays the most important role in impedance since the variation percentage of the velocity (3.760-6.860 km/s) is larger than the bulk density (2.0-2.8 g/cc) (Chapter 3). Accordingly, the influence of textural and petrophysical factors which causes variations in the acoustic velocity can be assessed and linked to the stratigraphic framework. Based on statistical

analysis in the studied low porous, mixed sediments, acoustic velocities are to some extent controlled by porosity and diagenetic properties but mostly by the mineral composition.

To demonstrate a wider perspective and a more general guideline we present the acoustic and petrophysical properties from various studies, each in different sedimentary systems (Figs. 5.1, 5.2). By comparing these datasets, it becomes apparent that two parameters mainly control the velocity variations; i.e., porosity and mineralogy.

5.2.1 Mineralogy

While the properties of pure lithologies have been intensively studied in the past, the attributes of multimineral sediments are rather underrepresented. Siliciclastic and carbonate sedimentary systems display different seismic signatures. Carbonates have high densities and velocities and show complex geometries (e.g. Kenter et al., 2007; Weger et al., 2009). Siliciclastic systems are marked by gentle geometries in which movement and deposition are controlled by gravity and flow showing lower velocities (Janson and Fomel, 2010). Hence, mixed lithology systems may complicate seismic interpretation.

In both the Gipsdalen and Tempelfjorden Groups, the analyzed samples show a wide range in carbonate content (0.2%-99.0%). The Gipsdalen samples vary between dolomitic and calcitic sediments to siliciclastic deposits with some samples of a mixed nature. The Tempelfjorden successions range from pure carbonate and mixed sediments to biosiliceous deposits.

Overall, in the studied dataset (Chapter 3; Fig. 5.1), P-wave velocities rise with increasing carbonate content from non-carbonate deposits (siliciclastic/biosiliceous) to mixed carbonate - non-carbonate sediments and finally to pure limestones and dolostones.

.

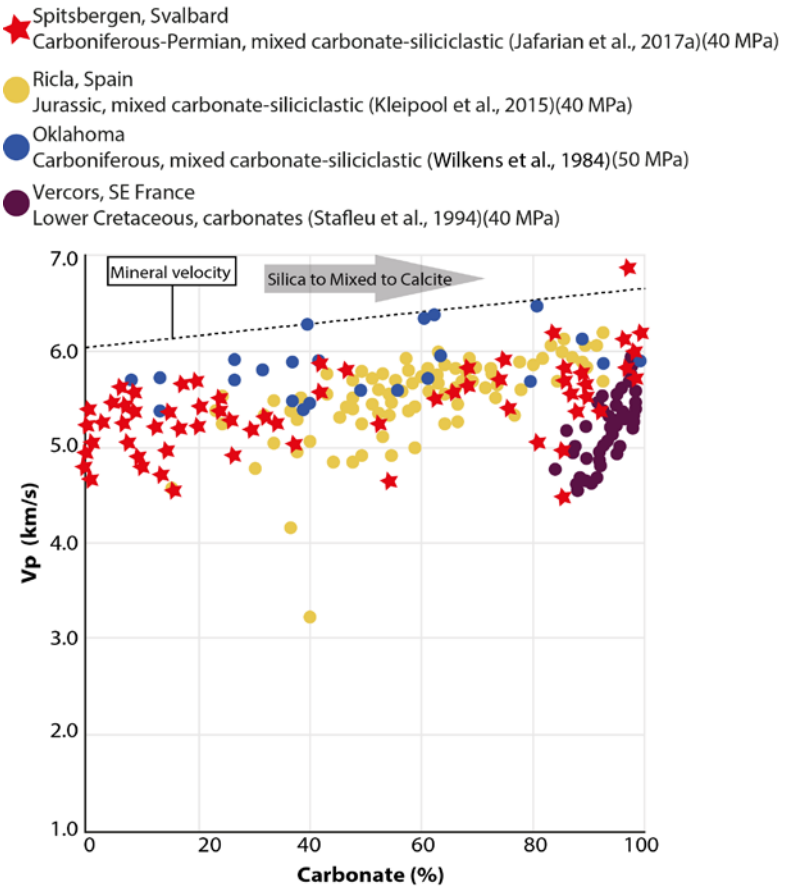

Fig. 5.1 Measured carbonate content and P-wave velocities of this study compared with carbonate and mixed siliciclastic-carbonate samples from other studies. The mineral velocity line displays the theoretical maximum velocity (Mavko et al., 2009) for SiO_2 (left) and $CaCO_3$ (right). Generally, P-wave velocities show a positive relationship with increasing carbonate content.

In other carbonates and mixed systems with low porosity values (Φ < 7%) (Fig. 5.1) such as (I) the Lower Cretaceous carbonate platform in Vercors, SE France (Stafleu et al., 1994), (II) the Carboniferous mixed sediments of southeast Oklahoma (Jack fork Formation; Wilkens et al., 1984), and (III) the mixed Jurassic sediments of the Ricla ramp system (Kleipool et al., 2015), the acoustic properties are primarily influenced by the carbonate content. The end points of the mineral velocity line at 0 and 100% carbonate represent the values for single crystal quartz and calcite, respectively (Fig. 5.1) (Mavko et al., 2009). The majority of the samples are positioned close to a mineral velocity

line indicating the overall composition control of velocity. As shown in Fig. 5-1, an increase in carbonate content results in a rise of the acoustic velocities.
We attribute most of the variance in velocity to the presence of non-carbonate grains such as clay, the amount and type of porosity or diagenetic properties (as discussed in the following paragraphs).

5.2.2 Porosity and density

Acoustic velocities are generally determined by the amount and type of porosity. The porosity of the studied samples ranges between 0.4% and 20.7% with an average of 2.2% (Chapter 3). Although velocity decreases with increasing porosity, the variability within a particular porosity range reaches up to ~2 km/s. Since the porosity domain of the studied sediments is narrow, the effect of pore type variations will be minor. Additionally, most of the porosity is invisible in thin sections, which suggest that it primarily occurs as micropores.
Bulk density including mineralogy and porosity follows the mineral composition and porosity trends. The Tempelfjorden samples display a wide range of bulk densities (2.0-2.7 g/cc). On the other hand, the Gipsdalen Group (2.4-2.8 g/cc) shows a narrow range but at the same time shows the highest bulk density values linked to dolostones
High porous ($\Phi > 20\%$) mono and multimineral marine datasets (Fig. 5.2) like (I) the Upper Cretaceous carbonates in Limburg, the Netherlands (Kenter et al., 1997a), (II) the Miocene carbonates of the Llucmajor platform on Mallorca, Spain (Verwer et al., 2008), (III) the Upper Jurassic mixed carbonate-siliciclastic rocks in the Boulonnais, northern France (Braaksma et al., 2003), and (IV) the Late Cretaceous mixed sediments of the South Provence Basin, SE France (Fournier and Borgomano, 2009), show a clear declining velocity trend with increasing porosity (Fig. 5.2). In the low porosity datasets such as (I) the Carboniferous-Permian mixed system of the Spitsbergen dataset (Jafarian et al., 2017a) and (II) the Upper Jurassic to Lower Cretaceous mixed sediments of the Neuquén Basin (Zeller et al., 2015a), this trend is also present but is less prominent. Therefore, in relative low-porous sediments ($\Phi < 10\%$), porosity still plays an important role controlling the acoustic properties, but its influence is less when compared to datasets with wider porosity domains.
The samples of carbonate systems show higher acoustic velocities for a given porosity compared to samples from mixed carbonate-siliciclastic systems (Fig. 5.2). The theoretical P-wave velocities of non-porous and non-carbonate minerals such as quartz and clays have lower velocities (Mavko et al., 2009).

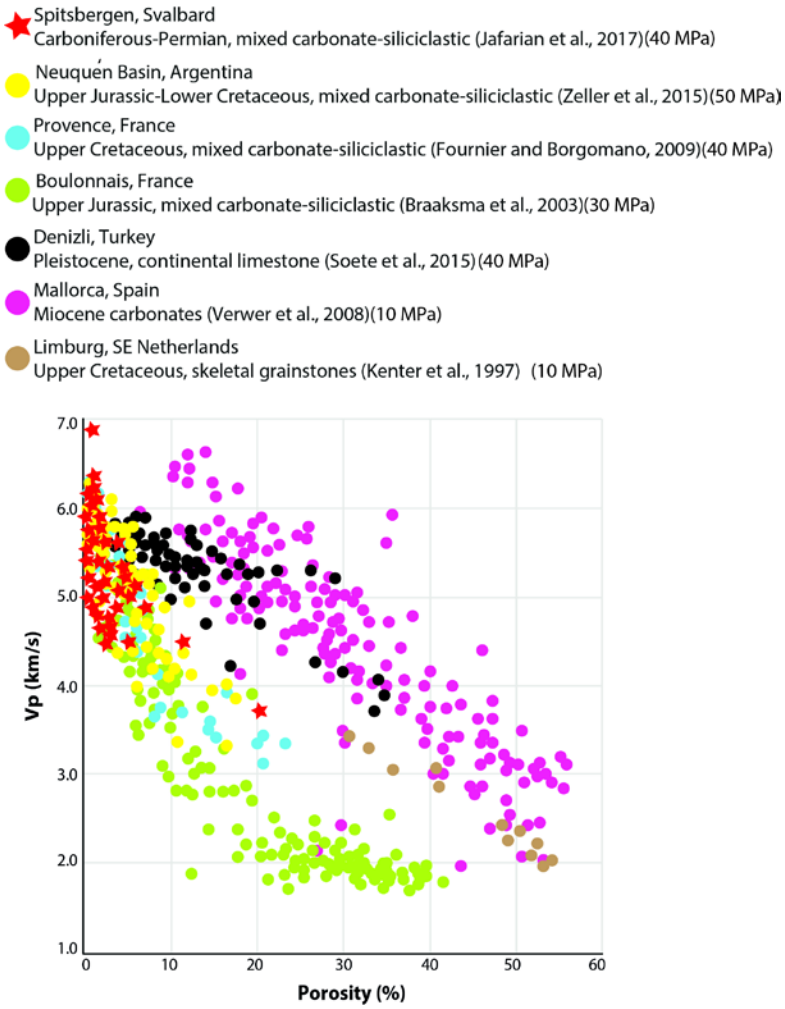

Fig. 5.2 Cross-plot of P-wave velocity versus porosity of different studies. In high porous datasets, the steepest negative inclinations are primarily caused by porosity. In low porous samples (Φ < 10%) such as the studied samples of Spitsbergen, this trend is less evident. The carbonate-silica ratio is the most important factor determining the variations in acoustic properties in the Spitsbergen samples.

5.2.3 Rock texture

The rock texture of the analyzed samples was described based on thin section observations, grain-size analysis, and mineralogical composition.

Grain-size

The grain-size analysis has been used to assess the impact of grain-size variations of the clastic portion on the acoustic properties. Generally, the clay content (<8 μm) plays a negative role on the acoustic velocities. In low porous, mixed carbonate-siliciclastic sediments in the Neuquén Basin (Argentina), Zeller et al. (2015a) reported that at a given porosity, shale successions have the lowest velocities with respect to sandstones and limestones. Kenter et al. (2007) indicated that the inverse effect of clay on acoustic properties is evident when the clay threshold exceeds 8%.

In Fig. 5.1, a critical threshold of 5–8% clay is shown, which inversely affects velocity in the low porous carbonate samples of Vercors (Stafleu et al., 1994) resulting in lower acoustic velocities compared to the mixed sediments. Kleipool et al. (2015) showed that the opposite influence of clay on velocities is evident where the clay threshold exceeds ~12% (Fig. 5.1).

At a given porosity in mixed systems, the Boulonnais samples (Braaksma et al., 2003) shown lower velocities when compared to the Provence sediments (Fournier and Borgomano, 2009) and the Spitsbergen samples (Jafarian et al., 2017a, in press). This effect can be explained by variations in the mineralogical and textural composition (Fig. 5.2). The Boulonnais sediments contain a higher amount of clay (0-50%) compared to the samples of the Provence dataset (0-4.5%) and the Spitsbergen samples (0-12.7%). The negative correlation of Vp and clay content as described in the abovementioned literature was not observed in the Provence and Spitsbergen samples. The clay content of the latter fall below the threshold value of 15% as proposed by Hossain and Zhou (2015), above which velocities tend to decrease.

Grain shape

The siliciclastic and biosiliceous samples (carbonate content < 20%) of the Gipsdalen and Tempelfjorden Groups are dominated by sand-sized grains (63-2000 μm), but with different shapes. The pore shape model of Soete et al. (2015) was used to determine the grain shapes present in these samples for showing a relationship between P-wave velocity and grain shapes. The spiculites consist of the accumulation of needle-shaped spicules originating from sponges of the group Demospongiae that acted as baffles, binders and even as constructors of reefs. The spicules, composed of opal, show parallel alignment and form the interconnected rigid skeleton which is comparable with the crystalline framestones texture in travertines of Soete et al. (2015).

The model indicates that in high porous travertines samples, the seismic velocities mainly depend on pore shapes. Soete et al. (2015) grouped the samples according to the dominance of three main pore shapes:

1. Rod- and cuboid-like pore shapes, which are elongated in one dimension
2. Cubic pores that are equidimensional
3. Blade- and plate-like pore shapes with a flattened form

Accordingly, rod-like pore shapes enhance the compressional-wave propagation, whereas plate-and blade-like pore shapes weaken the velocity. The latter shows the same dimensions as a fracture porosity of Xu and Payne (2009), which has an adverse impact on the velocity. Equidimensional pore shapes do not considerably affect the seismic velocity. It seems that this type of pore shape is similar to a separate-vug porosity that is mostly ineffective with regard to the velocity (Lucia and Conti, 1987; Doveton, 1994).

Siliciclastic samples of the analyzed dataset comprise of equidimensional quartz grains, which according to Soete et al. (2015), do not significantly influence the velocity. The rod-like shapes of spicules can explain the higher velocity of the deep-water biosiliceous samples of the Tempelfjorden Group compared to the shallow-water siliciclastic samples of the Gipsdalen Group (Fig. 5.3).

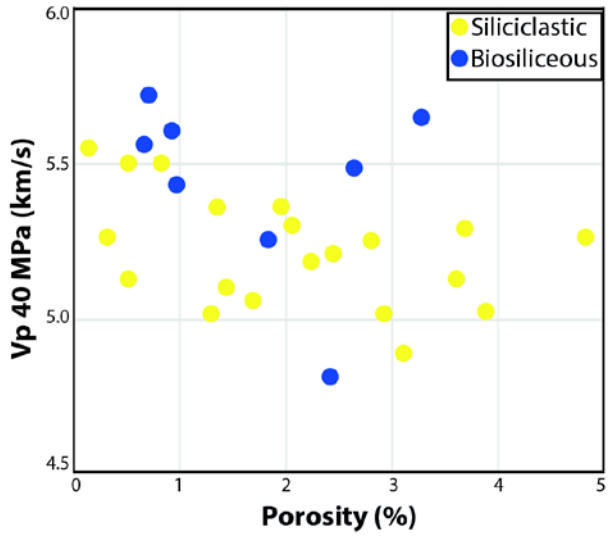

Fig. 5.3 Measured P-wave velocity versus porosity (< 4%) in biosiliceous sediments of the Tempelfjorden Group (blue dots) and siliciclastic sediments of the Gipsdalen Group (yellow dots). carbonate content < 20%. Due to the narrow porosity range, the impact of porosity on the acoustic velocities is obscured

Diagenetic alteration

Diagenetic effects can cause a homogenization or inversion of the petrophysical characteristics in which the appearance of the seismic reflectors will disappear or become inverted (Fournier and Borgomano, 2007).

In the studied tropical carbonates (T-factory) of the Gipsdalen Group, dolomitization and micritization are the dominant processes; whereas cool-water carbonates (C-factory) of the Tempelfjorden Group are marked by cementation and chertification.

Dolomitization

Diagenetic processes can change the mineralogy from aragonite/calcite to dolomite. Mavko et al. (2009) reported that pure calcite has a velocity of 6.64 km/s and pure dolomite of 7.34 km/s (Mavko et al., 2009). Anselmetti and Eberli (1993) stated that the two most important carbonate minerals calcite and dolomite show a minor Vp contrast. However, the type of dolomitization process and the associated pore characteristics control the seismic response. Some dolomitized samples from the Unda drill hole on the Bahamas (Anselmetti and Eberli, 1993) showed lower velocities while dolomitization destroyed most of the primary sedimentary structures, creating porosities of 49%. Whereas, in the studied Gipsdalen Group, the dolomitization process obscured the original texture and created interlocking crystals, which has the most positive impact on acoustic velocity.

The highest P-wave velocities of the Mallorca carbonate platform samples (Verwer et al., 2008) can be explained by a finely crystalline pervasive dolomitization in which the original textures generally are well preserved (Fig. 5.2). In this area, dolomitization was one of the earliest diagenetic events, and took place during a sea-level highstand succeeding a major fall in sea level (Pomar et al., 1996).

At a given porosity, the fabric-preserving dolomitization results in a significant increase in velocities due to the crystalline fabric and the higher matrix velocity of dolomite compared with calcite (Anselmetti and Eberli, 2001). In the Spitsbergen dataset, in which fabric destructive dolomitization probably occurred during early diagenesis within shallow burial depths in connection with the emersion of the platform surface, and resulted in a velocity increase. However, this increase is less pronounced than the fabric-preserving dolomitization of the Mallorca samples.

Chertification

Fournier and Borgomano (2009) documented that in sediments with a granular fabric, grain-to-grain contacts support the main medium for acoustic-wave propagation and acoustic energy loss at grain-to-grain boundaries,

similar to what is observed in siliciclastics (Verwer et al., 2008). However, crystal-dominated fabrics in which the primary grain-dominated fabric is recrystallized or cemented during diagenesis, creating interlocking crystals, also might form an effective acoustically connected frame for wave propagation. In the studied area, siliceous sponge spicules form the main constituent of the biosiliceous sediments. They are a source of widespread biogenic silica in the deep-marine environment. Due to remobilization of silica-rich waters in the subsurface, metastable carbonate grains and cements dissolved and chalcedony most commonly replaced them. This chertification (recrystallization) process provided the interlocking crystals framework for wave propagation resulting in an increase in acoustic velocities. In contrast, non-diagenetic siliciclastic samples are marked by the granular fabric and lower velocities.

Cementation

In the studied dataset, carbonates (carbonate content > 80%) and some mixed sediments samples of the Tempelfjorden Group (C-factory) comprise coarse-grained heterozoan biota with a sparitic crystalline infill. For a given carbonate content, the coarse-grained cemented sediments of the Tempelfjorden Group (C-Factory) show slightly higher velocities compared to the micritic-dominated sediments of the Gipsdalen Group (T-factory). This finding is in line with Soete et al. (2015) who showed that cement improves the contact between discrete constituents throughout the sample, which causes a more rigid self-supporting rock framework resulting in higher velocities.

Based on Figs. 5.1, 5.2, we can deduce that independent of lithology, porosity plays the most important role in predicting velocity and resulting acoustic impedance. The impact of mineralogy, which can be linked to the depositional environment, on the acoustic properties is well visible in sediments with limited porosity and variability in pore types such as in Ricla (Kleipool et al., 2015), the Neuquén Basin (Argentina) (Zeller et al., 2015a) and Spitsbergen. Variations in acoustic properties can become even more pronounced due to diagenetic overprinting such as dolomitization and cementation as we have already discussed.

5.2.4 Comparison of marine and continental carbonates

Soete et al. (2015) documented that velocities are higher for travertines than for marine carbonates due to a stiff crystalline framework, the so-called framestones (Soete et al., 2015). Fig. 5.2 demonstrates that at similar porosity, travertine samples possess higher velocities than marine carbonates and mixed systems. However, the dolomitization process in the Mallorca marine

carbonates (Verwer et al., 2008) has the greatest impact on acoustic properties and causes the highest velocity values.

5.3 Integrating outcrop observation and petrophysics to construct synthetic seismic models

Petrophysical properties; e.g., mineralogy, porosity, density and acoustic properties, are strongly influenced by depositional and diagenetic processes and therefore vary within a sequence stratigraphic framework (Anselmetti and Eberli, 1993; Braaksma et al., 2003; Verwer et al., 2008).
To show the spatial distribution of acoustic impedances within the sequence stratigraphic framework, they were assigned to the individual microfacies bodies in the Geological Model (GM). Shifts in the acoustic impedance log (reflection coefficient: R) were convoluted to seismic traces using a zero-phase Ricker wavelet (Ricker, 1953) at various frequencies (25, 35, 50, 100, 200, and 400 Hz).
High frequency seismic models (200 to 400 Hz) are used to indicate which transitions have the highest amplitude contrasts. The studied high frequency seismic profiles (400 Hz) have an approximate 14m wavelength (assuming an average velocity of 5.5 km/s) with a vertical resolution of about 3.5m (1/4-th of a wavelength) (Chapter 4). However, microfacies variations on a meter or sub-meter scale do not show up at the high frequencies spectrum. Thus, these models can show impedance variations on the scale of a few meters and highlight which details of the sedimentological variations that relate to the depositional setting and associated facies distribution are overlooked with respect to the low frequency models (25 Hz: 220m wavelength, 55m resolution).

5.3.1 Vertical and lateral heterogeneity of the sediments

The strength of the seismic reflection is controlled by the relative difference in the acoustic properties at the transition between two sediment bodies (Nichols, 1999). Within the Kapp Starostin Formation, the chert-dominated parasequences shift into limestones as a result of a third-order sea-level fall. Therefore, the carbonate content generally increases towards the top of the depositional parasequences. In the cool-water Tempelfjorden sediments, the high carbonate content corresponds to high velocities and impedances (Chapter 3). Since the carbonate content is a key factor controlling the acoustic velocity variations, the highest seismic amplitudes are linked to the carbonate facies, which have a high impedance contrast with the surrounding non-

carbonate facies. Thus, the transitions from non-carbonate sediments towards carbonates and vice versa result in hard-kick and soft-kick signals, respectively (Chapter 4; Figs. 4.9, 4.10). The impedance contrast at the sharp interfaces between biosiliceous sediments above and carbonates below is about 1.3 Nsm^{-3}. This acoustic impedance difference results in the high amplitude in seismic traces, which are coherent with the parasequence boundaries.

The parasequence boundary (PSB1) between the biosiliceous outer ramp strata of the Kapp Starostin Formation and the inner ramp carbonates of the Vøringen Member is a clear feature that can be observed in all profiles (Jafarian et al., in press). Toward lower frequencies (25 to 50 Hz) other parasequence boundaries are obliterated or show a mismatch between the seismic reflectors and the parasequence boundaries due to the longer seismic wavelength.

In NE Svalbard, the contrast in mineralogy is more significant within the individual parasequences. In central Spitsbergen, these changes are subtle (Chapter 4, Figs. 4.4, 4.5.). During the Permian, the deposits at NE Svalbard were located at a shallower water depth and frequently affected by lower-order sea-level fluctuations associated with overall stormier, high-energy conditions. Therefore, carbonates associated with shallower conditions including single limestone beds and sandstones occur interspersed within the chert-dominated parasequences resulting in sharp acoustic contrasts between both lithologies. The same occurs in the proximal part of the studied exposures (NE of NE Svalbard; west of central Spitsbergen). These microfacies alternating on a meter scale can be resolved by high frequency models (200, 400 Hz) but become obliterated toward lower frequencies (Chapter 4, Figs. 4.9, 4.10).

In central Spitsbergen and the distal part of the studied exposures (SW of NE Svalbard; east of central Spitsbergen), the shallower intervals (e.g. limestone beds, sandstones) pinch-out. Therefore, minor lithological variations are dominant in central Spitsbergen such as bedded to massive cherts transitions, which are marked by minimal physical contrasts. The impedance difference at these gradual boundaries is around 0.16 Nsm^{-3}, which causes low amplitudes seismic reflectors at high frequency profiles (200 to 400 Hz) (Chapter 4, Figs. 4.9, 4.10).

Hence, it can be deduced that, due to spatial microfacies distribution, the proximal part shows higher internal amplitude contrasts when compared to the distal part.

The facies pinch-outs and shifts in mineral composition from proximal to distal realms related to the sedimentary system, also cause lateral variations in amplitude strength and polarity of the seismic traces. This feature can be observed at the boundaries between two different parasequences and within

the single parasequences at high frequencies spectrum (200, 400 Hz) (Chapter 4; Figs. 4.9, 4.10).

5.3.2 Transition between the T-factory and the C-factory

The carbonate production within the studied areas switches from a cool-water factory (Tempelfjorden Group) to a tropical factory (Gipsdalen Group). The surface between tight heterozoan grainstones and mudstones with limited photozoan elements coincides with the sequence boundary (SB), which can be recognized as a low-amplitude soft-kick in the high frequency profiles (200 to 400 Hz) (Chapter 4; Figs. 4.9, 4.10).

The negative reflectors at this boundary can be explained by textural differences resulting from depositional and diagenetic processes. These observations agree with the results of Stafleu et al. (1994) who showed that in tight limestones of the Vercors (France), grain-size and texture might be the primary control on the acoustic properties. As we discussed in the diagenetic alteration section, coarser grain-sizes resulting from the high-energy depositional environment and cementation/chertification processes can explain the higher acoustic velocity and impedance of cool-water carbonates (Tempelfjorden Group) compared to the micrite-dominated tropical carbonates (Templet Member). The mudstone-grainstone boundary in Vercors shows a high impedance contrast. This transition does not only show a shift in terms of rock texture but also in the quantity of clay. The clay content significantly increases in mudstones, which reduces the acoustic velocities and therefore emphasizes the contrast in the seismic traces. We can say that facies boundaries by itself might not be distinct enough to be distinguished on seismic images only. In these low porous datasets, the mineralogical composition is the main trigger for changes in amplitude strength and polarity of the seismic signals. In the Spitsbergen dataset, however, the carbonate factory switchover is reflected as a gradual transition without major changes in mineral composition and is therefore less distinct in the synthetic seismic models.

5.3.3 Seismic reflection patterns

Generally, a carbonate ramp system is marked by lateral homogeneity and vertical heterogeneity (Schlager, 2005; Kleipool et al., 2015). The vertical heterogeneity of the sediments is resulting from relative sea-level fluctuations. Within the cool-water Tempelfjorden sediments, which are deposited on a storm-influenced ramp system, the main layers are laterally continuous and can be traced over large distances without significant changes in petrophysical properties (Chapter 4). The distinct seismic events that are detectable in

various seismic models are caused by abrupt vertical shifts in the mineral composition of the sediments, e.g. carbonate-chert shifts, resulting from sea-level fluctuations. Therefore, these major microfacies shifts are coherent with timelines and therefore with the strongest seismic reflectors.
This seismic reflection pattern is similar to the seismic traces of the lateral homogenous mixed sediments along the Ricla ramp system (Kleipool et al., 2015) in which major reflections are coherent with main facies shifts, thus stratigraphic time surfaces. In a Miocene carbonate succession, Kleipool et al. (2017) documented that seismic signatures follow geological time surfaces when cool-water carbonate factories are active. When carbonate-producing factories switch to a tropical factory, seismic signals follow microfacies boundaries instead of timelines. This can be explained by a complex platform morphology, which shows a shallow water lagoon surrounded by a reef barrier and a pronounced break of the slope into deeper waters. This morphology is characterized by high lateral lithological and physical contrasts from proximal to distal realms within a single microfacies tract.
The thicknesses (2-20m) of the sedimentary sequences produced by the T-factory (Gipsdalen Group) fall below seismic resolution. However, we expect that in high resolution seismic this tropical factory displays a facies dependent seismic signature.
We can conclude that differences in the seismic reflection pattern can be linked to the spatial distribution of the facies and the associated petrophysical properties resulting from carbonate-producing factories.

5.3.4 Depositional geometry

The studied 200 and 400 Hz synthetic seismic profiles provide information on a detailed depositional geometry such as microfacies pinch-outs (e.g. massive chert, sandstone, limestone) and sediment wedges (particularly in NE Svalbard) (Chapter4; Figs 4.9, 4.10). These features are obliterated towards lower frequencies, however general anticlinal and synclinal shapes resulting from thickness variations can be recognized in the whole frequency spectrum that has been applied.

5.3.5 Interpretation of seismic reflection pattern based on seismic profiles without prior knowledge of study area

Acoustic velocities measured in sedimentary rocks are influenced by various factors (e.g., porosity and pore type, mineralogy, fabric, texture); contrasts in acoustic velocities caused by natural variations are reflected in seismic datasets. Generally, velocity is primarily controlled by total porosity and lithology.

The acoustic ranges of measured sedimentary rocks often overlap, which makes prediction of lithologies and associated properties from seismic datasets a highly challenging task.
Anselmetti et al. (1997) reported that despite the differences in lithology and porosity of fine-grained limestones of Stock Island Formation and siliciclastic sediments of Long Key Formation (Florida Keys), both formations have the same petrophysical signature. Therefore, the resulting seismic response is very similar, which makes gradual transitions or intercalations of the two lithologies seismically undetectable.
The seismic patterns in the produced seismograms at industrial frequencies (25, 35 and 50 Hz; Figs. 4.9, 4.10) can be subdivided into two zones of high-amplitude hard-kick reflections at the top and the bottom, and a zone with high-amplitude soft-kick reflections between them. These zones could be formed by changes in porosity or lithology resulting from depositional and diagenetic alterations.
The lateral continuation of seismic reflections indicates minor physical contrast of the sediments over large distances. The vertical heterogeneities are caused by sea-level fluctuations and associated depositional and post-depositional changes (e.g. cementation, compaction, recrystallization). Since sequence stratigraphic cycle (sequence/parasequence) boundaries are marked by abrupt facies shift from for example shallower to deeper water depositional settings with high petrophysical contrasts, high amplitude wiggles are expected to occur at the interface of these transitions. This interpretation fits with the ramp-type setting discussed above. However, the ramp-type geometry is not clearly reflected by the seismic reflector patterns, which is interpreted to be related to the absence of large-scale depositional geometries. The shape of the seismic reflectors varies laterally and follows the topography of the depositional area. The latter results from local differences in accommodation space that could be linked to the tectonic events.

5.4 Summary and Outlook

The objective of this thesis is to understand the sequence architecture of a mixed carbonate to non-carbonate succession by using outcrop data, to capture the fine-scale heterogeneity within this stratigraphic framework and the appearance of these sediments in synthetic seismic profiles. The results presented in this thesis are an important step towards a better understanding of seismic datasets of carbonate to non-carbonate, low-porous sedimentary systems

5.4.1 General rules out of the analysis of the dataset

Heterogeneity

The multimineral Carboniferous-Permian succession displays a high degree of heterogeneity that relates to the sedimentary system, sea-level fluctuations, and post-depositional processes like diagenesis. A wide range of biota and facies developed during the northward movement of Spitsbergen as part of the Pangea continent, while oceanographic changes resulted in environmental shifts and the formation of T-factory and C-factory carbonate sediments. The sediments vary from shallow marine sandstones and limestones to deep marine cherts and shales. The mixed nature of the sediments demonstrates a high spatial variability of lithologies and facies, which resulted in a broad range of physical and textural properties. This variation allows for a comparison with a wide range of data known from the literature (e.g. McNeill et al., 2004; Braaksma et al., 2006; Kenter et al., 2007; Fournier and Borgomano, 2009).

Key rock properties that have an impact on the acoustic behavior

In the researched marine, low porous, mixed carbonate to non-carbonate system, the mineral composition of the sediments appears to be a key factor controlling the acoustic velocities. This interpretation is in agreement with the results in literature (e.g. Anselmetti and Eberli, 1993; Kleipool et al., 2015; Kittridge; 2015; Zeller et al., 2015a; Reijmer et al., in prep.). Overall, the carbonate to non-carbonate ratio plays a major role in the distribution of the acoustic properties. In a carbonate- to non-carbonate sedimentary system a positive carbonate content to P-wave velocity trend exists (Fig. 5.1). The inclination of this trend is controlled by the porosity, as well as the quantity and mineralogy of the non-carbonate portions. The impact of mineralogy on the velocities of a high porous system such as the Miocene carbonates of SE Spain (Kleipool et al., 2017), however, is less evident due to the primary effect of variations in porosity and pore type (Fig. 5.2). Generally, the negative inclination of the porosity – velocity trend has a higher impact than the positive inclination of carbonate content – velocity trend.

The post-depositional diagenetic alterations that have impacted the physical properties of the Spitsbergen strata comprise dolomitization, cementation, and recrystallization.

Dolomitization is the most important process that significantly changes the rock properties of the studied dataset. However acoustic properties may vary depending on the dolomitization process and the associated pore characteristics. This overprint may lead to an enhanced seismic velocity, as shown in the investigated samples, or a reduction of the velocity, when the

process results in an increase of the amount porosity (Anselmetti and Eberli, 1993).
The cherts formed through recrystallization provided the interlocking crystal scaffold for wave propagation leading to higher acoustic velocities for a given porosity.
The spiritic infill of interparticle pore space of the deposits slightly affects the acoustic properties. In general, cemented sediments show higher velocities compared to the micritic samples.

Synthetic seismic profiles

The synthetic seismic profiles display that in low porous, multimineral sediments, the spatial distribution of the facies and the associated petrophysical properties are decisive for the appearance of the synthetic seismic reflectors. This pattern confirms the data known from the literature (e.g. Kleipool et al., 2015; Zeller et al., 2015a). However, the large difference in mineralogical composition between two facies (the type of sediment) results in high amplitude contrasts when translating the acoustic impedances to seismic traces. In the studied ramp system, which was formed by a cool-water carbonate factory, these major changes in facies are caused by sea-level fluctuations and represent parasequence boundaries, and therefore timelines. Accordingly, in the cool-water factory, the rapid facies shifts are consistent with timelines; therefore, the strongest seismic reflectors are coherent with both. In T-factory carbonates the seismic signals tend to follow facies boundaries due to the lateral heterogeneity of the sediments resulting from a complex platform anatomy (Kleipool et al., 2017). Therefore, with the synthetic seismic models we can assess the effect of diagenesis, carbonate factory switchovers and stratigraphy on the impedance contrasts.

5.5 Future work

This study showed the possibilities and limitations of 2D synthetic seismic modeling when investigating the seismic response of multimineral sediments with a complex depositional geometry. Seismic reflectors in high frequency synthetic seismic models (200, 400 Hz) follow the stratal geometries and spatial distribution of the facies in detail. The low frequency profiles (e.g. 25 to 50 Hz) fail to show these details. However, they display some major transitions e.g. between the inner and outer ramp facies which are coherent with timelines.

Predicting the anatomy of sedimentary systems in the subsurface remains the main challenge in sedimentary geology. The limited resolution of conventional industrial seismic wavelets (e.g. 25 to 50 Hz) in 2D synthetic seismic profiles can be solved by 3D synthetic seismic acquisition and processing with a resolution of a few tens of meters over thousands of square kilometers (Nestvold, 1996; Dorn, 1998). The 3D seismic technology has been the key to success for exploration of hydrocarbon over the past century.

3D high-resolution synthetic seismic models can be constructed from outcrops using Petrel geophysical software, however outcrops permitting such an one to one link are very rare, to say the least. In this type of seismic models, reflections are placed in their proper vertical and horizontal positions, and allow for the discovery of complex geological structures (such as build-up structures, fault geometry, carbonate factory switchovers), but also enable to capture the spatial variability of facies in 3D detail. The work on synthetic seismic modelling and the evaluation of rock properties will be of use in the fields of quantitative interpretation of seismic datasets and towards the improvement of rock physics models.

Finally, the diagenetic controls on petrophysical properties (e.g. porosity, permeability) and consequently the reservoir characterization of the sediments should not be underestimated. While the study area was positioned in a tectonically stable condition during the Late Palaeozoic, we may be able to assess the sensitivity to diagenetic modification processes of the lithological variations of the individual sedimentary systems as produced by variations in sea level and climate. Additional geochemical studies will improve our present understanding of the depositional environment and the sensitivity of the sedimentary system to diagenetic modification that occurred during syn- and post-depositional processes. Further isotope studies are needed to reconstruct burial history, asses the timing of charge and estimate formation temperatures.

Detailed field mapping by drones and Lidar imaging in combination with high resolution satellite data will improve our concept of the spatial heterogeneity of the outcropping deposits and hence the translation of field data to seismic.

References

Adam, L., Batzle, M., Brevik, I., 2006. Gassmann's fluid substitution and shear modulus variability in carbonates at laboratory seismic and ultrasonic frequencies. Geophysics 71, 173-183.

Ahlborn, M., Stemmerik, L., Kalsto, T.K., 2014. 3D seismic analysis of karstified interbedded carbonates and evaporites, Lower Permian Gipsdalen Group, Loppa High, southwestern Barents Sea. Marine and Petroleum Geology 56, 16-33.

Alves, F., Almeida, J.A., Silva, A.P., 2014. Simulation of acoustic impedance images by stochastic inversion of post-stack seismic reflection amplitudes and well data. Journal of Petroleum Science and Engineering 121, 52-65.

Anell, I., Braathen, A., Olaussen, S., 2014. Regional constraints of the Sørkapp Basin: A Carboniferous relic or a Cretaceous depression. Marine and Petroleum Geology 54, 123-138.

Anselmetti, F.S., Eberli, G.P., 1993. Controls on sonic velocity in carbonates. Pure and Applied Geophysics 141, 287-323.

Anselmetti, F.S., Von Salis, G.A., Cunningham, K.J., Eberli, G.P., 1997. Acoustic properties of Neogene carbonates and siliciclastics from the subsurface of the Florida Keys: implications for seismic reflectivity. Marine Geology 144, 9-31.

Anselmetti, F.S., Eberli, G.P., 2001. Sonic velocity in carbonates: a combined production of depositional lithology and diagenetic alterations. In: Ginsburg, R.N. (Eds.), Subsurface Geology of a Prograding Carbonate Platform Margin, Great Bahama Bank: Results of the Bahamas Drilling Project, vol. 70. SEPM Special Publication, Tulsa, Oklahoma, USA, pp. 193-216.

Bacon, M., Simm, R., Redshaw, T., 2007. 3-D seismic interpretation, Cambridge University Press, p. 238.

Baechle, G., Weger, R., Eberli, G., 2005. Changes of shear moduli in carbonate rocks: Implications for Gassmann applicability. The Leading Edge 24, 507-510.

Baechle, G.T., Colpaert, A., Eberli, G.P., Weger, R.J., 2008. Effects of microporosity on sonic velocity in carbonate rocks. The Leading Edge 27, 1012-1018.

Beauchamp, B., 1994. Permian climatic cooling in the Canadian Arctic. In: Klein, G. (Ed.), Pangaea: paleoclimate, tectonics, and sedimentation during accretion, zenith, and breakup of a supercontinent, vol. 288. GSA Special Papers, pp. 229-246.

Beauchamp, B., Desrochers, A., 1997. Permian warm- to very cold-water carbonates and cherts in Northwest Pangaea. In: James, N.P., Clarke. J.A.D. (Eds.), Cool-water carbonates, vol. 56. SEPM Special Publication, Tulsa, Oklahoma, USA, pp. 327-347.

Beauchamp, B., Baud, A., 2002. Growth and demise of Permian biogenic chert along northwest Pangea: Evidence for end- Permian collapse of thermohaline circulation. Palaeogeography, Palaeoclimatology, Palaeoecology 184, 37-63.

Beauchamp, B., Olchowy, B., 2003. Early Permian buildups (Tolkien reefs) associated with subaqueous evaporites, Sverdrup Basin, Canadian Arctic: a record of syn- to post-tectonic differential subsidence and reciprocal uplift. In: Ahr, W.M., Harris, P.M., Morgan, W.A., Somerville, I.D. (Eds.), Permo-Carboniferous Carbonate Platforms and Reefs, vol. 78. SEPM Special Publication, Tulsa, Oklahoma, USA, 133-153.

Beauchamp, B., Wamsteeker, M., Peña, J., 2010. The Carboniferous-Permian reef play in the Sverdrup Basin: Dare to Dream. Search and Discovery Article #90172 at AAPG GeoConvention, Calgary, Alberta, Canada, May 10-14, 2010.

Beauchamp, B., Grasby, S., 2012. Permian lysocline shoaling and ocean acidification along NW Pangaea led to carbonate eradication and chert expansion. Palaeogeography, Palaeoclimatology, Palaeoecology 350, 73-90.

Bensing, J.P., James, N.P., Beauchamp, B., 2008. Carbonate deposition during a time of mid-latitude ocean cooling: Early Permian subtropical sedimentation in the Sverdrup Basin, Arctic Canada. Journal of Sedimentary Research 78, 2-15.

Benson, G.S., Franseen, E.K., Goldstein, R.H., Li, Z., 2014. Workflows for incorporating stratigraphic and diagenetic relationships into a reservoir analogue model from outcrops of Miocene carbonates in SE Spain. Petroleum Geoscience 20, 55-78.

Bellian, J.A., Kerans, C., Jennette, D.C., 2005. Digital outcrop models: applications of terrestrial scanning lidar technology in stratigraphic modelling. Journal of Sedimentary Research 75, 166-176.

Birkenmajer, K., 1964. Devonian, Carboniferous and Permian Formations of Hornsund, Vestspitsbergen. Studia Geologica Polonica 11, 47-123.

Birkenmajer, K., 1984. Cyclic sedimentation in mixed alluvial to marginal-marine conditions: The Treskelodden Formation (?Upper Carboniferous and Lower Permian) at Hornsund, south Spitsbergen. Studia Geologica Polonica 80, 25-46.

Blazejowski, B., 2009. Foraminifers from the Treskelodden Formation (Carboniferous-Permian) of south Spitsbergen. Polish Polar Research 30, 193-230.

Blomeier, D., Scheibner, C., Forke, H., 2009. Facies arrangement and cyclostratigraphic architecture of a shallow-marine, warm-water carbonate platform: the Late Carboniferous Ny Friesland Platform in eastern

Spitsbergen (Pyefjellet Beds, Wordiekammen Formation, Gipsdalen Group). Facies 55, 291-324.

Blomeier, D., Dustira, A.M., Forke, H., Scheibner, C., 2011. Environmental change in the Early Permian of NE Svalbard: from a warm-water carbonate platform (Gipshuken Formation) to a temperate, mixed siliciclastic-carbonate ramp (Kapp Starostin Formation). Facies 57, 493-523.

Blomeier, D., Dustira, A.M., Forke, H., Scheibner, C., 2013. Facies analysis and depositional environments of a storm-dominated, temperate to cold, mixed siliceous–carbonate ramp: The Permian Kapp Starostin Formation in NE Svalbard. Norwegian Journal of Geology 93, 75-93.

Bourbié, T., Coussy, O., Zinszner, B., 1987. Acoustics of Porous Media, Gulf Publishing Co, Houston, Texas, USA, p. 334.

Braaksma, H., Kenter, J.A.M., Proust, J.N., Dijkmans, V., Van Hoek, T., Mahieux, G., Drijkoningen, G.G., 2003. Controls on acoustic properties of Upper Jurassic siliciclastic rocks (Boulonnais, northern France). Geophysics 68, 58-69.

Braaksma, H., Proust, J.N., Kenter, J.A.M., Drijkoningen, G.G., Filippidou, N., 2006. Sedimentological, petrophysical and seismic characterization of an Upper Jurassic shoreface dominated shelf-margin (The Boulonnais, northern France). Journal of Sedimentary Research 76, 175-199.

Bracco Gartner, G.L., 2000. High resolution impedance models of outcrops and their applications in seismic interpretations. PhD Thesis. VU University Amsterdam, The Netherlands, p. 144.

Buggisch, W., Blomeier, D., Joachimski, M.M., 2012. Facies, diagenesis and carbon isotopes of the Early Permian Gipshuken Formation (Svalbard)[Fazies, Kohlenstoffisotopie und diagenetische Erscheinungen der randmarinen Gipshuken Formation im Unterperm von Spitzbergen]. Zeitschrift der Deutschen Gesellschaft für Geowissenschaften 163, 309-321.

Castagna, J.P., 1993. Petrophysical imaging using AVO. The Leading Edge 12, 172-178.

Christensen, N.I., Szymanski, D.L., 1991. Seismic properties and the origin of reflectivity from a classic Paleozoic sedimentary sequence, Valley and Ridge province, southern Appalachians. GSA Bulletin 103, 277-289.

Colpaert, A., Pickard, N., Mienert, J., Henriksen, L.B., Rafaelsen, B., Andreassen, K., 2007. 3D seismic analysis of an Upper Palaeozoic carbonate succession of the Eastern Finnmark platform area, Norwegian Barents Sea. Sedimentary Geology 197, 79-98.

Cutbill, J.L., Challinor, A., 1965. Revision of the stratigraphical scheme for the Carboniferous and Permian rocks of Spitsbergen and Bjørnøya. Geological Magazine 102, 418-439.

Dallmann, W.K., Gjelberg, J.G., Harland, W.B., Johannessen, E.P., Keilen, H.B., Lønøy, A., Nilsson, I., Worsley, D., 1999. The Upper Palaeozoic lithostratigraphy. In: Dallmann, W.K. (Ed.), Lithostratigraphic lexicon of Svalbard, Norsk Polarinstitutt, Tromsø, pp. 25-126.

Dean Jr, W.E., 1974. Determination of carbonate and organic matter in calcareous sediments and sedimentary rocks by loss on ignition: comparison with other methods. Journal of Sedimentary Petrology 44, 242-248.

De Jong, K., 2015. Synthetic seismic profile of lateral variations in the Sobrarbe delta (Pyrenees, northern Spain). Unpublished MSc Thesis. VU University Amsterdam, The Netherlands, p. 56.

Dorn, A.G., 1998. Modern 3-D seismic interpretation. The Leading Edge 17, 1262-1272.

Doveton, J.H., 1994. Geological log interpretation—Reading the rocks from wireline logs, vol. 29. SEPM Short Course, p. 169.

Dunham, R.J., 1962. Classification of carbonate rocks according to depositional texture. In: Ham, W.E. (Ed.), Classification of carbonate rocks, vol. 1. AAPG Memoir, pp. 108-171.

Dustira, A.M., Wignall, P.B., Joachimski, M., Blomeier, D., Hartkopf-Fröder, C., Bond, D., 2013. Gradual onset of anoxia across the Permian–Triassic Boundary in Svalbard, Norway. Palaeogeography, Palaeoclimatology, Palaeoecology 374, 303-313.

Earnest, C.M., 1984. Modern thermogravimetry. Analytical Chemistry 56, 1471-1486.

Earnest, C.M., 1988. Compositional analysis by thermogravimetry, ASTM-STP 997, Philadelphia, Pennsylvania, USA, p. 293.

Eberli, G.P., Anselmetti, F.S., Kenter, J.A.M., McNeill, D.F., Melim, L.A., 2001. Calibration of seismic sequence stratigraphy with cores and logs. In: Ginsburg, R.N. (Ed.), Subsurface geology of a prograding carbonate platform margin, Great Bahama Bank: Results of the Bahamas drilling project, vol. 70. SEPM Special Publication, Tulsa, Oklahoma, USA, pp. 241-265.

Eberli, G.P., Anselmetti, F.S., Kroon, D., Sato, T., Wright, J.D., 2002. The chronostratigraphic significance of seismic reflectors along the Bahamas Transect. Marine Geology 185, 1-17.

Eberli, G.P., Baechle, G.T., Anselmetti, F.S., Incze, M.L., 2003. Factors controlling elastic properties in carbonate sediments and rocks. The Leading Edge 22, 654-660.

Eberli, G.P., Anselmetti, F.S., Betzler, C., Van Konijnenburg, J.H., Bernoulli, D., 2004. Carbonate platform to basin transitions on seismic data and in outcrops, Great Bahama Bank and the Maiella platform margin, Italy. In:

Eberli, G.P., Massaferro, J.L., Sarg, J.F. (Eds.), Seismic imaging of carbonate reservoirs and systems, vol. 81. AAPG Memoir, pp. 207-250.

Ehrenberg, S., Nielsen, E.B., Svånå, T.A., Stemmerik, L.A., 1998. Depositional evolution of the Finnmark Carbonate Platform, Barents Sea: results from wells 7128/6-1 and 7128/4-1. Norwegian Journal of Geology 78, 185-224

Ehrenberg, S., Pickard, N., Henriksen, L., Svånå, T.A., Gutteridge, P., Macdonald, D., 2001. A depositional and sequence stratigraphic model for cold-water, spiculitic strata based on the Kapp Starostin Formation (Permian) of Spitsbergen and equivalent deposits from the Barents Sea. AAPG Bulletin 85, 2061-2088.

Ehrenberg, S., Eberli, G.P., Bracco Gartner, G.L., 2004. Data report: Porosity and permeability of Miocene carbonate platforms on the Marion Plateau, ODP Leg 194. In: Anselmetti, F.S., Isern, A.R., Blum, P., Betzler, C. (Eds.), Proceedings ODP, Scientific Results 194, Ocean Drilling Program, College Station, Texas, USA, p. 217.

Elvevold, S., 2015. Georesources. In: Dallmann, W.K. (Ed.), Geoscience Atlas of Svalbard, Norwegian Polar Institute, Tromsø, Norway, p. 292.

Falivene, O., Arbues, P., Ledo, J., Benjumea, B., Munoz, J.A., Fernandez, O., Martinez, S., 2010. Synthetic seismic models from outcrop-derived reservoir-scale three-dimensional facies models: The Eocene Ainsa turbidite system (southern Pyrenees). AAPG Bulletin 94, 317-343.

Fedorowski, J., 1982. Some rugose corals from the Upper Permian of East Greenland. In: Peel, J.S. (Ed.), Palaeontology of Greenland: short contributions, Grønlands Geologiske Undersøgelse, Copenhagen, Denmark, p. 91.

Flügel, E., 2004. Microfacies of Carbonate Rocks, Springer, Berlin, Germany, p. 976.

Fournier, F., Borgomano, J., 2007. Geological significance of seismic reflections and imaging of the reservoir architecture in the Malampaya gas field (Philippines). AAPG Bulletin 91, 235-258.

Fournier, F., Borgomano, J., 2009. Critical porosity and elastic properties of microporous mixed carbonate-siliciclastic rocks. Geophysics 74, 93-109.

Fournier, F., Léonide, P., Kleipool, L., Toullec, R., Reijmer, J.J.G., Borgomano, J., Klootwijk, T., Van Der Molen, J., 2014. Pore space evolution and elastic properties of platform carbonates (Urgonian limestone, Barremian-Aptian, SE France). Sedimentary Geology 308, 1-17.

Fredriksen, K., 1988. Sedimentologiske og diagenetiske undersøkelser av Kapp Starostin Formasjonen på Akseløya og Mariaholmen, Bellsund, Svalbard. Unpublished MSc Thesis. University of Tromsø, Norway, p. 162.

Gardner, G., Gardner, L., Gregory, A., 1974. Formation velocity and density-the diagnostic basics for stratigraphic traps. Geophysics 39, 770-780.

Gassmann, F., 1951. Elastic waves through a packing of spheres. Geophysics 16, 673-685.

Gates, L.M., James, N.P., Beauchamp, B., 2004. A glass ramp: shallow-water Permian spiculitic chert sedimentation, Sverdrup basin, Arctic Canada. Sedimentary Geology 168, 125-147.

Golonka, J., 2002. Plate-tectonic maps of the Phanerozoic. In: Kiessling, W., Flügel, E., Golonka, J. (Eds.), Phanerozoic reef patterns, vol. 72. SEPM Special Publications, Tulsa, Oklahoma, USA, pp. 21–70.

Groen, R.D., 2010. From a restricted carbonate platform to a temperate, storm-dominated ramp: The onset of the Permian Chert Event in central Spitsbergen. Unpublished MSc Thesis. VU University Amsterdam, The Netherlands, p. 105.

Helland-Hansen, W., Helle, H., Sunde, K., 1994. Seismic modeling of Tertiary sandstone clinothems, Spitsbergen. Basin Research 6, 181-191.

Han, D., Nur, A., Morgan, D., 1986. Effects of porosity and clay content on wave velocities in sandstones. Geophysics 51, 2093-2107.

Haq, B., Schutter, S., 2008. A chronology of Paleozoic sea-Level changes. Science 322, 64-68.

Hodgetts, D., Howell, J.A., 2000. Synthetic seismic modelling of a large-scale geological cross-section from the Book Cliffs, Utah, USA. Petroleum Geoscience 6, 221-229.

Hossain, Z., Zhou, Y., 2015. Petrophysics and rock physics modelling of diagenetically altered sandstone. Interpretation 3, 107-120.

Hüneke, H., Joachimski, M., Buggisch, W., Lützner, H., 2001. Marine Carbonate Facies in Response to Climate and Nutrient Level: The Upper Carboniferous and Permian of Central Spitsbergen (Svalbard). Facies 45, 93-136.

Iijima, A., Hein, J.R., Siever, R., 1983. An introduction to siliceous deposits in the Pacific region. Developments in Sedimentology 36, 1-6.

Jacquin, T., Arnaud-Vanneau, A., Arnaud, H., Ravenne, C., Vail, P., 1991. Systems tracts and depositional sequences in a carbonate setting: A study of continuous outcrops from platform to basin at the scale of seismic lines. Marine and Petroleum Geology 8, 122-139.

Jafarian, E., Kleipool, L.M., Scheibner, C., Blomeier, D., Reijmer, J.J.G., 2017a. Variations in petrophysical properties of Upper Palaeozoic mixed carbonate and non-carbonate deposits, Spitsbergen, Svalbard Archipelago. Journal of Petroleum Geology 40, 59-83.

Jafarian, E., Reijmer, J.J.G., Blomeier, D., 2017b. Facies arrangement and cyclostratigraphic architecture of the Templet Member and the Kapp Starostin Formation (Permian) on Spitsbergen, Svalbard. Norwegian Journal of Geology 97, 213-231.

Jafarian, E., De Jong, K., Kleipool, L.M., Scheibner, C., Blomeier, D., Reijmer, J.J.G., in press. Synthetic seismic model of a Permian biosiliceous carbonate – carbonate depositional system (Spitsbergen, Svalbard Archipelago). Manuscript submitted to "Marine and Petroleum Geology".

James, N.P., 1997. The cool-water carbonate depositional realm. In: James, N.P., Clarke, J.A.D. (Eds.), Cool-Water Carbonates, vol. 56. SEPM Special Publication, Tulsa, pp. 1- 20.

Janson, X., Eberli, G.P., Bonnaffe, F., Gaumet, F., De Casanove, V., 2007. Seismic expressions of a Miocene prograding carbonate margin, Mut Basin, Turkey. AAPG Bulletin 91, 685-713.

Janson, X., Fomel, S., 2010. 3D Forward Seismic Model of an Outcrop-Based Geocellular Model. In: Martinsen, O., Pulham, A., Haughton, P., Sullivan, M. (Eds.), Outcrops Revitalized: Tools, Techniques and Applications, SEPM Concepts in Sedimentology and Paleontology, Tulsa, Oklahoma, pp. 87-106.

Janson, X., Lucia, F.J., 2014. Relationship between Acoustic and Petrophysical Properties of Permian Dolograinstones, p. 40. Search and Discovery Article #41263.

Johannessen, E.P., Steel, R.J., 1992. Mid-Carboniferous extension and rift-infill sequences in the Billefjorden Trough, Svalbard. Norwegian Journal of Geology 72, 35-48

Kenter, J., Fouke, B., Reinders, M., 1997a. Effects of differential cementation on the sonic velocities of Upper Cretaceous skeletal grainstones (southeastern Netherlands). Journal of Sedimentary Research 67, 178-185.

Kenter, J., Podladchikov, F., Reinders, M., Van der Gaast, S., Fouke, B., Sonnenfeld, M., 1997b. Parameters controlling sonic velocities in a mixed carbonate-siliciclastics Permian shelf-margin (upper San Andres formation, Last Chance Canyon, New Mexico). Geophysics 62, 505-520.

Kenter, J., Bracco Gartner, G.L., Schlager, W., 2001. Seismic models of a mixed carbonate-siliciclastic shelf margin: Permian upper San Andres Formation, Last Chance Canyon, New Mexico. Geophysics 66, 1744-1748.

Kenter, J., Braaksma, H., Verwer, K., Van Lanen, X., 2007. Acoustic behavior of sedimentary rocks: Geologic properties versus Poisson's ratios. Geophysics 26, 436-444.

Kittridge, M.G., 2015. Investigating the influence of mineralogy and pore shape on the velocity of carbonate rocks: Insights from extant global data sets. Interpretation 3, 15–31.

Kleipool, L.M., Reijmer, J.J.G, Bádenas, B., Aurell, M., 2015. Variations in petrophysical properties along a mixed siliciclastic carbonate ramp (Upper Jurassic, Ricla, NE Spain). Marine and Petroleum Geology 68, 158-177.

Kleipool, L.M., De Jong, K., De Vaal, E.L., Reijmer, J.J.G., 2017. Seismic characterization of switching platform geometries and dominant carbonate producers (Miocene, Las Negras, Spain). Sedimentology 64, 1676-1707.

Klicpera, A., Michel, J., Westphal, H., 2015. Facies patterns of a tropical heterozoan carbonate platform under eutrophic conditions: the Banc d'Arguin, Mauritania. Facies 61, 1-24.

Larssen, G.B., Elvebakk, G., Henriksen, L.B., Kristensen, S.E., Nilsson, I., Samuelsberg, T.J., Svånå, T.A., Stemmerik, L., Worsley, D., 2002. Upper Palaeozoic lithostratigraphy of the Southern Norwegian Barents Sea. Norwegian Petroleum Directorate (NPD) Bulletin 9, p. 76.

Laya, J.C., Tucker, M.E., 2012. Facies analysis and depositional environments of Permian carbonates of the Venezuelan Andes: Palaeogeographic implications for Northern Gondwana. Palaeogeography, Palaeoclimatology, Palaeoecology 331, 1-26.

Lerch, B., Karlsen, D.A., Matapour, Z., Seland, R., Backer-Owe, K., 2016. Organic geochemistry of Barents Sea petroleum: thermal maturity and alteration and mixing processes in oils and condensates. Journal of Petroleum Geology 39, 125-48.

Loizeau, J., Arbouille, D., Santiago, S., Vernet, J., 1994. Evaluation of a wide range laser diffraction grain size analyser for use with sediments. Sedimentology 41, 353-361.

Lucia, F.J., Conti, R.D., 1987. Rock fabric, permeability, and log relationships in an upward-shoaling, vuggy carbonate sequence, Bureau of Economic Geology, University of Texas at Austin, Geological Circular 87-5, p. 22.

McNeill, D.F., Cunningham, K.J., Guertin, L.A., Anselmetti, F.S., 2004. Depositional themes of mixed carbonate-siliciclastics in the south Florida Neogene: application to ancient deposits. In: Integration of Outcrop and Modern Analogs in Reservoir Modeling, vol. 80. AAPG Memoir, pp. 23-43.

Malkowski, K., Hoffman, A., 1979. Semi-quantitative facies model for the Kapp Starostin Formation (Permian), Spitsbergen. Acta Palaeontologica Polonica 24, 217-230.

Mangerud, G., Konieczny, R.M., 1993. Palynology of the Permian succession of Spitsbergen, Svalbard. Polar Research 12, 65-93.

Mavko, G., Mukerji, T., Dvorkin, J., 2009. The rock physics handbook: Tools for seismic analysis of porous media, Cambridge University Press, New York, USA, p. 511.

May, B.T., Hron, F., 1978. Synthetic seismic sections of typical petroleum traps. Geophysics 43, 1119-1147.

McCave, I., Bryant, R.J., Cook, H., Coughanowr, C., 1986. Evaluation of a laser-diffraction-size analyzer for use with natural sediments. Journal of Sedimentary Petrology 56, 561-564.

Michel, J., Vicens, G.M., Westphal, H., 2011. Modern heterozoan carbonates from a eutrophic tropical shelf (Mauritania). Journal of Sedimentary Research 81, 641-655.

Montgomery, S.L., 1998. Thirtyone Formation, Permian Basin, Texas: Structural and lithologic heterogeneity in a Lower Devonian chert reservoir. AAPG Bulletin 82, 1-24.

Morton, R.A., 1981. Formation of storm deposits by wind-forced currents in the Gulf of Mexico and the North Sea. In: Nio, S.D., Shuttenhelm, R.T.E., Van Weering, T.J. (Eds.), Holocene Marine Sedimentation in the North Sea Basin, vol. 5. International Association of Sedimentologists (IAS) Special Publication, pp. 385-396.

Mørk, A., Embry, A.F., Weitschat, W., 1989. Triassic transgressive-regressive cycles in the Sverdrup Basin, Svalbard and the Barents Shelf. In: Collinsen, J. (Ed.), Correlation in hydrocarbon exploration, Norwegian Petroleum Society, Graham & Trotman, London, pp. 113-130.

Nakrem, H.A., Nilsson, I., Mangerud, G., 1992. Permian biostratigraphy of Svalbard (Arctic Norway) — a review. International Geology Review 34, 933–959.

Nakrem, H.A., Orchard, M.J., Weitschat, W., Hounslow, M.W., Beatty, T.W., Mørk, A., 2008. Triassic conodonts from Svalbard and their Boreal correlations. Polar Research 27, 523-539.

Nestvold, E.O., 1996. The impact of 3-D seismic data on exploration, field development, and production. In: Weimer, P., Thomas, D.L. (Eds.), Applications of 3-D Seismic Data to Exploration and Production, vol. 42. AAPG Studies in Geology, pp. 1-7.

Nichols, G., 1999. Sedimentology and stratigraphy, second ed. Wiley-Blackwell, Oxford, United Kingdom, p. 419.

O'brien, R.M., 2007. A caution regarding rules of thumb for variance inflation factors. Quality & Quantity 41, 673-690.

Pomar, L., Ward, W.C., Green, D.G., 1996. Upper Miocene reef complex of the Llucmajor area, Mallorca, Spain. In: Franseen, E., Esteban, M., Ward, W.C., Rouchy, J.M. (Eds.), Models for Carbonate Stratigraphy from Miocene Reef Complexes of the Mediterranean Regions, vol. 5. SEPM Concepts in Sedimentology and Paleontology, pp. 191-225.

Rafaelsen, B., Elvebakk, G., Andreassen, K., Stemmerik, L., Colpaert, A., Samuelsberg, T.J., 2008. From detached to attached carbonate buildup complexes—3D seismic data from the Upper Palaeozoic, Finnmark Platform, southwestern Barents Sea. Sedimentary Geology 206, 17-32.

Raymer, L., Hunt, E., Gardner, J., 1980. An improved sonic transit time-to-porosity transform. SPWLA 21st Annual Logging Symposium, p. 1-12.

Reid, C.M., James, N.P., Beauchamp, B., Kyser, T.K., 2007. Faunal turnover and changing oceanography: Late Palaeozoic warm-to cool water carbonates, Sverdrup Basin, Canadian Arctic Archipelago. Palaeogeography, Palaeoclimatology, Palaeoecology 249, 128–159.

Reijmer, J.J.G., Bauch, T., Schäfer, P., 2012. Carbonate facies patterns in surface sediments of upwelling and non-upwelling shelf environments (Panama, East Pacific). Sedimentology 59, 32-56.

Reijmer, J.J.G., Worms, S., De Jong, K., Nooitgedacht, C., Kleipool, L.M., Arbués, P. Synthetic seismic profile of lateral variations in the Sobrarbe delta (Pyrenees, northern Spain). In Prep.

Reymond, C.E., Zihrul, K.S., Halfar, J., Riegl, B., Humphreys, A., Westphal, H., 2016. Heterozoan carbonates from the equatorial rocky reefs of the Galápagos Archipelago. Sedimentology 63, 940-958.

Ricker, N., 1953. The form and laws of propagation of seismic wavelets. Geophysics 18, 10-40.

Rogers, J.P., Longman, M.W., 2001. An introduction to chert reservoirs of North America. AAPG Bulletin 85, 1-5.

Rudolph, K.W., Schlager, W., Biddle, K.T., 1989. Seismic models of a carbonate foreslope-to-basin transition, Picco di Vallandro, Dolomite Alps, northern Italy. Geology 17, 453-456.

Ruppel, S., Hovorka, S., 1995. Controls on reservoir development in Devonian chert: Permian basin, Texas. AAPG Bulletin 79, 1757-1784.

Saller, A., Vanhorn, D., Miller, J., Guy, B., 1991. Reservoir geology of Devonian carbonates and chert-implications for Tertiary recovery, Dollarhide Field, Andrews County, Texas. AAPG Bulletin 75, 86-107.

Schlager, W., 2005. Carbonate sedimentology and sequence stratigraphy, vol. 8. SEPM Concepts in sedimentology and paleontology, Tulsa, Oklahoma, USA, p. 200.

Schneider, J., 2013. Upper Carboniferous - lower Permian warm-water carbonates from Hornsund and Bellsund, Spitsbergen: Lithology, diagenesis, depositional environment and petrophysical properties. Unpublished MSc Thesis. VU University, Amsterdam, The Netherlands, p. 169.

Schoenberger, M., 1974. Resolution comparison of minimum-phase and zero-phase signals. Geophysics 39, 826-833.

Schroeder, L.D., Sjoquist, D.L., Stephan, P.E., 1986. Understanding regression analysis: An introductory guide, Sage, Newbury Park, California, USA, p. 96.

Schwab, A.M., Cronin, B.T., Ferreira, H., 2007. Seismic expression of channel outcrops: Offset stacked versus amalgamated channel systems. Marine and Petroleum Geology 24, 504-514.

Scotese, C.R., Langford, R.P., 1995. Pangaea and the paleogeography of the Permian. In: Scholle, P.A., Peryt, T.M., Ulmer-Scholle, D.S. (Eds.), The Permian of northern Pangaea, Paleogeography, paleoclimates, stratigraphy, vol. 1. Springer, Berlin Heidelberg, New York, pp. 3-19.

Seidler, L., Steel, R.J., Stemmerik, L., Surlyk, F., 2004. North Atlantic marine rifting in the Early Triassic: new evidence from East Greenland. Journal of the Geological Society 161, 583-592.

Soete, J., Kleipool, L.M., Claes, H., Claes, S., Hamaekers, H., Kele, S., Özkul, M., Foubert, A., Reijmer, J.J.G., Swennen, R., 2015. Acoustic properties in travertines and their relation to porosity and pore types. Marine and Petroleum Geology 59, 320-335.

Stafleu, J., 1994. Seismic models of outcrops as an aid in seismic Interpretation. PhD Thesis. VU University Amsterdam, The Netherlands, p. 223.

Stafleu, J., Everts, A.J., Kenter, J.A., 1994. Seismic models of a prograding carbonate platform: Vercors, south-east France. Marine and Petroleum Geology 11, 514-527.

Stafleu, J., Sonnenfeld, M.D., 1994. Seismic models of a shelf margin depositional sequence: Upper San Andres Formation, Last Chance Canyon, New Mexico. Journal of Sedimentary Research 64, 481-499.

Steel, R.J., Worsley, D., 1984. Svalbard's post-Caledonian strata—an atlas of sedimentation patterns and paleogeographic evolution. In: Spencer, A.M., Holter, E., Johnsen, S.O., Mørk, A., Nysæther, E., Songstad, P., Spinnangr, Å. (Eds.), Petroleum Geology of the North European Margin, Norwegian Petroleum Society, Graham & Trotman Ltd., London, pp. 109-135.

Stemmerik, L., Worsley, D., 1989. Late Palaeozoic sequence correlations, North Greenland, Svalbard and the Barents Shelf. In: Collinson, J.D. (Ed.), Correlation in hydrocarbon exploration, Norwegian Petroleum Society, Graham & Trotman Ltd., London, pp. 99–111.

Stemmerik, L., Worsley, D., 1995. Permian history of the Barents Shelf Area. In: Scholle, P., Peryt, T., Ulmer-Scholle, D. (Eds.), The Permian of Northern Pangaea: Sedimentary Basins and Economic Resources, vol. 2. Springer-Verlag, Berlin, Heidelberg, pp. 81-97.

Stemmerik, L., Elvebakk, G., Worsley, D., 1999. Upper Palaeozoic carbonate reservoirs on the Norwegian Arctic Shelf: delineation of reservoir models with application to the Loppa High. Petroleum Geoscience 5, 173-187.

Stemmerik, L., Worsley, D., 2005. 30 years on - Arctic Upper Palaeozoic stratigraphy, depositional evolution and hydrocarbon prospectivity. Norwegian Journal of Geology 85, 151-168.

Surdam, R.C., Stanley, K.O., 1981. Diagenesis and migration of hydrocrabons in the Monterey Formation, Pismo Syncline, California. In: Garrison, R.E., Douglas, R.G. (Eds.), The Monterey Formation and related siliceous rocks of

California, Society of Economic Paleontologists and Mineralogists, Pacific Section, Los Angeles, pp. 317-327.

Tomás, S., Zitzmann, M., Homann, M., Rumpf, M., Amour, F., Benisek, M., Marcano, G., Mutti, M., Betzler, C., 2009. From ramp to platform: building a 3D model of depositional geometries and facies architectures in transitional carbonates in the Miocene, northern Sardinia. Facies 56, 195-210.

Tucker, M.E., Wright, V.P., 2009. Carbonate sedimentology, Blackwell Science, Oxford, p. 482.

Van Wagoner, J.C., Mitchum, R.M., Campion, K.M., Rahmanian, V.D., 1990. Siliciclastic sequence stratigraphy in well logs, cores, and outcrops: Concepts for high-resolution correlation of time and facies, vol. 7. AAPG Methods in Exploration, AAPG, Tulsa, p. 55.

Vernik, L., Nur, A., 1992. Petrophysical classification of siliciclastics for lithology and porosity prediction from seismic velocities. AAPG Bulletin 76, 1295-1309.

Verwer, K., Braaksma, H., Kenter, J., 2008. Acoustic properties of carbonates: Effects of rock texture and implications for fluid substitution. Geophysics 73, 51-65.

Verwer, K., Merino-Tomé, O., Kenter, J.A.M., Della Porta, G., 2009. Evolution of a highrelief carbonate platform slope using 3D digital outcrop models: Lower Jurassic Djebel Bou Dahar, High Atlas, Morocco. Journal of Sedimentary Research 79, 416-439.

Verwer, K., Eberli, G.P., Weger, R.J., 2011. Effect of pore structure on electrical resistivity in carbonates. AAPG Bulletin 95, 175-190.

Wang, Z., 2001. Fundamentals of seismic rock physics. Geophysics 66, 398-412.

Warrlich, G., Bosence, D., Waltham, D., 2005. 3D and 4D controls on carbonate depositional systems: sedimentological and sequence stratigraphic analysis of an attached carbonate platform and atoll (Miocene, Níjar Basin, SE Spain). Sedimentology 52, 363-389.

Weger, R.J., Eberli, G.P., Baechle, G.T., Massaferro, J.L., Sun, Y.F., 2009. Quantification of pore structure and its effect on sonic velocity and permeability in carbonates. AAPG Bulletin 93, 1297-1317.

Wentworth, C.K., 1922. A scale of grade and class terms for clastic sediments. Journal of Geology 30, 377-392.

Wignall, P.B., Morante, R., Newton, R., 1998. The Permo–Triassic transition in Spitsbergen: δ^{13}Corg chemostratigraphy, Fe and S geochemistry, facies, fauna and trace fossils. Geological Magazine 135, 47-62.

Wilkens, R., Simmons, G., Caruso, L., 1984. The ratio VP/VS as a discriminant of composition for siliceous limestones. Geophysics 49, 1850-1860.

Wyllie, M., Gregory, A., Gardner, L., 1956. Elastic wave velocities in heterogeneous and porous media. Geophysics 21, 41-70.

Xu, S., Payne, M., 2009. Modeling elastic properties in carbonate rocks. The Leading Edge 28, 66-74.

Zeller, M., Eberli, G.P., Weger, R.J., Giunta, D.L., Massaferro, J.L., 2014. Seismic expressions of the Quintuco-Vaca Muerta system based on outcrop facies and geometry. In: IX Congreso de Exploración y Desarrollo de Hidrocarburos, Simposio de Recursos No Convenionales: Ampliando el Horizonte Energético, pp. 209-224.

Zeller, M., Reid, S.B., Eberli, G.P., Weger, R.J., Massaferro, J.L., 2015a. Sequence architecture and heterogeneities of a field - Scale Vaca Muerta analog (Neuquén Basin, Argentina) - From outcrop to synthetic seismic. Marine and Petroleum Geology 66, 829-847.

Zeller, M., Verwer, K., Eberli, G.P., Massaferro, J.L., Schwarz, E., Spalletti, L., 2015b. Depositional controls on mixed carbonate–siliciclastic cycles and sequences on gently inclined shelf profiles. Sedimentology 62, 2009-2037.

Zhao, L., Nasser, M., Han, D., 2013. Quantitative geophysical pore-type classification and its geological implication in carbonate reservoirs. Geophysical Prospecting 61, 827-841.

Ziegler, A., Hulver, M., Rowley, D., 1997. Permian World Topography and Climate. In: Martini, I. (Ed.), Late Glacial and Postglacial Environmental Changes: Quaternary, Carboniferous–Permian and Proterozoic, Oxford University Press, New York, Oxford, pp. 111-146.

Samenvatting

Carbonaat sedimenten worden gevormd door verscheidene biogene en niet-biogene processen. Ze worden gekenmerkt door hun heterogene voorkomen en vormen zich binnen een uniek sedimentair milieu. Het geproduceerde sediment blijft of in het productiegebied, bijvoorbeeld bij koraalriffen en modder heuvels (mud mounds), of is beschikbaar voor sediment transport naar de aangrenzende hellingen, het continentale plat of omliggende bekkens. De productie van sediment en transport mechanismes verschillen aanzienlijk ten opzichte van siliciclastische afzettingen. Die sedimenten zijn het gevolg van van erosie op andere plaatsen en de geproduceerde sedimenten worden in het depositionele milieu gebracht via verschillende transport processen, bijvoorbeeld water, wind, of gletsjers.

Carbonaat groei en productie zijn gebonden aan mariene, zout water, dan wel lacustriene, zoet water, of terrestrische milieus. In mariene werelden zijn licht, watertemperatuur, de aanvoer van nutrienten en tot op zekere hoogte saliniteit de meest dominante factoren die de productie van sedimenten sturen. Daarnaast kunnen individuele oceanografische factoren een rol spelen, bijvoorbeeld stromingen, opwelling/niet-opwelling, oceaanwinden, seizoensgebonden variaties, getijden en de invoer van siliciclastisch sediment.

Carbonaat afzettingen kunnen na depositie onderworpen worden aan texturele en kristallografische veranderingen, deze komen tot stand door zogenoemde diagenetische processen. Sommige van de oorspronkelijke metastabiele carbonaathoudende mineralen, bijvoorbeeld aragoniet en hoog-magnesium calciet, zijn gevoelig voor veranderingen in de oorspronkelijke condities waaronder de sedimenten zijn afgezet. Voornamelijk druk, temperatuur en de chemische samenstelling van circulerende vloeistoffen kunnen in de ondergrond sterk veranderen en het oorsponkelijke sedimentaire gesteente omzetten.

Aangezien de biosfeer en depositionele milieus drastisch zijn veranderd in tijd en ruimte, zijn de meerderheid van de carbonaat afzettingen uniek betreffende de compositie van het sediment en hun ruimtelijke distributie.

Het Perm wordt gekenmerkt door klimatologische, oceanografische en ecologische veranderingen, als gevolg van de vorming van het supercontinent Pangea. Tijdens het Boven-Paleozoïcum veranderde de samenstelling van de sedimenten die werden afgezet in de arctische en subarctische delen van het noordelijk halfrond. De sedimenten lieten een geleidelijke afkoeling zien, welke was af te lezen aan hun biogene samenstelling; van warme en aride

omstandigheden naar koud-water condities. Deze verandering ging gepaard met een verdieping van het afzettingsmilieu in de regio van Spitsbergen.
Het doel van deze thesis was om met behulp van observaties aan diverse ontsluitingen een gedetailleerd onderzoek te doen naar de fysieke en texturele eigenschappen van carbonaat en niet-carbonaathoudend gesteente. Voorts werd de invloed van deze variaties op het gedrag van synthetische seismische signalen onderzocht. De gemeten fysische eigenschappen van het gesteente, zoals porositeit, dichtheid en akoestische snelheden, worden in deze thesis geëvalueerd voor de onderzochte gesteentes. Daarnaast worden texturele kenmerken zoals de korrelgrootteverdeling en de mineralogie bestudeerd. Vervolgens werden synthetische seismische modellen geconstrueerd met behulp van de hiervoor genoemde ruimtelijke, fysieke en texturele informatie. De geconstrueerde synthetisch seismische profielen kunnen vervolgens dienen als richtlijnen voor de interpretatie van seismische profielen gebaseerd op seismisch onderzoek van gesteenteformaties die niet aan het oppervlak treden en verborgen zitten in de diepe ondergrond.
Het Arctische eiland Spitsbergen, ligt op de noordwestelijke hoek van de Barentsz Zee, en toont uitstekende ontsluitingen van Boven-Paleozoïsche sedimentaire opeenvolgingen. De afzettingen van het Laat-Carboon tot Vroeg-Perm op Spitsbergen worden gekenmerkt door een gemengde samenstelling van siliclastische - en tropische carbonaat sedimenten die zijn gevormd op een laag hoekige carbonaat helling. De geïdentificeerde sedimentaire sequenties zijn afgezet tijdens een periode waarin de zeespiegel langzaam daalde, een algemene regressie. Deze trend is duidelijk te zien aan de bovenkant van de successie, omdat deze uiteindelijk eindigt met een hiaat in sedimentatie, een stop in het afzetten van sedimenten in een marien milieu.
De Vroege tot Late Permische sedimenten op Spitsbergen zijn samengesteld uit hoornsteen met fijne silica naaldjes (spiculitic chert) in combinatie met koudwater carbonaten. Het afzettingsmilieu is geïnterpreteerd als carbonaat platform met een geringe helling dat gesitueerd was op een midden breedtegraad. Het werd gekenmerkt door een relatief laag-energetische milieu dat regelmatig werd verstoord door stormen. Opwelling van kouder diep-water resulteerde niet alleen in een toename van de trofische omstandigheden maar vooral ook in een toevoer van silica. Dit resulteerde uiteindelijk in de sedimentatie van hoornsteen afzettingen met fijne silica naaldjes.
De afzettingen tonen sterke ruimtelijke variatie in lithologieën, wat resulteert in een brede verscheidenheid aan petrofysische en texturele eigenschappen. Het ontbreken van porositeit is een van de meest karakteristieke eigenschappen van de bestudeerde sedimentaire gesteentes. Variatie in de mineralogische samenstelling (silica versus carbonaat) is een andere bepalende parameter voor de gemeten akoestische snelheid van deze

gesteentes. Deze verscheidenheid resulteert in het voorkomen van hoge amplitude reflecties in de synthetische seismogrammen.
Bij hoge frequenties geven de synthetische seismogrammen van de Spitsbergen-ontsluitingen de variaties van facies en de bijbehorende wijzigingen in de petrofysische eigenschappen zeer goed weer. Bij lagere frequenties daarentegen worden deze variaties bijna allemaal uitgewist, de contrasten vervagen. Echter, de carbonaat naar niet-carbonaat transities blijven zichtbaar vanwege hun hoge impedantie contrasten. De eerste orde verschuivingen in het afzettingssysteem die in het veld zijn aangetroffen zijn gekenmerkt door het voorkomen van zogenaamde sequentie grenzen en het interessante is dat juist die grenzen herkenbaar blijven in de lage-frequentie-profielen.
De studie van de fysische eigenschappen en het synthetisch modelleren van gesteenteontsluitingen laat zien dat men door middel van dit soort exercities de geologische wereld te zien aan het aardoppervlak en de geofysische weergave van de wereld in de ondergrond dichter bij elkaar kan brengen.

Summary

Carbonate deposits enclose a broad variety of biogenic and non-biogenic constituents. They are characterized by their heterogeneous appearance and produce sediment within their depositional environment that either remains in the production area, e.g. reefs, mud mounds, or is available for sediment export to the adjacent slopes, shelves or surrounding basins. This sedimentation production and export process differs significantly from those observed for siliciclastic deposits while these sediments are the product of erosion elsewhere and brought into the depositional setting through various transport processes, e.g. water, wind, glaciers.

Carbonate growth and production are tied to the marine realm, lacustrine environments or terrestrial settings. In marine environments light, water temperature, nutrient supply and to some extend salinity are the most dominant controls. In addition, individual oceanographic factors may play a role, e.g. ocean currents, upwelling/non-upwelling, winds, seasonal variations, tides, and siliciclastic input.

Carbonate deposits may be subjected to extensive diagenetic alteration during burial or exposure. Some of the original metastable carbonate minerals, e.g. aragonite and High-Magnesium calcite, are sensitive for changes in subsurface conditions like pressure, temperature and the chemical composition of circulating fluids.

Since the biosphere and the depositional settings have changed drastically through time and space, the majority of the carbonate deposits are unique as to their sediment composition and sediment distribution.

The Permian time is characterized by pronounced climatic, oceanographic and environmental changes, due to the formation of the supercontinent Pangea. During the Upper Palaeozoic, the sediments present in Arctic and sub-Arctic parts of the Northern Hemisphere recorded a gradual cooling from warm and arid to cold-water conditions, which was accompanied by a deepening of the depositional environments in the Spitsbergen region.

By using outcrop observations, this thesis aimed to provide a detailed investigation of the physical and textural properties of carbonate and non-carbonate rocks and the impact of these variations on the appearance of synthetic seismic signals. The measured rock's physical properties, e.g. porosity, density and acoustic velocities, are evaluated. Additionally, textural characteristics such as the grain size distribution and the mineralogy are assessed. The synthetic seismic models are constructed using spatial, physical and textural information; the constructed profiles could serve as guidelines for seismic datasets from the subsurface.

The Arctic island of Spitsbergen, located at the northwestern corner of the

Barents Sea Shelf, shows outstanding exposures of an Upper Palaeozoic sedimentary succession. The Late Carboniferous to Early Permian strata on Spitsbergen are characterized by a mixed composition of siliciclastic and tropical carbonate sediments that are deposited on a carbonate shelf. The identified sedimentary sequences record an overall marine regression towards the top of this succession, which ultimately produced a hiatus in sedimentation.

The Early to Late Permian sediments on Spitsbergen are composed of spiculitic cherts in combination with cold-water carbonates. The succession is interpreted to have accumulated on a ramp-type carbonate platform in a mid-latitude, relative low-energy setting that was periodically perturbed by storm events. Upwelling resulted in elevated trophic resources on the ramp and supplied the silica required for spiculitic chert deposition.

The deposits show the high spatial variability of lithologies, resulting in a wide range of petrophysical and textural properties. The absence of porosity is one of the most characteristic properties of the studied carbonate and non-carbonate sediments. Variations in mineralogical composition (silica versus carbonate) are an important controlling parameter for acoustic velocity and consequently causes high amplitude reflections in the synthetic seismic seismograms.

At high frequencies, the synthetic seismograms of the Spitsbergen outcrops mimic the facies variations and associated changes in petrophysical properties, which become obliterated at lower frequencies. Carbonate to non-carbonate transitions remain visible because of their high impedance contrasts. These first order shifts in the depositional system are in line with the major sequence boundaries and are recognizable in the low frequency profiles.

The study of physical properties and synthetic modelling of outcrops shows that we can bring together the geological world exposed at the earths surface and the geophysical representation we compose of its interior.

Acknowledgements

After a period of intense learning, today is the day; writing this acknowledgment as the finishing touch on my dissertation. I would like to reflect on the people who have supported and helped me so much throughout this period in one way or another.

First and foremost, I would like to express my deepest gratitude to my promoter John Reijmer, who has been a tremendous help to me, not only in academic life but also in my personal life. John has given me a lot of freedom to develop my scientific work, believed in my work, and given me courage and inspiration in this way. John has been beyond a great support for me. John, thank you for your time and patience in supervising me. Sincere thanks also go to my co-promoter Lucas Kleipool, someone from whom I learned a lot. Luuk has supported me not only by providing valuable advice to develop my research, but also emotionally through the rough road to finish this thesis. I am also grateful to my other co-promoters, Dierk Blomeier and Christian Scheibner, for their consistent support. Thank you very much, for your ideas, for the fruitful discussions, for your continuous efforts to improve my papers and thesis. We have been a team; hoping our collaboration may develop further in the future.

I would like to thank the members of the reading committee, prof.dr. Christian Betzler, prof.dr. Jean Borgomano, prof.dr. Maria Mutti, prof.dr. W. van Westrenen, dr. Jan Stafleu, for dedicating their precious time to read my work and offering valuable feedback which improved the quality of this thesis.

I thank M.Sc. students Ralph Groen, Mahtab Mozafari and Jan Schneider of the Vrije Universiteit Amsterdam for their contributions; and Bouke Lacet and Wynanda Koot for preparing the thin-sections and plugs at the VU University Amsterdam.

I dedicate my grateful to my colleagues at the sedimentology group of the Vrije Universiteit Amsterdam who have helped me get through this process. Especially, I would like to thank Fenny, Barbara, Luuk, Rieneke, Monica, Carlette, Cas, Koos, Jeroen, Els, Thomas, and Max. I had a great time working with all of you. Many thanks for your enthusiasm and the great times we spend together.

I also wish to thank my Iranian friends for making our life in Amsterdam so much more enjoyable. I consider myself to be very lucky to have so many Iranian friends I could rely on them for support.

I would like to express my deepest gratitude to my family. My parents, Hassan and Mahboubeh, my brothers, and my sister for their endless support and encouragement. I would like to thank my parents-in-law, my brothers-in-law, and my sister-in-law for their continuous support.

Last but not least, I am really grateful to my dear husband, Seyedesmaeil Mousavi, for his unconditional support, patience, and attention. My son, Parham, is an absolute joy and brings happiness to me every second. I am forever indebted to you all!